Illinois State University

ISU ReD: Research and eData

Theses and Dissertations

4-6-2018

Alkyne Combustion: Experimental and Computational Studies of Formyl Radical Production

Matthew Charles Drummer
Illinois State University, mcdrumm@ilstu.edu

Follow this and additional works at: https://ir.library.illinoisstate.edu/etd

Part of the Physical Chemistry Commons

Recommended Citation

Drummer, Matthew Charles, "Alkyne Combustion: Experimental and Computational Studies of Formyl Radical Production" (2018). *Theses and Dissertations*. 853.
https://ir.library.illinoisstate.edu/etd/853

This Thesis is brought to you for free and open access by ISU ReD: Research and eData. It has been accepted for inclusion in Theses and Dissertations by an authorized administrator of ISU ReD: Research and eData. For more information, please contact ISUReD@ilstu.edu.

www.manaraa.com

ALKYNE COMBUSTION: EXPERIMENTAL AND COMPUTATIONAL STUDIES OF FORMYL RADICAL PRODUCTION

Matthew C. Drummer

154 Pages

According to the U.S. Energy Information Administration, the United States consumed a total of 97.4 trillion BTUs (British Thermal Unit, 1 BTU = 1.055 kJ) of energy in 2016 with over 80% of that energy consumption source being fossil fuel combustion. Before a combustion reaction reaches its end products, a number of intermediate products form and may react with other abundant atmospheric species to form aerosol particles and acid rain, both of which have potentially negative impacts on both human-made structures and the natural environment.

In an effort to counteract the consequences of fossil fuel combustion, scientists are interested in gaining insight into the reaction mechanisms of hydrocarbon combustion reactions to understand how, and which, intermediate products form. One of the many intermediate products formed in hydrocarbon combustion reactions is the formyl radical, HCO. Discovered in 1934, HCO radical has since been proven to form in many hundreds of combustion reactions and plays key roles in both atmospheric and interstellar chemistry, namely as a donor of hydroxyl radicals.

While alkane combustion has been studied extensively in the past, alkene and alkyne combustion has received little attention beyond the short-chain species: ethylene, propene, acetylene, and propyne. Due to receiving little attention, the formation of HCO radical during alkyne combustion reactions is focused on in this project. This thesis provides results from both

www.manaraa.com

experimental and theoretical studies on the reactions of triplet oxygen atoms, $O(^3P)$, with the hydroxyl-substituted alkynes, propargyl alcohol and 3-butyn-1-ol.

Preliminary experimental studies of alkyne combustion revealed strong variations in HCO radical absorption intensity across different alkyne species. The most dramatic difference in HCO radical absorption intensity was observed between the combustion of propyne and propargyl alcohol, where propargyl alcohol gave a much stronger signal for HCO radical than propyne. Both compounds are three-carbon alkynes, with the only difference being the hydroxyl substituent of propargyl alcohol. This study attempts to explain these variations via computational investigation. Utilizing quantum mechanical methods, potential energy profiles have been mapped out to reveal the energetics of reaction pathways that result in the formation of HCO radical. Isoformyl radical, HOC, is also investigated computationally in this project as it is the higher energy isomer of HCO radical and may isomerize to the lower energy state.

The computational portion of this study reveals a higher number of HCO/HOC radical formation pathways for the alcohol-substituted alkynes and focuses on the reactions of $O(^3P)$ + propargyl alcohol and $O(^3P)$ + 3-butyn-1-ol. The experimental portion of this study involves the detection of HCO radical as it forms during alkyne combustion via Cavity Ring-down Laser Absorption Spectroscopy (CRDLAS).

KEYWORDS: combustion; alkyne; formyl; radical; experimental; computational

www.manaraa.com

ALKYNE COMBUSTION: EXPERIMENTAL AND COMPUTATIONAL STUDIES OF FORMYL RADICAL PRODUCTION

MATTHEW C. DRUMMER

A Thesis Submitted in Partial
Fulfillment of the Requirements
For the Degree of

MASTER OF SCIENCE

Department of Chemistry

ILLINOIS STATE UNIVERSITY

2018

www.manaraa.com

©2018 Matthew C. Drummer

www.manaraa.com

ALKYNE COMBUSTION: EXPERIMENTAL AND COMPUTATIONAL STUDIES OF FORMYL RADICAL PRODUCTION

MATTHEW C. DRUMMER

COMMITTEE MEMBERS:

Jean M. Standard, Chair

Isabel X. Green

Christopher C. Mulligan

www.manaraa.com

ACKNOWLEDGMENTS

I would like to thank all of those who made this thesis possible. First, thank you to Dr. Jean Standard for taking me in as a graduate student and being an amazing research mentor and teacher of both computational and quantum chemistry. Second, thank you to Dr. Bob Quandt for sparking my interest in physical chemistry research and teaching me vital laboratory skills during my undergraduate years. Third, thank you to the faculty and staff of the Department of Chemistry at Illinois State University for nurturing a strong sense of community and fellowship among both undergraduate and graduate students. Finally, many thanks to Lori and Gary Drummer for all of their support and providing me with the means to further my education and pursue a career in science.

M.C.D.

www.manaraa.com

CONTENTS

		Page
ACKNOWLEDGMENTS		i
CONTENTS		ii
TABLES		iv
FIGURES		v
CHAPTER		
I.	INTRODUCTION	1
II.	EXPERIMENTAL METHODS	11
III.	COMPUTATIONAL METHODS	15
IV.	RESULTS	18
	Experimental Detection of HCO in the Reaction of $O(^3P)$ + Propargyl Alcohol	18
	Computational Results for $O(^3P)$ + Propargyl Alcohol	23
	Geometries: $O(^3P)$ + Propargyl Alcohol	24
	Potential Energy Profiles: $O(^3P)$ + Propargyl Alcohol	28
	Minimum Energy Crossing Point	41
	NRT Analysis: $O(^3P)$ + Propargyl Alcohol	43
	Computational Results for $O(^3P)$ + 3-Butyn-1-ol	53
	Geometries: $O(^3P)$ + 3-Butyn-1-ol	53
	Potential Energy Profiles: $O(^3P)$ + 3-Butyn-1-ol	56
	NRT Analysis: $O(^3P)$ + 3-Butyn-1-ol	62
	Subsequent Pathways	69

www.manaraa.com

V. CONCLUSION 72

REFERENCES 75

APPENDIX A: ALL OPTIMIZED STRUCTURES FOR O(^{3}P) + PROPARGYL ALCOHOL AND O(^{3}P) + 3-BUTYN-1-OL AT THE M06-2X/CC-PVTZ LEVEL 81

APPENDIX B: CARTESIAN COORDINATES FOR ALL OPTIMIZED STRUCTURES FOR O(^{3}P) + PROPARGYL ALCOHOL AND O(^{3}P) + 3-BUTYN-1-OL AT THE M06-2X/CC-PVTZ LEVEL 116

www.manaraa.com

TABLES

Table Page

1. Selected bond lengths and angles for structures on the triplet potential energy surface of O(^{3}P) + propargyl alcohol, calculated at the M06-2X/cc-pVTZ and MP2/6-311++G(d,p) levels of theory. 25

2. Continued bond lengths and angles for structures on the triplet potential energy surface of O(^{3}P) + propargyl alcohol, calculated at the M06-2X/cc-pVTZ and MP2/6-311++G(d,p) levels of theory. 26

3. Selected bond lengths and angles for structures on the singlet potential energy surface of O(^{3}P) + propargyl alcohol, calculated at the M06-2X/cc-pVTZ and MP2/6-311++G(d,p) levels of theory. 27

4. Relative energies for structures on the triplet potential energy surface, computed using the M06-2X, MP2, and CCSD(T)//M06-2X single point methods. 29

5. Continued relative energies for structures on the triplet potential energy surface, computed using the M06-2X, MP2, and CCSD(T)//M06-2X single point methods. 30

6. Continued relative energies for structures on the triplet potential energy surface, computed using the M06-2X, MP2, and CCSD(T)//M06-2X single point methods. 31

7. MECP results, calculated at the M06-2X/cc-pVTZ level of theory. 42

8. Selected bond lengths and angles for structures on the triplet potential energy surface of O(^{3}P) + 3-butyn-1-ol, calculated at the M06-2X/cc-pVTZ and MP2/6-311++G(d,p) levels of theory. 54

9. Continued selected bond lengths and angles for structures on the triplet potential energy surface of O(^{3}P) + 3-butyn-1-ol, calculated at the M06-2X/cc-pVTZ and MP2/6-311++G(d,p) levels of theory. 55

www.manaraa.com

FIGURES

Figure Page

1. Buettner's absorption spectrum of HCO (average of 10 runs) for the reaction of $O(^3P)$ + propyne. 4

2. Buettner's absorption spectrum of HCO (average of 10 runs) for the reaction of $O(^3P)$ + propargyl alcohol. 4

3. Relative HCO absorbance intensities for a series of alkynes. 5

4. Plot for level of theory vs basis set size. As accuracy increases, so does computational cost. 7

5. Potential energy profile for the reaction of $O(^3P)$ + propargyl alcohol at the MP2/6-311++G(d,p) level of theory. 8

6. Potential energy profile for the reaction of $O(^3P)$ + propyne at the MP2/6-311++G(d,p) level of theory (black = triplet, red = singlet). 9

7. Diagram of the CRDLAS experimental setup. 11

8. Example for 1 of 1536 data points from a single 613-617 nm scan (ring-down time: ~15 μs). 18

9. Absorption spectrum for HCO in the reaction of $O(^3P)$ + propargyl alcohol. This spectrum is an average of 10 individual runs. 19

10. Absorption spectrum for HCO in the reaction of $O(^3P)$ + butyne. This spectrum is an average of 10 individual runs. 20

11. Absorption spectrum for HCO in the reaction of $O(^3P)$ + pentyne. This spectrum is an average of 10 individual runs. 21

12. Comparison of absorption spectra for HCO in the reaction of $O(^3P)$ + propyne (left) and $O(^3P)$ + propargyl alcohol (right). Left spectrum is an average of 15 individual runs and the right spectrum is an average of 8 individual runs. 22

13. Comparison of absorption spectra for HCO in the reaction of $O(^3P)$ + butyne (left) and $O(^3P)$ + 3-butyn-1-ol (right). Left spectrum is an average of 10 individual spectra and the right spectrum is an average of 10 individual runs. 22

14. Numbering scheme for the $O(^3P)$ + propargyl alcohol reaction. 24

15. Established triplet surface pathways, CCSD(T)// M06-2x/cc-pVTZ level, key IM and TS structures shown. 33

www.manaraa.com

Figure Page

16. Established singlet surface pathways, CCSD(T)//M06-2x/cc-pVTZ level. 33

17. Established triplet surface pathways, M06-2x/cc-pVTZ level. 34

18. Established singlet surface pathways, M06-2x/cc-pVTZ level. 34

19. Established triplet surface pathways, MP2/6-311++G(d,p) level. 35

20. Established singlet surface pathways, MP2/6-311++G(d,p) level. 35

21. Isomerization of the formyl radical, computed at the CCSD(T)//M06-2x/cc-pVTZ level of theory. 36

22. Novel HCO Pathway (branching off from IM-1T), CCSD(T)//M06-2x/cc-pVTZ level. 38

23. Novel HCO Pathway (branching off from IM-2T), CCSD(T)//M06-2x/cc-pVTZ level. 39

24. Novel HCO Pathway (branching off of IM-4T), CCSD(T)//M06-2x/cc-pVTZ level. 40

25. Structures for IM-1T (top left), MECP (top right), and IM-1S (bottom), calculated at the M06-2x/cc-pVTZ level. 42

26. NSD Data for the Established HCO Pathway, calculated at the M06-2x/cc-pVTZ level of theory. 44

27. NBO Data for the Established HCO Pathway, calculated at the M06-2x/cc-pVTZ level of theory. 45

28. NSD Data for a novel HCO Pathway (IM-1T), calculated at the M06-2x/cc-pVTZ level of theory. 46

29. NBO Data for a novel HCO Pathway (IM-1T), calculated at the M06-2x/cc-pVTZ level of theory. 47

30. NSD Data for a novel HOC Pathway (IM-2T), calculated at the M06-2x/cc-pVTZ level of theory. 48

31. NBO Data for a novel HOC Pathway (IM-2T), calculated at the M06-2x/cc-pVTZ level of theory. 49

www.manaraa.com

Figure Page

32. NSD Data for a novel HOC Pathway (IM-4T), calculated at the M06-2x/cc-pVTZ level of theory. 50

33. NBO Data for a novel HOC Pathway (IM-4T), calculated at the M06-2x/cc-pVTZ level of theory. 50

34. NSD Data for a novel HOC Pathway (IM-4T), calculated at the M06-2x/cc-pVTZ level of theory. 51

35. NBO Data for a novel HOC Pathway (IM-4T), calculated at the M06-2x/cc-pVTZ level of theory. 51

36. NSD Data for a novel HCO Pathway (IM-4T), calculated at the M06-2x/cc-pVTZ level of theory. 52

37. NBO Data for a novel HCO Pathway (IM-4T), calculated at the M06-2x/cc-pVTZ level of theory. 52

38. Numbering scheme for the $O(^3P)$ + 3-butyn-1-ol reaction. 53

39. Two HCO formation pathways for $O(^3P)$ + 3-butyn-1-ol, M06-2x/cc-pVTZ level. 57

40. Two HCO formation pathways for $O(^3P)$ + 3-butyn-1-ol, CCSD(T)//M06-2x/cc-pVTZ level. 57

41. Additional HCO/HOC formation pathways for $O(^3P)$ + 3-butyn-1-ol, M06-2x/cc-pVTZ level. 58

42. Additional HCO/HOC formation pathways for $O(^3P)$ + 3-butyn-1-ol, CCSD(T)//M06-2x/cc-pVTZ level. 59

43. Final HOC dissociation pathway found for $O(^3P)$ + 3-butyn-1-ol, M06-2x/cc-pVTZ level. 60

44. Final HOC dissociation pathway found for $O(^3P)$ + 3-butyn-1-ol, CCSD(T)//M06-2x/cc-pVTZ. 61

45. NSD Data for the HCO pathway shown in Figure 39, calculated at the M06-2x/cc-pVTZ level of theory. 62

46. NBO Data for the HCO pathway shown in Figure 39, calculated at the M06-2x/cc-pVTZ level of theory. 63

www.manaraa.com

Figure Page

47. NSD Data for the other HCO pathway shown in Figure 39, calculated at the M06-2x/ cc-pVTZ level of theory. 64

48. NBO Data for the other HCO pathway shown in Figure 39, calculated at the M06-2x/ cc-pVTZ level of theory. 65

49. NSD Data for the HCO pathway shown in Figure 41, calculated at the M06-2x/ cc-pVTZ level of theory. 65

50. NBO Data for the HCO pathway shown in Figure 41, calculated at the M06-2x/ cc-pVTZ level of theory. 66

51. NSD Data for the HOC pathway shown in Figure 41, calculated at the M06-2x/ cc-pVTZ level of theory. 66

52. NBO Data for the HOC pathway shown in Figure 41, calculated at the M06-2x/ cc-pVTZ level of theory. 67

53. NSD Data for the HOC pathway shown in Figure 43, calculated at the M06-2x/ cc-pVTZ level of theory. 67

54. NBO Data for the HOC pathway shown in Figure 43, calculated at the M06-2x/ cc-pVTZ level of theory. 68

55. Subsequent dissociation pathway for HOC, CCSD(T)//M06-2x/cc-pVTZ level. 70

56. Subsequent dissociation pathway for HOC, CCSD(T)//M06-2x/cc-pVTZ level. 70

57. Subsequent dissociation pathway for HCO, CCSD(T)//M06-2x/cc-pVTZ level. 71

www.manaraa.com

CHAPTER I

INTRODUCTION

The combustion of hydrocarbons has been a subject of interest to scientists for a whole host of reasons, including both its contributions to human advancement and its potential environmental consequences. The industrial-scale process of burning fossil fuels such as petroleum, coal, and natural gas allows for large yields in energy that is put to work within various sectors including transportation, residential/commercial energy utilization, and the generation of electrical power.[1] The U.S. Energy Information Administration (EIA) estimates that a total of 97,394 trillion BTUs (British Thermal Unit, 1 BTU = 1.055 kJ) of energy were consumed by the United States alone in 2016, with the current total estimated consumption of 2017 at 97,310 trillion BTUs.[2] With fossil fuel combustion making up over 80% of total energy consumption in the United States,[2] the effects of chemical byproducts from these combustion reactions, therefore, come into question. Perhaps the most profound effect of combustion byproducts is the phenomenon of global climate change in which human activities of energy consumption have led to the highest levels of atmospheric CO_2 in 650,000 years (404.07 ppm), increased global temperature of 1.7° F, increased loss of land ice (281.0 gigatonnes per year), and a rise in sea level of about seven inches over the past 100 years.[3]

Scientists are interested in studying the reaction mechanisms of hydrocarbon combustion in an effort to gain further insight into how combustion reactions work and the intermediate byproducts that are inevitably released into the atmosphere. Scientific research into the mechanisms and effects of hydrocarbon combustion spans a number of fields, including physical chemistry, and such mechansisms have been studied experimentally and computationally by physical chemists for over two decades.[4-6] Through experimentation and computational methods,

www.manaraa.com

physical chemists have detected key reaction pathways that have been proven to exist throughout many hundreds of saturated hydrocarbon combustion reactions. However, the combustion of the unsaturated analogs of these hydrocarbons remains widely uninvestigated. Investigations of the combustion of unsaturated hydrocarbons have mostly been focused on short-chain alkenes and alkynes. Short-chain alkenes that have been studied extensively include ethylene[7-9] and propene.[10-12] Investigations on the combustion of alkynes have been conducted mainly on acetylene[13-17] and propyne.[18-20] Research on the reactions of $O(^3P)$ + short-chain alkenes have been carried out by the Cvetanović group, in which temperature dependence was observed for the combustion of ethylene, propene, and 1-butene.[21] In addition, the Cvetanović group determined that radical intermediates are produced during these combustion reactions before the final products, CO_2 and H_2O, are formed.[21] The high temperature conditions of a combustion reaction allow for the dehydrogenation of saturated hydrocarbons to their corresponding unsaturated forms, as described by equations (1) and (2).[22] Following the dissociation of molecular oxygen, equation (3), alkene and alkyne species may react with $O(^3P)$ atoms to form many products, as shown in equations (4) and (5),

$$\text{alkane} + \text{heat} \rightarrow \text{alkene} + 2H \qquad (1)$$

$$\text{alkene} + \text{heat} \rightarrow \text{alkyne} + 2H \qquad (2)$$

$$O_2 + \text{heat} \rightarrow 2O(^3P) \qquad (3)$$

$$\text{alkene} + O(^3P) \rightarrow \text{products} \qquad (4)$$

$$\text{alkyne} + O(^3P) \rightarrow \text{products} \qquad (5)$$

www.manaraa.com

Numerous product channels exist in an alkyne + $O(^3P)$ reaction, including CO, H_2, and various radical species. Reaction pathways of alkenes and alkynes with $O(^3P)$ have been studied by several research groups and a number of recurring reaction pathways have been discovered, including the formation of the formyl radical, HCO.[23] The formyl radical, HCO, was first reported by Vaidya in 1934 and has since been proven to be an abundantly observed intermediate in many hundreds of combustion reactions.[24] For example, research conducted by the Bersohn group delved into the HCO radical formation pathways within the $O(^3P)$ + alkene systems.[25] The formyl radical is a highly reactive atmospheric compound that may react and result in the formation of hydroxyl radicals, OH, a species that reacts with other atmospheric compounds to form aerosol particles and acid rain.[22] HCO radical plays significant roles in combustion, atmospheric, and interstellar chemical reactions, particularly as a donor of hydrogen atoms.[26] Experimental HCO radical detection in $O(^3P)$ + alkyne reactions remains largely uninvestigated due to the complications of detecting HCO radical via laser-induced fluorescence (LIF), a widely utilized gas-phase spectroscopic method.[27] The complications of employing LIF to study HCO radical formation stems from an interference of the $O(^3P)$ precursor, SO_2, which absorbs in the same region as the B ← X transition of HCO radical observed in LIF (~230 nm). Cavity ring-down laser absorption spectroscopy (CRDLAS) allows one to observe the $\tilde{A}^2A''(0,9,0) \leftarrow \tilde{X}\ ^2A'(0,0,0)$ transition of HCO radical (613-617 nm) without any interference from SO_2.

The Quandt group has conducted CRDLAS experiments to demonstrate the formation of HCO radical within the reactions of $O(^3P)$ with propyne, butyne, 3-butyn-2-one, 3-butyn-1-ol, pentyne, propargyl ether, propargyl amine, and propargyl alcohol.[28] These studies revealed wide variations in HCO radical absorption intensity across the different $O(^3P)$ + alkyne reactions. For example, absorption spectra collected by the Quandt group[28] for propyne and propargyl alcohol

www.manaraa.com

are shown in Figures 1 and 2, respectively. It was observed that the reaction of $O(^3P)$ with propyne and butyne resulted in detectable HCO radical absorption, whereas $O(^3P)$ + pentyne resulted in data that was far too noisy to distinguish HCO radical formation. Propargyl alcohol consistently gave the strongest intensity signal for HCO radical.

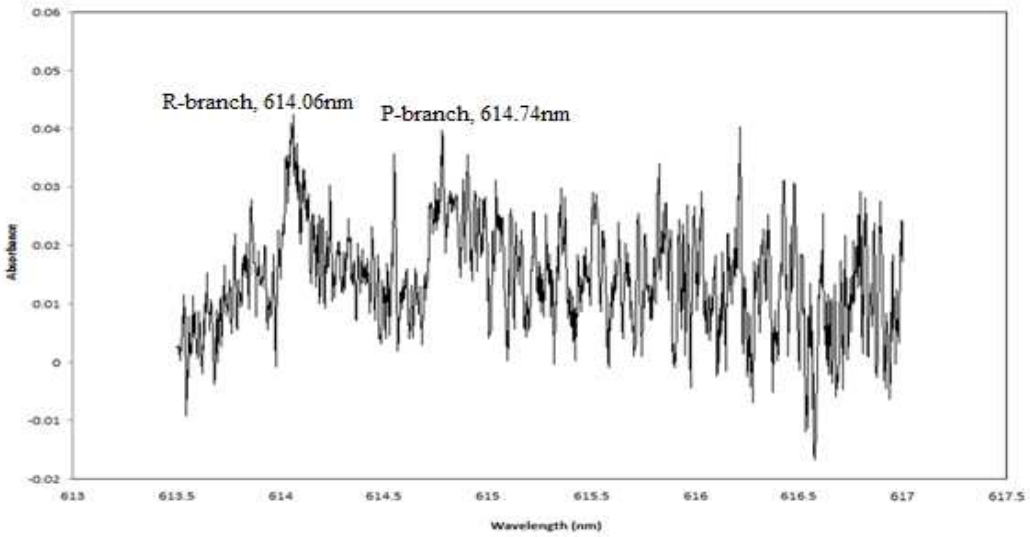

Figure 1. Buettner's absorption spectrum of HCO (average of 10 runs) for the reaction of $O(^3P)$ + propyne.[28]

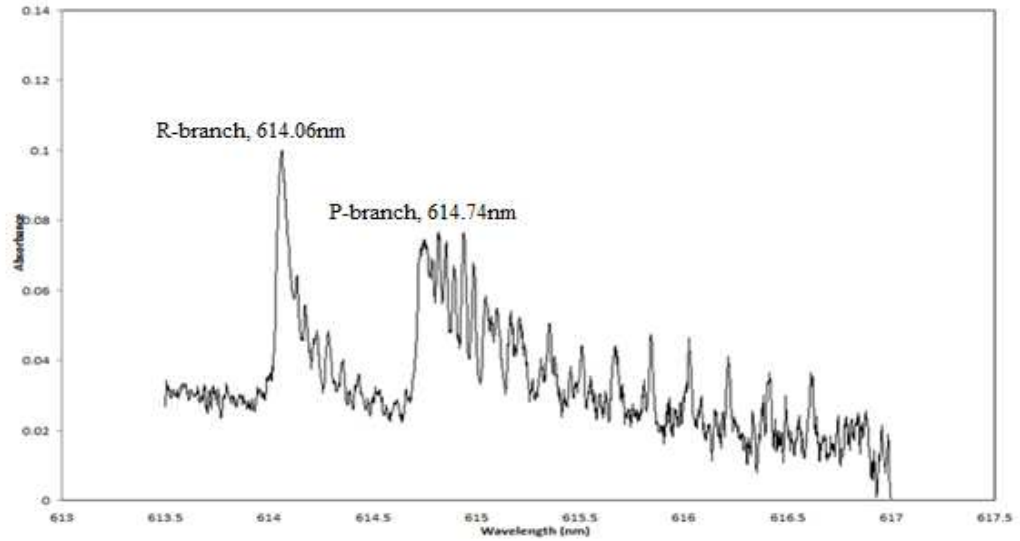

Figure 2. Buettner's absorption spectrum of HCO (average of 10 runs) for the reaction of $O(^3P)$ + propargyl alcohol.[28]

www.manaraa.com

Previous experimental work in the Quandt research lab found a relatively large signal in the absorption spectrum for HCO radical formation in propargyl alcohol + $O(^3P)$.[28] Formyl radical signals were acquired for a series of other alkynes as well, with their relative absorbance intensities compared in Figure 3. Absorbance values below 0.02 have been covered by a dark area to represent where the signal becomes indistinguishable from the noise. Prior to the studies conducted by the Quandt and Standard lab groups, the reaction pathway of propargyl alcohol has gone uninvestigated and, thus, has become a topic of interest as hydroxyl-substituted alkynes gave the strongest absorbance signal for HCO radical after reacting with triplet oxygen.

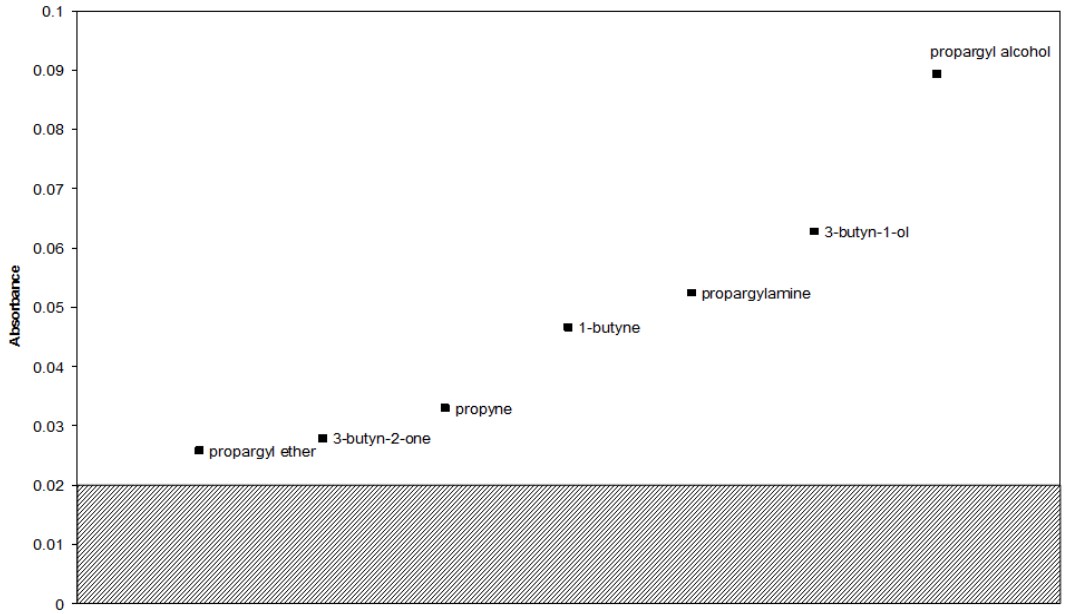

Figure 3. Relative HCO absorbance intensities for a series of alkynes.[28]

Through computational methods, the Quandt and Standard research groups studied the potential energy surfaces of $O(^3P)$ + alkyne reactions to better understand the reaction mechanisms behind formyl radical formation.[28,29] Previous computational work in the Quandt and Standard groups have led to new insight into how HCO radical forms during combustion

www.manaraa.com

reactions.[28-29] Computational methods have been employed to investigate novel reaction pathways that may explain the strong HCO radical signal seen in the propargyl alcohol + O(^{3}P) reaction. The Quandt and Standard groups utilized quantum mechanical calculations for the optimization of equilibrium geometries, vibrational frequencies, and potential energies at the B3LYP/cc-pVTZ, M06-2x/cc-pVTZ, and MP2/6-311++G(d,p) levels of theory. More accurate potential energy values were obtained by performing single-point energy calculations on each optimized structure at the CCSD(T)/cc-pVTZ//M06-2x/cc-pVTZ level of theory.

Figure 4 illustrates the relative accuracy and computational cost of different levels of theory and basis set sizes. The concurrent utilization of high levels of theory with large basis set sizes results in highly accurate optimization results. However, computational costs increase with accuracy. For this reason, the CCSD(T) level of theory was not feasibly applicable for full optimizations of the various reagent, IM, TS, and product structures for this project. Instead, methods with lower computational costs were employed for optimizing geometries and vibrational frequencies. Once this has been accomplished, the higher level CCSD(T) was used to optimize only the potential energies of each structure.

www.manaraa.com

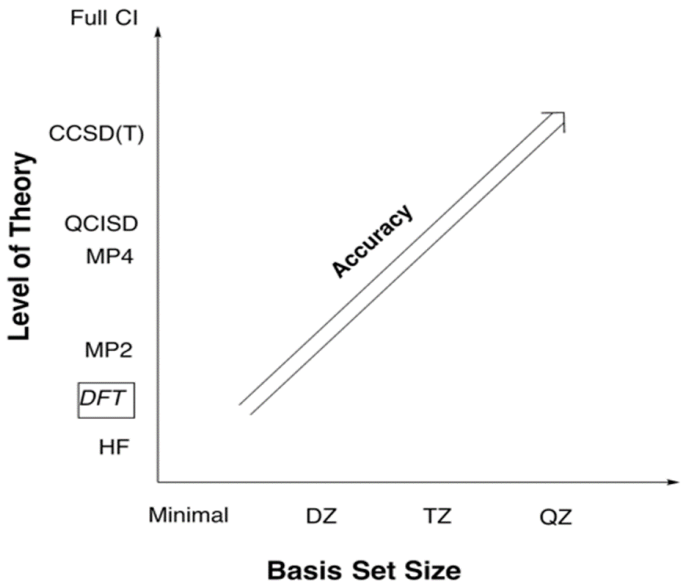

Figure 4. Plot for level of theory vs basis set size. As accuracy increases, so does computational cost.

Thus far, only a few pathways in the reaction of $O(^3P)$ + propargyl alcohol have been studied and were investigated at the MP2/6-311++G(d,p) level of theory, as seen in Figure 5. The pathways shown in Figure 5 exist on the triplet potential energy surface of the $O(^3P)$ + propargyl alcohol reaction. The relative energies of all intermediate (IM) and transition state (TS) structures in Figure 5 have been improved upon and are presented in this project. Optimization of potential energies was achieved by first collecting optimized geometries, vibrational frequencies, and energies at the M06-2x level of theory followed by single-point energy calculations at the CCSD(T)/cc-pVTZ level of theory.

www.manaraa.com

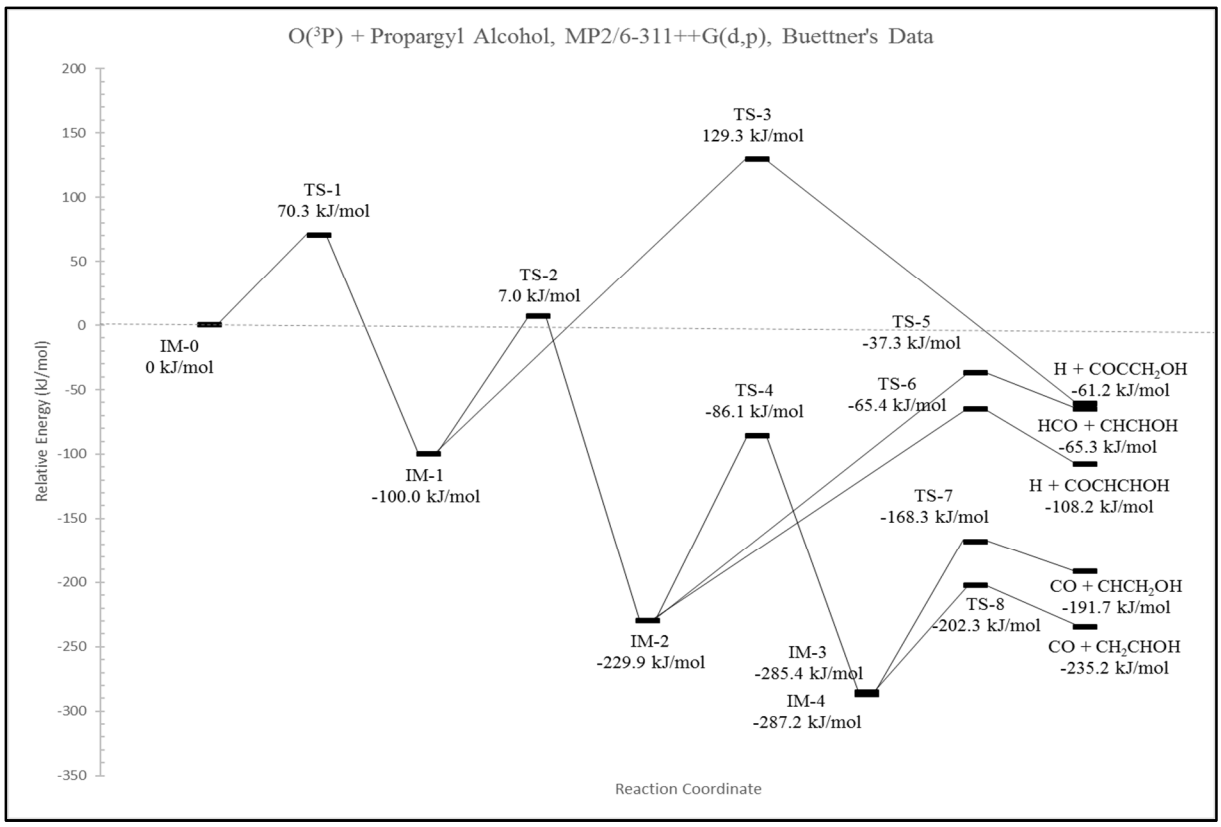

Figure 5. Potential energy profile for the reaction of $O(^3P)$ + propargyl alcohol at the MP2/6-311++G(d,p) level of theory.[28]

As seen in Figure 6, both the triplet (black) and singlet (red) pathways were computed by the Quandt and Standard groups for the $O(^3P)$ + propyne reaction. While the singlet surface pathways do not yield HCO radical, intersystem crossing (ISC) may occur in which a triplet IM may cross over to the singlet surface or vice versa. ISC plays an important role in many atmospheric and combustion reactions as it helps explain the branching ratios and intersections of product channels in the reactions of $O(^3P)$ + alkanes, alkenes, and alkynes.[30] ISC between the singlet and triplet surfaces is of interest because of the accessibility of the singlet potential energy surface after the initiation of the reaction on the triplet surface.

www.manaraa.com

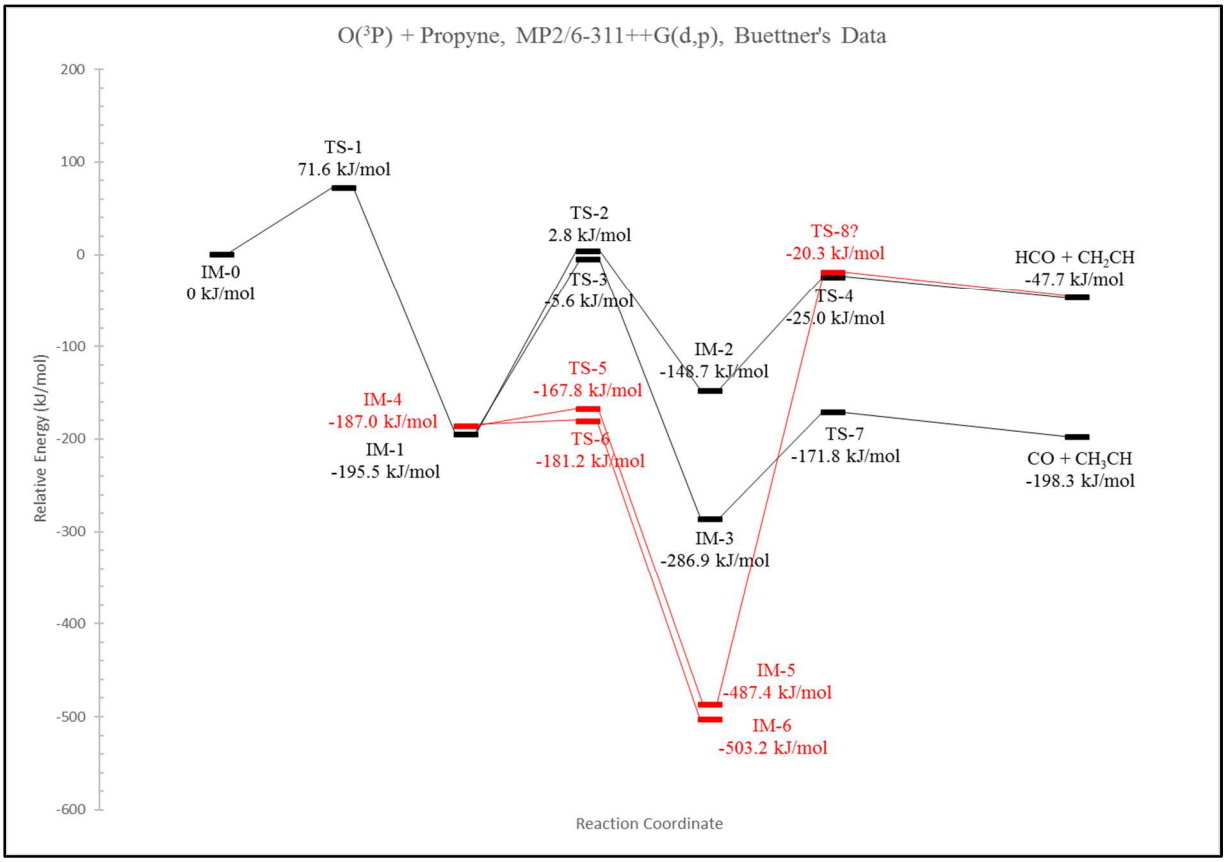

Figure 6. Potential energy profile for the reaction of $O(^3P)$ + propyne at the MP2/6-311++G(d,p) level of theory (black = triplet, red = singlet).[28]

The potential energy profile (PEP) is a plot of potential energy as a function of reaction coordinate. As the reaction progresses, IM and TS structures reveal important information about the combustion reaction of interest, such as relative energy barriers that indicate which reaction pathways are preferred. Calculated vibrational frequencies confirm whether a structure is an IM (all vibrational frequencies are positive) or a TS (one vibrational frequency is imaginary).

Buettner explored the reaction pathways for the reactions of $O(^3P)$ + propyne, butyne, pentyne, and propargyl alcohol at the MP2 level of theory.[28] This project expands upon Buettner's findings and offers possible explanations as to why propargyl alcohol gave the highest intensity absorption signal for HCO radical in the CRDLAS studies.

www.manaraa.com

The first accomplishment presented in this thesis is the rebuilt PEP of $O(^3P)$ + propargyl alcohol at the CCSD(T)/cc-pVTZ//M06-2x/cc-pVTZ level of theory because M06-2x has been proven to yield optimized geometries and energies that are more consistent with CCSD(T) for the reaction of propyne + $O(^3P)$ than other benchmarked levels of theory.[29] The HCO radical formation pathway found by Buettner will hereby be referred to as the "established HCO radical pathway." In addition to building a new PEP starting from Buettner's MP2/6-311++G(d,p) structures, novel pathways of formyl radical production have also been investigated. All novel pathways presented here branch off from IM structures within the established HCO radical formation pathway. The formation of the isoformyl radical, HOC, is also investigated and presented here as it isomerizes to the lower energy formyl radical, HCO. Reaction mechanisms of HCO and HOC radical production are investigated and presented in this thesis via Natural Resonance Theory (NRT) analysis, from which bond orders and spin densities are obtained. Finally, this project is concluded with the study of the reaction of $O(^3P)$ + 3-butyn-1-ol. Full equilibrium geometry, vibrational frequency, and energy optimizations have been carried out at the M06-2x/cc-pVTZ level of theory with single-point energy calculations collected at the CCSD(T)/cc-pVTZ level. Both the $O(^3P)$ + propargyl alcohol and $O(^3P)$ + 3-butyn-1-ol reactions have received a full NRT analysis, which is presented in chapter IV.

www.manaraa.com

CHAPTER II

EXPERIMENTAL METHODS

The experimental portion of this project was completed in the Quandt research group. HCO radical product formation was detected via Cavity Ringdown Laser Absorption Spectroscopy (CRDLAS).[28] The experimental set up, as seen in Figure 7, involved flowing reagent gaseous species through a stainless steel cavity consisting of two 27 cm tubes connected to an 8 cm stainless steel cubic cell. Reagents were introduced into the cavity by flowing the appropriate gas/vapor through small tubes connected to the system and were evacuated with a vacuum pump (base pressure of ~1 torr). Each end of the cavity was sealed off from the atmosphere by highly reflective mirrors (Los Gatos Research, R>99.999%).

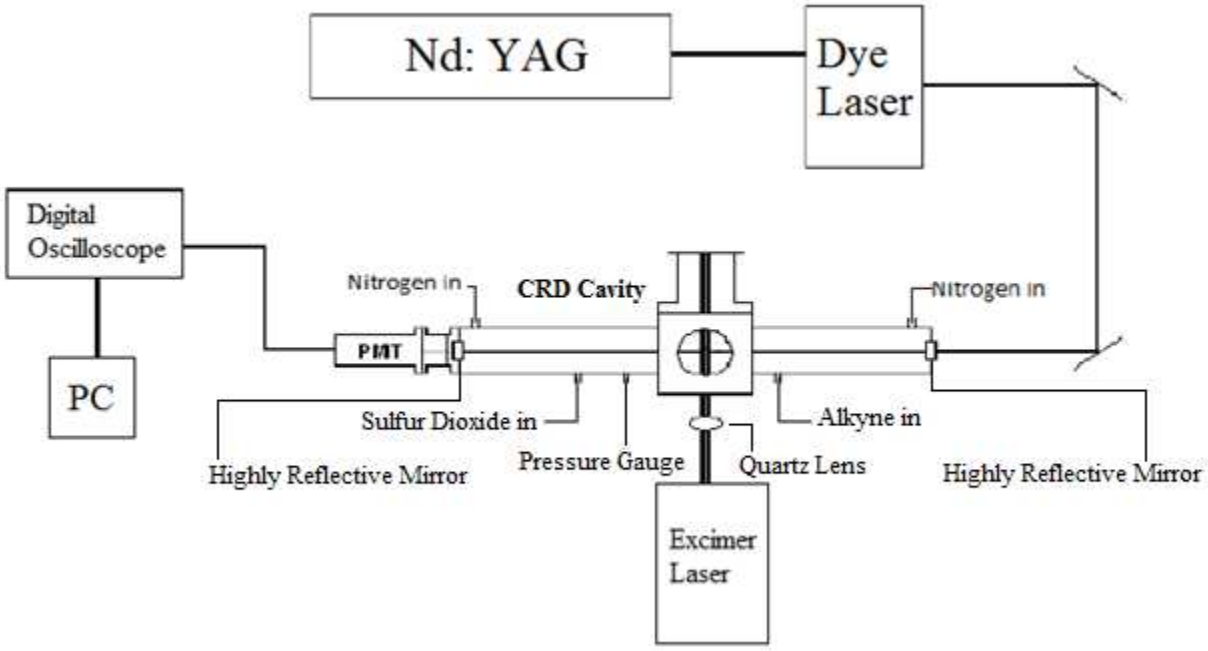

Figure 7. Diagram of the CRDLAS experimental setup.

www.manaraa.com

Reactions were probed using a Nd:YAG laser (Continuum Surelite II, operating at 1064 nm) which passed through a tunable pumped dye laser (Continuum ND6000). The YAG/dye laser setup fired at a frequency of 2 Hz and at a power of 5-10 mJ. The dye used for the dye pump was rhodamine 640, providing a wavelength range of 605-630 nm with a peak wavelength of 613 nm. One end of the stainless steel cavity featured a photomultiplier tube (PMT) for detection of light decay. This detector was then connected to a digital oscilloscope (PicoScope 2207A, Pico Technologies) which was connected to a PC with a USB adapter to record the ringdown data. Typical ringdown times ranged from 30-70 μs.

CRDLAS is a modification of a technique known as Cavity Attenuated Phase Shift (CAPS), which was developed initially to quantify the reflectivity of mirrors. CAPS uses continuous wave laser light to measure the phase shift between the input and output light in the cavity.[31] However, this technique was limited in its sensitivity due to fluctuations in the phase angle. CRDLAS differs from CAPS in that the modulated light entering the cavity is pulsed, as opposed to continuous. Instead of measuring the phase shift angle, CRDLAS relies on the time it takes for the light intensity to decay after a given pulse. The intensity decay observed in a CRDLAS experiment can be expressed as a first-order relationship between the initial intensity of modulated light and intensity decay as a function of time, equation (6).

$$I(t) = I_0 e^{-t/\tau} \qquad (6)$$

Here, $I(t)$ is the intensity at time t, I_0 is the initial intensity, and τ is the ringdown time. The ringdown time, τ, is defined as the amount of time it takes for the light to exponentially decay inside the cavity and is hastened by the presence of a chemical species that absorbs light at

www.manaraa.com

a wavelength that is within the scan-range of the spectrometer. According to the Beer-Lambert Law, absorption (A) equals the concentration of analyte (c) times the molar absorptivity (ε) and path length (l), equation (7).

$$A = \varepsilon l c \qquad (7)$$

CRDLAS allows for the detection of minute product concentrations (~10 ppb) by compensating with a large path length. The highly reflective mirrors allow the probe light to reflect back and forth within the cavity, resulting in an effective path length of ~20 km.

The generation of O(^{3}P) atoms was achieved via photolysis of SO_2 at 193 nm, shown in equation (8), using an Ar/F Excimer Laser (Lambda Physik Compex 110), operating at a frequency of 2 Hz and a power of 94-114 mJ.

$$SO_2 + hv(193\ nm) \rightarrow SO\left(A\ ^3\Pi\right) + O(\ ^3P) \qquad (8)$$

The scan range chosen for probing HCO radical was 613-617 nm. HCO radical also shows absorption in the UV range at 230 nm for its ground to second excited state transition (B ← X), however, the precursor for O(^{3}P) (SO_2) absorbs strongly in the UV region and so 613-617 nm was chosen as the region to look for HCO radical formation as the P and R bands (band origins at 614.4 nm and 613.8 nm, respectively) are found in that region for the formyl radical $\tilde{A}^2A''(0,9,0) \leftarrow \tilde{X}^2A'(0,0,0)$ transition.

Nitrogen gas was flowed through the cavity in addition to SO_2 and the alkyne of interest. The N_2 acted as a vibrational relaxant for HCO radical as well as a barrier to protect the mirrors

www.manaraa.com

against build-up of contaminants during an experiment. Typical pressures were about 4 torr with a reagent gas ratio of 1:1:2 (N_2:SO_2:alkyne) and were monitored using a digital barometer. The statistical program language, R, was utilized to process the ringdown time data (exponential decay time *vs.* wavelength) into an absorption spectrum (absorption *vs.* wavelength).[32] Experimental studies were conducted on propyne, butyne, pentyne, and propargyl alcohol (Aldrich, 99%). CRDLAS results are presented and discussed in chapter IV.

www.manaraa.com

CHAPTER III

COMPUTATIONAL METHODS

Quantum mechanical methods were employed to gain insight into the mechanisms at play within the alkyne + O(^{3}P) reactions of interest. Previous work by Buettner[28] revealed varying degrees of signal intensity for the absorption spectrum of HCO radical without plausible explanation for the observed intensity variation across alkyne species. Computational methods were utilized to search for reaction pathways to help explain the higher intensity HCO radical absorption observed for the reaction of O(^{3}P) with hydroxyl-substituted alkynes (propargyl alcohol and 3-butyn-1-ol). Both the triplet and singlet potential energy surfaces of the O(^{3}P) + propargyl alcohol and O(^{3}P) + 3-butyn-1-ol reactions were investigated and are presented here. While formyl radical production is only observed on the triplet potential energy surface of these reactions, the singlet surface is easily accessible via ISC and is, thus, relevant to this study.

Theoretical investigations were carried out using the Gaussian 09 software package.[33] Calculations were performed at the M06-2x/cc-pVTZ level of theory, a DFT-based functional that has proven to yield energy values comparable to higher levels of theory without the computational cost.[29] Previous work in the Quandt and Standard groups have employed the MP2(Full) method with a 6-311++G(d,p) basis set for geometry optimizations.[28,29] When MP2 potential energy values were compared to CCSD(T) single-point energy values, it was observed that MP2 consistently predicted higher energy barriers due to the shorter estimation of bond lengths. To acquire more reliable geometries with low resource cost, the M06-2x functional was adopted as it yielded potential energy values that were more comparable to the values found at the highly reliable CCSD(T)/cc-pVTZ level. The computational methods discussed here have been performed for the reactions of O(^{3}P) with propargyl alcohol and 3-butyn-1-ol.

www.manaraa.com

Once optimized geometries, vibrational frequencies, and potential energies are obtained at the M06-2x/cc-pVTZ level of theory, a higher level of theory may be employed to obtain more accurate potential energy values. The coupled cluster method, CCSD(T)/cc-pVTZ, was utilized to conduct single-point energy calculations on the optimized M06-2x/cc-pVTZ structures.

The collected vibrational frequency data was utilized to identify structures as either intermediates (IM) or transition states (TS). TS structures exist at the saddle point of the potential energy surface of a reaction and have imaginary values for the frequency that describes the transition, such as a hydrogen shift or a dissociation. IM structures exist at local minima on the potential energy surface and have all positive, real values for their vibrational frequencies. Intrinsic reaction coordinate (IRC) calculations were carried out on most TS structures to verify that a given TS connected two IM structures along the reaction coordinate. The output file for an IRC may show 100 or more structures that connect a TS structure to its corresponding precursor and product IM structures.

Minimum energy crossing point (MECP) calculations have also been performed for the propargyl alcohol/3-butyn-1-ol + O(^{3}P) reactions to reveal where intersystem crossing (ISC) occurs within the reaction pathway.[34,35] ISC is the phenomenon by which a reaction crosses from the triplet surface to the singlet surface or vice versa. Typically, ISC can be thought of as a seam on the three dimensional potential energy surface of the reaction. The MECP calculation will find the lowest energy point on the ISC seam and provides the point within the reaction pathway and the geometric parameters for which crossing may occur.

Finally, a Natural Resonance Theory (NRT) analysis was carried out on the reactions discussed in this project. NRT is a method developed by Frank Weinhold of University of Wisconsin-Madison[36-40] and provides two key pieces of information that are crucial for

www.manaraa.com

understanding the reaction mechanisms at play: natural spin density (NSD) and natural bond order (NBO). NSD reveals the movement of the unpaired electrons on the triplet potential energy surface as the reaction progresses and confirms that the dissociated HCO/HOC molecules have a total NSD of 1, indicating a radical species. NBO provides bond order information throughout the progression of the reaction and confirms bond breakage during the dissociation steps of the reaction mechanism. For example, the C1-C2 bond order drops to zero in the established pathway when HCO radical dissociates.

www.manaraa.com

CHAPTER IV

RESULTS

Experimental Detection of HCO in the Reaction of $O(^3P)$ + Propargyl Alcohol

The raw data collected via CRDLAS indicates the amount of time it takes for the light of a single laser pulse to decay within the cavity and is known as the ring-down time. The Nd:YAG laser fires at a frequency of 2 Hz through the dye pump laser, which varies the wavelength by approximately 0.002 nm every pulse. The lasers must pulse ~1500 times for a given run to generate a single absorption spectrum for HCO radical. The statistical language program, R, is used to convert ring-down times to absorbance intensities, which is then plotted as a function of wavelength. Figure 8 shows an example of raw, ring-down data collected via CRDLAS for the reaction of $O(^3P)$ + propargyl alcohol.

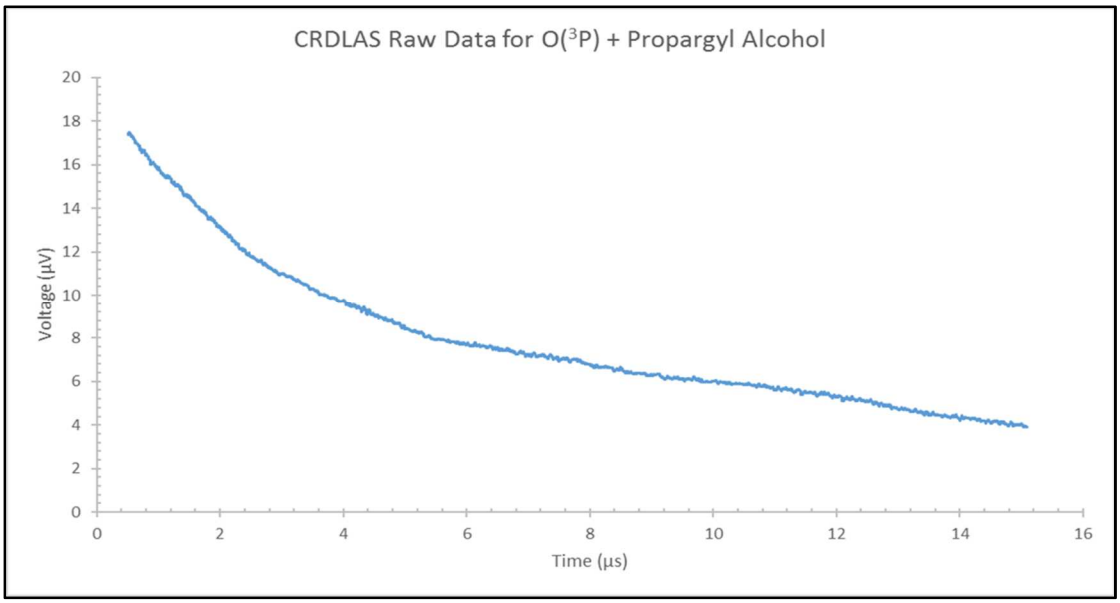

Figure 8. Example for 1 of 1536 data points from a single 613-617 nm scan (ring-down time: ~15 µs).

www.manaraa.com

HCO radical formation was confirmed for the reaction of O(^{3}P) + propargyl alcohol via CRDLAS and its absorption spectrum is shown in Figure 9. The $\tilde{A}\,^2A''(0,9,0) \leftarrow \tilde{X}\,^2A'(0,0,0)$ transition of HCO radical was observed in the 613-617 nm range with R and P branch origins at 614.06 nm and 614.74 nm, respectively. While ground state HCO radical has a bent geometry, the first excited state of HCO radical takes on a linear conformation, resulting in the observed P and R branches. The collected spectrum for HCO radical is in good agreement with Buettner's studies and the literature,[26] confirming the collected spectrum as a signature of HCO radical.

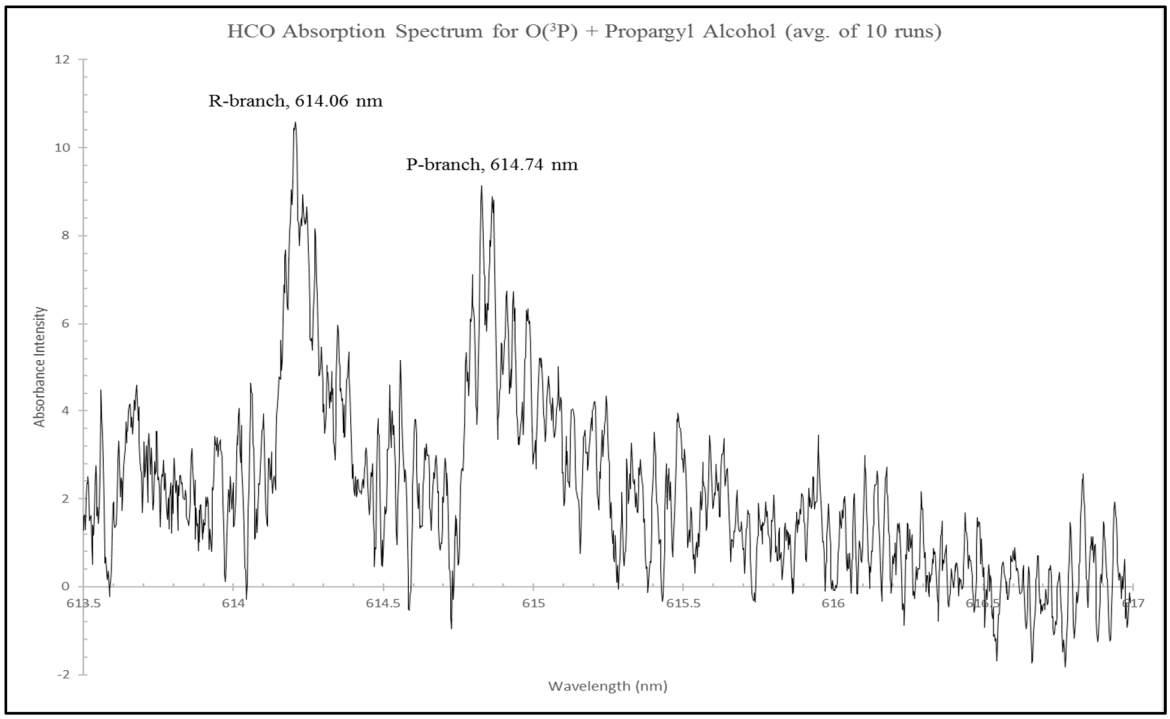

Figure 9. Absorption spectrum for HCO in the reaction of O(^{3}P) + propargyl alcohol. This spectrum is an average of 10 individual runs.

www.manaraa.com

HCO radical absorption spectra were collected for other O(^{3}P) + alkyne reactions as well to illustrate the varying degrees of intensity observed across different species. During data collection for this project, the O(^{3}P) + butyne and O(^{3}P) + pentyne reactions were also probed for HCO radical formation and the resultant spectra are shown in Figures 10 and 11. As seen in Figure 11, the S/N ratio is too great to confirm the formation of HCO radical in the reaction of O(^{3}P) + pentyne and further experimentation and/or computation is desirable to explain the buried P and R branches in the spectrum.

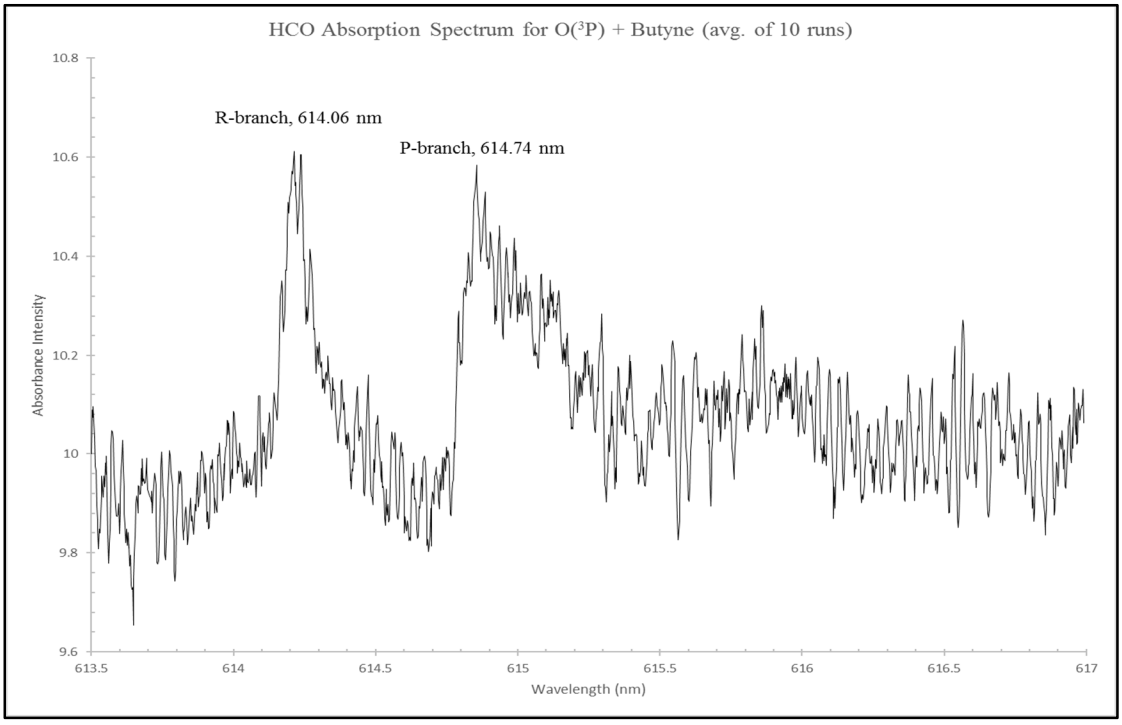

Figure 10. Absorption spectrum for HCO in the reaction of O(^{3}P) + butyne. This spectrum is an average of 10 individual runs.

www.manaraa.com

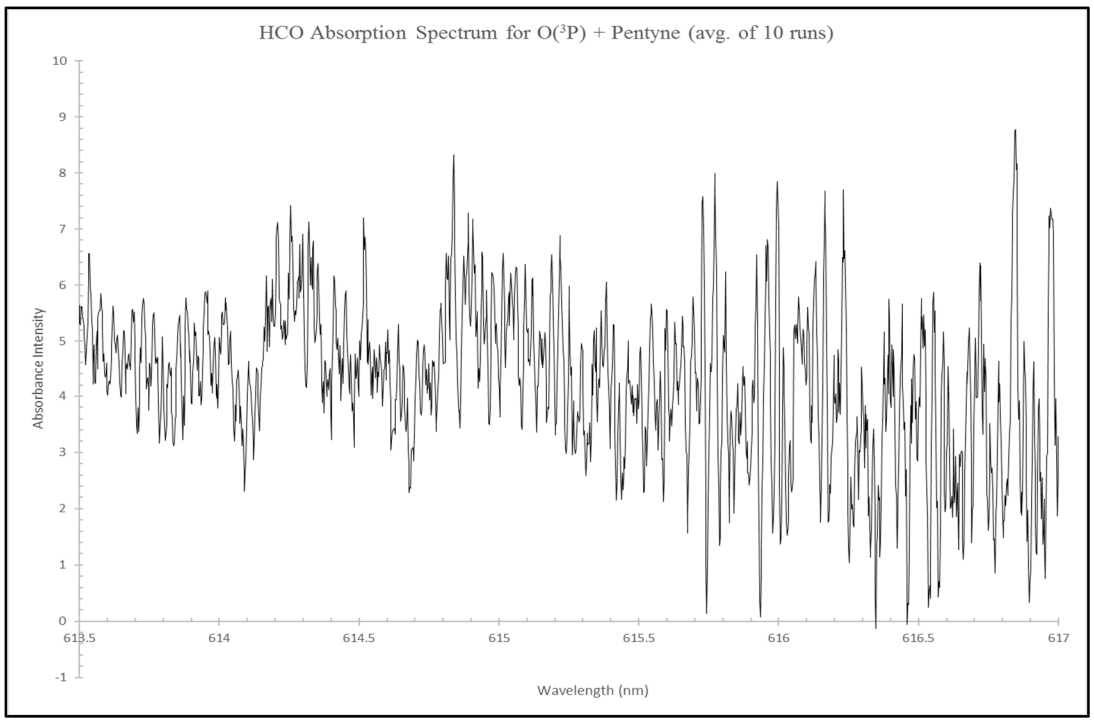

Figure 11. Absorption spectrum for HCO in the reaction of $O(^3P)$ + pentyne. This spectrum is an average of 10 individual runs.

www.manaraa.com

As seen in Figures 9-11, the intensity of HCO radical absorption varies greatly. These variations also were observed in the studies conducted by Buettner and are shown in Figures 12 and 13.

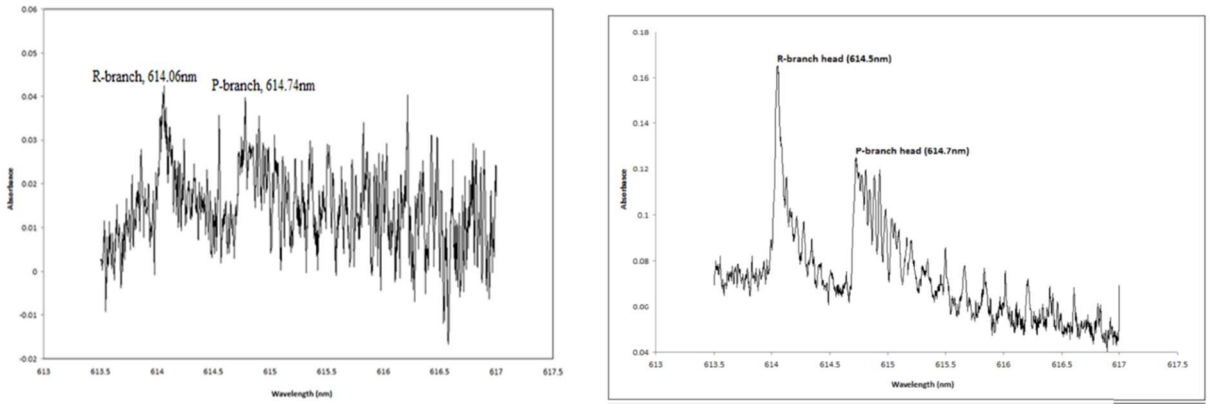

Figure 12. Comparison of absorption spectra for HCO in the reaction of $O(^3P)$ + propyne (left) and $O(^3P)$ + propargyl alcohol (right). Left spectrum is an average of 15 individual runs and the right spectrum is an average of 8 individual runs.[28]

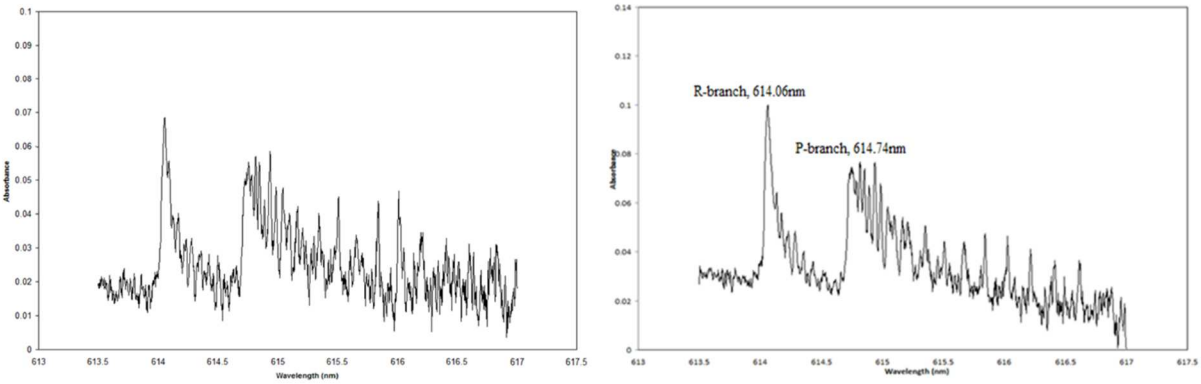

Figure 13. Comparison of absorption spectra for HCO in the reaction of $O(^3P)$ + butyne (left) and $O(^3P)$ + 3-butyn-1-ol (right). Left spectrum is an average of 10 individual spectra and the right spectrum is an average of 10 individual runs.[28]

www.manaraa.com

Hydroxyl-substituted alkynes, when reacted with $O(^3P)$, produced the strongest absorption signals for HCO radical. The difference in HCO radical absorption intensity observed between $O(^3P)$ + propyne and $O(^3P)$ + propargyl alcohol, shown in Figure 12, is worth further discussion. The HCO radical spectrum for $O(^3P)$ + propyne was generated by averaging 15 individual runs together, while the HCO radical spectrum for $O(^3P)$ + propargyl alcohol is an average of just 8 individual runs. Despite holding the reagent gas ratios constant between each experimental run, the collected spectra for $O(^3P)$ + propargyl alcohol consistently showed the highest absorption intensity. While it is difficult to quantify the HCO radical product in these reactions, there seems to be a clear, observable difference in the concentration of HCO radical produced between propyne and propargyl alcohol. Up to this point, no plausible explanation for the variations of HCO radical absorption (shown above) has been proposed.

Computational Results for $O(^3P)$ + Propargyl Alcohol

While the results from the computational investigation of the singlet potential energy surface are reported here, only the results from the triplet potential energy surface will be thoroughly discussed as HCO radical is only formed on the triplet surface. The numbering system for $O(^3P)$ + propargyl alcohol reaction is shown in Figure 14.

www.manaraa.com

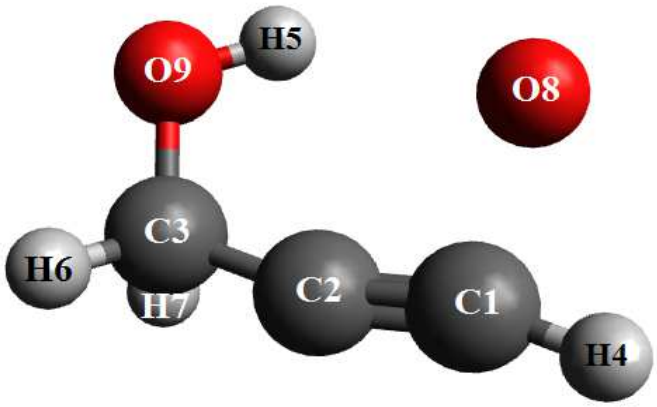

Figure 14. Numbering scheme for the O(^{3}P) + propargyl alcohol reaction.

Geometries: O(^{3}P) + Propargyl Alcohol

Relevant bond lengths and angles for each IM and TS on the O(^{3}P) + propargyl alcohol triplet and singlet potential energy surfaces have been tabulated and are presented in tables 1-3. All geometries reported here are at the M06-2x/cc-pVTZ and MP2/6-311++G(d,p) levels of theory. Bond lengths agreed well across all optimized M06-2x and MP2 structures on both the triplet and singlet potential energy surfaces, with a maximum difference of just 0.085 Å. In general, there is good agreement between the M06-2x and MP2 bond angles with only a few deviations worth noting. First, the optimized structures for IM-5T show a difference of 8.7° between the M06-2x and MP2 results for the C1-C2-C3 bond angle. Larger geometric deviations are observed on the singlet surface for a few species. TS-2S shows a 16.2° difference between the M06-2x and MP2 structures for the C1-C2-C3 bond angle and a 15.4° difference for the C2-C1-O8 bond angle. In addition, TS-8S shows a 9° difference between M06-2x and MP2 for the C1-C2-C3 bond angle and an 18.9° difference for the C2-C1-O8 bond angle.

www.manaraa.com

Table 1. Selected bond lengths and angles for structures on the triplet potential energy surface of $O(^3P)$ + propargyl alcohol, calculated at the M06-2x/cc-pVTZ and MP2/6-311++G(d,p) levels of theory. The difference between the two levels, Δ, is also reported. The numbering scheme is shown in Figure 14.

Species	Level/Basis Set	C1-H4 (Å)	C1-C2 (Å)	C2-C3 (Å)	C1-O8 (Å)	C3-O9 (Å)	O9-H5 (Å)	<C1-C2-C3 (°)	<C2-C1-O8 (°)	<H4-C1-O8 (°)	<C2-C3-O9 (°)	<C3-O9-H5 (°)
CHCCH2OH	M06-2x/cc-pVTZ	1.062	1.197	1.466	-	1.412	0.960	178.000	-	-	113.000	108.300
	MP2/6-311++G(d,p)	1.065	1.218	1.466	-	1.422	0.961	179.700	-	-	112.800	107.000
	Δ	0.003	0.021	0.000	-	0.010	0.001	1.700	-	-	-0.200	-1.300
TS-1T	M06-2x/cc-pVTZ	1.064	1.218	1.464	1.972	1.408	0.965	164.100	95.600	101.200	111.300	107.600
	MP2/6-311++G(d,p)	1.066	1.211	1.463	1.847	1.416	0.965	165.500	98.400	101.300	111.600	106.500
	Δ	0.002	-0.007	-0.001	-0.125	0.008	0.000	1.400	2.800	0.100	0.300	-1.100
IM-1T	M06-2x/cc-pVTZ	1.097	1.416	1.477	1.232	1.408	0.966	129.700	120.700	120.800	112.100	107.500
	MP2/6-311++G(d,p)	1.105	1.461	1.480	1.199	1.417	0.966	125.700	120.900	122.400	111.200	105.900
	Δ	0.008	0.045	0.003	-0.033	0.009	0.000	-4.000	0.200	1.600	-0.900	-1.600
TS-2T	M06-2x/cc-pVTZ	1.098	1.422	1.433	1.230	1.357	0.962	138.700	121.400	122.000	120.000	109.600
	MP2/6-311++G(d,p)	1.109	1.457	1.445	1.198	1.366	0.963	138.500	124.300	122.700	118.900	107.900
	Δ	0.011	0.035	0.012	-0.032	0.009	0.001	-0.200	2.900	0.700	-1.100	-1.700
IM-2T	M06-2x/cc-pVTZ	1.103	1.442	1.461	1.219	1.364	0.961	121.300	123.000	120.600	114.400	109.600
	MP2/6-311++G(d,p)	1.112	1.481	1.465	1.190	1.370	0.962	120.800	124.100	121.800	113.500	108.400
	Δ	0.009	0.039	0.004	-0.029	0.006	0.001	-0.500	1.100	1.200	-0.900	-1.200
TS-3T	M06-2x/cc-pVTZ	-	1.378	1.500	1.212	1.405	0.964	132.100	135.700	-	111.400	109.400
	MP2/6-311++G(d,p)	-	1.393	1.508	1.201	1.413	0.964	130.600	138.500	-	110.600	108.000
	Δ	-	0.015	0.008	-0.011	0.008	0.000	-1.500	2.800	-	-0.800	-1.400
IM-3T	M06-2x/cc-pVTZ	-	1.435	1.492	1.194	1.397	0.964	123.200	128.300	-	115.800	109.300
	MP2/6-311++G(d,p)	-	1.461	1.502	1.196	1.413	0.963	120.700	127.300	-	113.700	107.300
	Δ	-	0.026	0.010	0.002	0.016	-0.001	-2.500	-1.000	-	-2.100	-2.000
TS-4T	M06-2x/cc-pVTZ	1.115	-	1.329	1.180	1.364	0.961	-	-	125.500	122.000	109.700
	MP2/6-311++G(d,p)	1.116	-	1.327	1.199	1.354	0.962	-	-	125.800	121.900	108.700
	Δ	0.001	-	-0.002	0.019	-0.010	0.001	-	-	0.300	-0.100	-1.000
TS-5T	M06-2x/cc-pVTZ	-	-	1.467	1.133	1.423	0.960	-	-	-	109.100	108.600
	MP2/6-311++G(d,p)	-	-	1.477	1.148	1.431	0.961	-	-	-	108.700	107.000
	Δ	-	-	0.010	0.015	0.008	0.001	-	-	-	-0.400	-1.600
TS-6T	M06-2x/cc-pVTZ	-	1.444	1.392	1.228	1.327	0.978	121.000	127.200	-	123.000	109.100
	MP2/6-311++G(d,p)	-	1.529	1.335	1.217	1.326	0.978	119.000	123.000	-	126.900	107.300
	Δ	-	0.085	-0.057	-0.011	-0.001	0.000	-2.000	-4.200	-	3.900	-1.800
IM-4T	M06-2x/cc-pVTZ	-	1.518	1.491	1.173	1.360	0.960	114.100	128.000	-	113.300	110.100
	MP2/6-311++G(d,p)	-	1.521	1.495	1.185	1.367	0.961	114.500	128.300	-	112.800	108.700
	Δ	-	0.003	0.004	0.012	0.007	0.001	0.400	0.300	-	-0.500	-1.400
TS-7T	M06-2x/cc-pVTZ	-	-	1.464	1.136	1.369	0.960	-	-	-	116.200	109.600
	MP2/6-311++G(d,p)	-	-	1.468	1.150	1.376	0.962	-	-	-	114.200	108.100
	Δ	-	-	0.004	0.014	0.007	0.002	-	-	-	-2.000	-1.500
TS-8T	M06-2x/cc-pVTZ	1.085	1.373	1.500	1.307	1.362	-	123.400	122.600	115.100	99.000	-
	MP2/6-311++G(d,p)	Did not converge										
	Δ	-										
IM-5T	M06-2x/cc-pVTZ	1.083	1.322	1.483	1.355	1.386	-	130.000	124.800	112.300	103.400	-
	MP2/6-311++G(d,p)	1.085	1.296	1.479	1.364	1.389	-	138.700	128.500	110.300	106.200	-
	Δ	0.002	-0.026	-0.004	0.009	0.003	-	8.700	3.700	-2.000	2.800	-
TS-9T	M06-2x/cc-pVTZ	1.081	1.375	1.450	1.320	1.275	-	124.300	117.400	116.400	117.400	-
	MP2/6-311++G(d,p)	1.083	1.381	1.460	1.325	1.280	-	124.200	120.000	116.100	117.400	-
	Δ	0.002	0.006	0.010	0.005	0.005	-	-0.100	2.600	-0.300	0.000	-
IM-6T	M06-2x/cc-pVTZ	1.076	1.462	1.404	1.329	1.267	-	123.500	119.700	117.000	121.000	-
	MP2/6-311++G(d,p)	1.082	1.484	1.464	1.363	1.201	-	118.600	114.500	113.500	122.200	-
	Δ	0.006	0.022	0.060	0.034	-0.066	-	-4.900	-5.200	-3.500	1.200	-

www.manaraa.com

Table 2. Continued bond lengths and angles for structures on the triplet potential energy surface of $O(^3P)$ + propargyl alcohol, calculated at the M06-2x/cc-pVTZ and MP2/6-311++G(d,p) levels of theory. The difference between the two levels, Δ, is also reported. The numbering scheme is shown in Figure 14.

Species	Level/Basis Set	C1-H4 (Å)	C1-C2 (Å)	C2-C3 (Å)	C1-O8 (Å)	C3-O9 (Å)	O9-H5 (Å)	<C1-C2-C3 (°)	<C2-C1-O8 (°)	<H4-C1-O8 (°)	<C2-C3-O9 (°)	<C3-O9-H5 (°)
TS-10T	M06-2x/cc-pVTZ	1.089	1.315	-	1.342	1.190	-	-	128.500	111.900	-	-
	MP2/6-311++G(d,p)	1.092	1.307	-	1.336	1.202	-	-	129.600	111.800	-	-
	Δ	0.003	-0.008	-	-0.006	0.012	-	-	1.100	-0.100	-	-
TS-11T	M06-2x/cc-pVTZ	1.102	1.444	1.458	1.219	1.335	0.964	120.700	123.500	121.600	125.500	111.200
	MP2/6-311++G(d,p)	1.111	1.462	1.459	1.206	1.342	0.964	119.900	124.800	122.200	125.400	109.200
	Δ	0.009	0.018	0.001	-0.013	0.007	0.000	-0.800	1.300	0.600	-0.100	-2.000
IM-7T	M06-2x/cc-pVTZ	1.106	1.506	1.478	1.197	1.338	0.965	112.900	124.500	120.900	124.200	111.300
	MP2/6-311++G(d,p)	1.109	1.510	1.488	1.211	1.349	0.964	113.600	125.100	120.900	122.800	109.300
	Δ	0.003	0.004	0.010	0.014	0.011	-0.001	0.700	0.600	0.000	-1.400	-2.000
TS-12T	M06-2x/cc-pVTZ	1.100	1.441	-	1.223	1.270	0.985	-	123.300	120.300	-	113.000
	MP2/6-311++G(d,p)	1.108	1.469	-	1.205	1.273	0.986	-	124.400	121.200	-	110.100
	Δ	0.008	0.028	-	-0.018	0.003	0.001	-	1.100	0.900	-	-2.900
TS-13T	M06-2x/cc-pVTZ	-	1.471	1.495	1.265	1.260	-	110.500	121.300	-	120.000	-
	MP2/6-311++G(d,p)	Did not converge.										
	Δ	-										
IM-8T	M06-2x/cc-pVTZ	-	1.478	1.514	1.331	1.201	-	111.800	124.000	-	123.900	-
	MP2/6-311++G(d,p)	-	1.489	1.517	1.340	1.214	-	112.200	123.600	-	124.100	-
	Δ	-	0.011	0.003	0.009	0.013	-	0.400	-0.400	-	0.200	-
TS-14T	M06-2x/cc-pVTZ	-	-	1.441	1.270	1.223	-	-	-	-	123.300	-
	MP2/6-311++G(d,p)	-	-	1.469	1.273	1.205	-	-	-	-	124.400	-
	Δ	-	-	0.028	0.003	-0.018	-	-	-	-	1.100	-
TS-15T	M06-2x/cc-pVTZ	-	1.341	-	1.305	1.194	-	-	130.100	-	-	-
	MP2/6-311++G(d,p)	-	1.339	-	1.285	1.222	-	-	129.900	-	-	-
	Δ	-	-0.002	-	-0.020	0.028	-	-	-0.200	-	-	-
TS-16T	M06-2x/cc-pVTZ	-	1.497	1.533	1.261	1.335	0.965	109.200	110.900	-	121.500	111.400
	MP2/6-311++G(d,p)	Did not converge.										
	Δ	-										
IM-9T	M06-2x/cc-pVTZ	-	1.528	1.489	1.289	1.339	0.965	117.700	111.900	-	123.700	111.300
	MP2/6-311++G(d,p)	-	1.535	1.497	1.298	1.348	0.964	116.700	111.600	-	122.500	109.500
	Δ	-	0.007	0.008	0.009	0.009	-0.001	-1.000	-0.300	-	-1.200	-1.800
TS-17T-a	M06-2x/cc-pVTZ	-	-	1.357	1.250	1.345	0.964	-	-	-	127.700	110.100
	MP2/6-311++G(d,p)	-	-	1.347	1.258	1.351	0.964	-	-	-	127.700	108.400
	Δ	-	-	-0.010	0.008	0.006	0.000	-	-	-	0.000	-1.700
TS-17T-b	M06-2x/cc-pVTZ	-	1.361	-	1.269	1.285	0.972	-	126.800	-	-	113.300
	MP2/6-311++G(d,p)	-	1.348	-	1.273	1.281	0.974	-	128.900	-	-	111.400
	Δ	-	-0.013	-	0.004	-0.004	0.002	-	2.100	-	-	-1.900
TS-18T	M06-2x/cc-pVTZ	1.095	1.480	1.350	1.253	1.347	0.960	130.200	118.900	123.200	121.400	109.900
	MP2/6-311++G(d,p)	Did not converge.										
	Δ	-										
IM-10T	M06-2x/cc-pVTZ	1.102	1.477	1.308	1.374	1.364	0.959	134.900	114.300	107.100	123.600	109.200
	MP2/6-311++G(d,p)	1.100	1.480	1.291	1.388	1.368	0.959	137.000	113.800	106.800	124.500	108.000
	Δ	-0.002	0.003	-0.017	0.014	0.004	0.000	2.100	-0.500	-0.300	0.900	-1.200
TS-19T	M06-2x/cc-pVTZ	1.103	1.497	1.331	1.373	1.344	0.961	126.600	117.500	111.700	125.900	108.200
	MP2/6-311++G(d,p)	1.103	1.496	1.331	1.383	1.358	0.961	131.600	116.200	111.700	123.700	106.100
	Δ	0.000	-0.001	0.000	0.010	0.014	0.000	5.000	-1.300	0.000	-2.200	-2.100
IM-11T	M06-2x/cc-pVTZ	1.104	1.502	1.313	1.361	1.329	0.963	122.700	116.400	107.200	130.600	110.100
	MP2/6-311++G(d,p)	1.103	1.504	1.298	1.373	1.328	0.963	123.800	116.000	108.000	131.700	108.500
	Δ	-0.001	0.002	-0.015	0.012	-0.001	0.000	1.100	-0.400	0.800	1.100	-1.600
TS-20T	M06-2x/cc-pVTZ	1.101	-	1.311	1.215	1.327	0.965	-	-	121.400	128.600	109.900
	MP2/6-311++G(d,p)	1.109	-	1.327	1.205	1.329	0.965	-	-	121.900	128.100	108.300
	Δ	0.008	-	0.016	-0.010	0.002	0.000	-	-	0.500	-0.500	-1.600

www.manaraa.com

Table 3. Selected bond lengths and angles for structures on the singlet potential energy surface of $O(^3P)$ + propargyl alcohol, calculated at the M06-2x/cc-pVTZ and MP2/6-311++G(d,p) levels of theory. The difference between the two levels, Δ, is also reported. The numbering scheme is shown in Figure 14.

Species	Level/Basis Set	C1-H4 (Å)	C1-C2 (Å)	C2-C3 (Å)	C1-O8 (Å)	C3-O9 (Å)	O9-H5 (Å)	<C1-C2-C3 (°)	<C2-C1-O8 (°)	<H4-C1-O8 (°)	<C2-C3-O9 (°)	<C3-O9-H5 (°)
CHCCH2OH	M06-2x/cc-pVTZ	1.062	1.197	1.466	-	1.412	0.960	178.000	-	-	113.000	108.300
	MP2/6-311++G(d,p)	1.065	1.218	1.466	-	1.422	0.961	179.700	-	-	112.800	107.000
	Δ	0.003	0.021	0.000	-	0.010	0.001	1.700	-	-	-0.200	-1.300
IM-1S	M06-2x/cc-pVTZ	1.101	1.423	1.448	1.223	1.404	0.964	117.700	115.000	123.300	120.100	108.100
	MP2/6-311++G(d,p)	1.103	1.433	1.451	1.237	1.414	0.963	117.200	113.800	123.600	120.800	107.000
	Δ	0.002	0.010	0.003	0.014	0.010	-0.001	-0.500	-1.200	0.300	0.700	-1.100
TS-2S	M06-2x/cc-pVTZ	1.098	1.422	1.433	1.230	1.357	0.962	138.700	121.400	122.000	120.000	109.600
	MP2/6-311++G(d,p)	1.139	1.411	1.447	1.220	1.411	0.962	122.500	136.800	122.500	122.400	108.800
	Δ	0.041	-0.011	0.014	-0.010	0.054	0.000	-16.200	15.400	0.500	2.400	-0.800
IM-2S	M06-2x/cc-pVTZ	1.100	1.439	1.355	1.228	1.314	0.993	119.100	123.600	118.900	124.400	106.500
	MP2/6-311++G(d,p)	1.102	1.443	1.366	1.241	1.323	0.992	119.400	123.300	119.100	124.200	105.200
	Δ	0.002	0.004	0.011	0.013	0.009	-0.001	0.300	-0.300	0.200	-0.200	-1.300
TS-3S	M06-2x/cc-pVTZ	1.141	1.398	1.428	1.205	1.394	0.963	120.800	140.000	122.500	123.700	109.700
	MP2/6-311++G(d,p)	1.152	1.401	1.434	1.216	1.401	0.963	120.400	142.400	123.400	124.200	108.500
	Δ	0.011	0.003	0.006	0.011	0.007	0.000	-0.400	2.400	0.900	0.500	-1.200
IM-3S	M06-2x/cc-pVTZ	-	1.311	1.508	1.154	1.414	0.960	121.400	178.800	-	114.200	108.700
	MP2/6-311++G(d,p)	-	1.326	1.506	1.166	1.426	0.961	121.000	178.600	-	114.200	106.800
	Δ	-	0.015	-0.002	0.012	0.012	0.001	-0.400	-0.200	-	0.000	-1.900
TS-6S	M06-2x/cc-pVTZ	-	-	1.405	1.126	1.384	0.961	-	-	-	123.000	109.900
	MP2/6-311++G(d,p)	-	-	1.424	1.140	1.388	0.966	-	-	-	119.600	105.400
	Δ	-	-	0.019	0.014	0.004	0.005	-	-	-	-3.400	-4.500
TS-8S	M06-2x/cc-pVTZ	-	1.400	1.428	1.163	1.377	0.961	107.400	160.900	-	117.700	110.500
	MP2/6-311++G(d,p)	-	1.448	1.424	1.194	1.365	0.962	116.400	142.000	-	117.900	109.100
	Δ	-	0.048	-0.004	0.031	-0.012	0.001	9.000	-18.900	-	0.200	-1.400
TS-19S	M06-2x/cc-pVTZ	1.147	1.389	1.433	1.202	1.392	0.963	122.600	141.500	122.600	118.800	107.900
	MP2/6-311++G(d,p)	Did not converge.										
	Δ	-										
TS-10S	M06-2x/cc-pVTZ	-	-	1.235	1.137	1.319	0.962	-	-	-	153.500	110.900
	MP2/6-311++G(d,p)	-	-	1.257	1.155	1.324	0.963	-	-	-	154.700	109.500
	Δ	-	-	0.022	0.018	0.005	0.001	-	-	-	1.200	-1.400
TS-11S	M06-2x/cc-pVTZ	-	1.436	1.480	1.159	1.397	0.960	87.500	167.600	-	115.500	108.400
	MP2/6-311++G(d,p)	-	1.426	1.498	1.177	1.407	0.960	85.800	174.100	-	115.000	106.700
	Δ	-	-0.010	0.018	0.018	0.010	0.000	-1.700	6.500	-	-0.500	-1.700

www.manaraa.com

Potential Energy Profiles: O(^{3}P) + Propargyl Alcohol

All potential energies presented in this section are referenced relative to the reactants of the reaction, propargyl alcohol and O(^{3}P). Computational work by Buettner has explored the potential energy profiles (PEPs) for the reactions of various alkynes and substituted alkynes with O(^{3}P) at the MP2/6-311++G(d,p) level of theory.[28] Dilday's investigation of O(^{3}P) + propyne demonstrated that the M06-2x functional provides relative energies closer to the CCSD(T) single point results than does MP2.[29] Triplet surface relative energies at the MP2(Full), M06-2x, and CCSD(T) single point levels of theory are reported in tables 1-5, which confirms the previous observations that M06-2x energies agree better with CCSD(T) single-point energies than does MP2. For this reason, all single-point energy calculations at the CCSD(T)/cc-pVTZ level of theory were carried out on the M06-2x/cc-pVTZ optimized geometries. All energies reported in this thesis are corrected for vibrational zero-point energies unless stated otherwise.

www.manaraa.com

Table 4. Relative energies for structures on the triplet potential energy surface, computed using the M06-2x, MP2, and CCSD(T)//M06-2x single point methods. Relative energy differences, Δ, for M06-2x and MP2 results compared to CCSD(T) single-point results are also shown.

Species	Level of Theory	Rel. E (kJ/mol)
TS-1T	M06-2x	-7.25
	MP2(Full)	77.41
	CCSD(T) Single Point	10.40
	Δ : M06-2x - CCSD(T)	-17.65
	Δ : MP2(Full) - CCSD(T)	67.02
IM-1T	M06-2x	-248.96
	MP2(Full)	-187.50
	CCSD(T) Single Point	-220.27
	Δ : M06-2x - CCSD(T)	-28.69
	Δ : MP2(Full) - CCSD(T)	32.77
TS-2T	M06-2x	-63.33
	MP2(Full)	9.66
	CCSD(T) Single Point	-30.60
	Δ : M06-2x - CCSD(T)	-32.73
	Δ : MP2(Full) - CCSD(T)	40.25
IM-2T	M06-2x	-278.32
	MP2(Full)	-222.21
	CCSD(T) Single Point	-255.02
	Δ : M06-2x - CCSD(T)	-23.29
	Δ : MP2(Full) - CCSD(T)	32.81
TS-3T	M06-2x	-60.58
	MP2(Full)	-154.84
	CCSD(T) Single Point	-35.52
	Δ : M06-2x - CCSD(T)	-25.06
	Δ : MP2(Full) - CCSD(T)	-119.32
IM-3T	M06-2x	-309.97
	MP2(Full)	-280.51
	CCSD(T) Single Point	-288.26
	Δ : M06-2x - CCSD(T)	-21.71
	Δ : MP2(Full) - CCSD(T)	7.75
TS-4T	M06-2x	-93.85
	MP2(Full)	-41.89
	CCSD(T) Single Point	-72.06
	Δ : M06-2x - CCSD(T)	-21.79
	Δ : MP2(Full) - CCSD(T)	30.17
CHOHCH+HCO	M06-2x	-115.64
	MP2(Full)	-75.98
	CCSD(T) Single Point	-103.56
	Δ : M06-2x - CCSD(T)	-12.08
	Δ : MP2(Full) - CCSD(T)	27.58

Species	Level of Theory	Rel. E (kJ/mol)
TS-5T	M06-2x	-199.48
	MP2(Full)	-171.58
	CCSD(T) Single Point	-176.31
	Δ : M06-2x - CCSD(T)	-23.16
	Δ : MP2(Full) - CCSD(T)	4.73
CH2OHCH+CO	M06-2x	-253.38
	MP2(Full)	-199.40
	CCSD(T) Single Point	-194.95
	Δ : M06-2x - CCSD(T)	-58.43
	Δ : MP2(Full) - CCSD(T)	-4.46
TS-6T	M06-2x	-193.64
	MP2(Full)	-113.19
	CCSD(T) Single Point	-162.97
	Δ : M06-2x - CCSD(T)	-30.67
	Δ : MP2(Full) - CCSD(T)	49.78
IM-4T	M06-2x	-291.03
	MP2(Full)	-276.16
	CCSD(T) Single Point	-274.36
	Δ : M06-2x - CCSD(T)	-16.67
	Δ : MP2(Full) - CCSD(T)	-1.79
TS-7T	M06-2x	-229.52
	MP2(Full)	-206.37
	CCSD(T) Single Point	-214.25
	Δ : M06-2x - CCSD(T)	-15.27
	Δ : MP2(Full) - CCSD(T)	7.88
CHOHCH2+CO	M06-2x	-249.12
	MP2(Full)	-245.39
	CCSD(T) Single Point	-242.59
	Δ : M06-2x - CCSD(T)	-6.53
	Δ : MP2(Full) - CCSD(T)	-2.80
TS-8T	M06-2x	-116.43
	MP2(Full)	-
	CCSD(T) Single Point	-81.84
	Δ : M06-2x - CCSD(T)	-34.59
	Δ : MP2(Full) - CCSD(T)	-
IM-5T	M06-2x	-121.39
	MP2(Full)	-40.38
	CCSD(T) Single Point	-93.06
	Δ : M06-2x - CCSD(T)	-28.33
	Δ : MP2(Full) - CCSD(T)	52.68

www.manaraa.com

Table 5. Continued relative energies for structures on the triplet potential energy surface, computed using the M06-2x, MP2, and CCSD(T)//M06-2x single point methods. Relative energy differences, Δ, for M06-2x and MP2 results compared to CCSD(T) single-point results are also shown.

Species	Level of Theory	Rel. E (kJ/mol)
TS-9T	M06-2x	-95.27
	MP2(Full)	-42.51
	CCSD(T) Single Point	-65.78
	Δ : M06-2x - CCSD(T)	-29.48
	Δ : MP2(Full) - CCSD(T)	23.28
IM-6T	M06-2x	-285.86
	MP2(Full)	-220.53
	CCSD(T) Single Point	-258.92
	Δ : M06-2x - CCSD(T)	-26.94
	Δ : MP2(Full) - CCSD(T)	38.40
TS-10T	M06-2x	-130.12
	MP2(Full)	-72.86
	CCSD(T) Single Point	-108.93
	Δ : M06-2x - CCSD(T)	-21.20
	Δ : MP2(Full) - CCSD(T)	36.07
HCO+CHCHOH	M06-2x	-140.74
	MP2(Full)	-101.43
	CCSD(T) Single Point	-120.69
	Δ : M06-2x - CCSD(T)	-20.05
	Δ : MP2(Full) - CCSD(T)	19.25
TS-11T	M06-2x	-78.51
	MP2(Full)	-23.55
	CCSD(T) Single Point	-41.61
	Δ : M06-2x - CCSD(T)	-36.90
	Δ : MP2(Full) - CCSD(T)	18.05
IM-7T	M06-2x	-226.40
	MP2(Full)	-202.24
	CCSD(T) Single Point	-201.51
	Δ : M06-2x - CCSD(T)	-24.89
	Δ : MP2(Full) - CCSD(T)	-0.74
TS-12T	M06-2x	-89.46
	MP2(Full)	-25.74
	CCSD(T) Single Point	-69.48
	Δ : M06-2x - CCSD(T)	-19.97
	Δ : MP2(Full) - CCSD(T)	43.74
HOC+CH2CHO	M06-2x	-120.66
	MP2(Full)	-61.60
	CCSD(T) Single Point	-104.83
	Δ : M06-2x - CCSD(T)	-15.83
	Δ : MP2(Full) - CCSD(T)	43.23

Species	Level of Theory	Rel. E (kJ/mol)
TS-13T	M06-2x	-185.31
	MP2(Full)	-
	CCSD(T) Single Point	-157.42
	Δ : M06-2x - CCSD(T)	-27.88
	Δ : MP2(Full) - CCSD(T)	-
IM-8T	M06-2x	-241.30
	MP2(Full)	-215.83
	CCSD(T) Single Point	-215.88
	Δ : M06-2x - CCSD(T)	-25.42
	Δ : MP2(Full) - CCSD(T)	0.05
TS-14T	M06-2x	-89.46
	MP2(Full)	-25.74
	CCSD(T) Single Point	-69.48
	Δ : M06-2x - CCSD(T)	-19.97
	Δ : MP2(Full) - CCSD(T)	43.74
HOC+CH2CHO	M06-2x	-120.66
	MP2(Full)	-61.60
	CCSD(T) Single Point	-227.29
	Δ : M06-2x - CCSD(T)	106.62
	Δ : MP2(Full) - CCSD(T)	165.69
TS-15T	M06-2x	-141.22
	MP2(Full)	-83.05
	CCSD(T) Single Point	-114.36
	Δ : M06-2x - CCSD(T)	-26.87
	Δ : MP2(Full) - CCSD(T)	31.31
HCO+CH2COH	M06-2x	-163.17
	MP2(Full)	-123.12
	CCSD(T) Single Point	-146.39
	Δ : M06-2x - CCSD(T)	-16.79
	Δ : MP2(Full) - CCSD(T)	23.27
TS-16T	M06-2x	-27.67
	MP2(Full)	-
	CCSD(T) Single Point	-1.64
	Δ : M06-2x - CCSD(T)	-26.04
	Δ : MP2(Full) - CCSD(T)	-
IM-9T	M06-2x	-27.50
	MP2(Full)	23.29
	CCSD(T) Single Point	-2.18
	Δ : M06-2x - CCSD(T)	-25.32
	Δ : MP2(Full) - CCSD(T)	25.48

www.manaraa.com

Table 6. Continued relative energies for structures on the triplet potential energy surface, computed using the M06-2x, MP2, and CCSD(T)//M06-2x single point methods. Relative energy differences, Δ, for M06-2x and MP2 results compared to CCSD(T) single-point results are also shown.

Species	Level of Theory	Rel. E (kJ/mol)
*TS-17A	M06-2x	35.25
	MP2(Full)	122.04
	CCSD(T) Single Point	62.42
	Δ : M06-2x - CCSD(T)	-27.17
	Δ : MP2(Full) - CCSD(T)	59.61
*TS-17B	M06-2x	30.78
	MP2(Full)	88.42
	CCSD(T) Single Point	56.00
	Δ : M06-2x - CCSD(T)	-25.23
	Δ : MP2(Full) - CCSD(T)	32.42
TS-18T	M06-2x	-53.10
	MP2(Full)	-202.82
	CCSD(T) Single Point	-23.10
	Δ : M06-2x - CCSD(T)	-30.01
	Δ : MP2(Full) - CCSD(T)	-179.72
IM-10T	M06-2x	-126.81
	MP2(Full)	-44.04
	CCSD(T) Single Point	-100.01
	Δ : M06-2x - CCSD(T)	-26.80
	Δ : MP2(Full) - CCSD(T)	55.97
TS-19T	M06-2x	50.33
	MP2(Full)	114.90
	CCSD(T) Single Point	77.39
	Δ : M06-2x - CCSD(T)	-27.05
	Δ : MP2(Full) - CCSD(T)	37.51
IM-11T	M06-2x	-142.16
	MP2(Full)	-64.85
	CCSD(T) Single Point	-113.30
	Δ : M06-2x - CCSD(T)	-28.86
	Δ : MP2(Full) - CCSD(T)	48.44
TS-20T	M06-2x	-11.91
	MP2(Full)	58.90
	CCSD(T) Single Point	7.16
	Δ : M06-2x - CCSD(T)	-19.07
	Δ : MP2(Full) - CCSD(T)	51.74
CH2O+CHCOH	M06-2x	-21.09
	MP2(Full)	-12.11
	CCSD(T) Single Point	-2.36
	Δ : M06-2x - CCSD(T)	-18.73
	Δ : MP2(Full) - CCSD(T)	-9.75

*Two different HOC dissociations are possible here.

www.manaraa.com

CCSD(T) single-point energies were used to construct PEPs of higher accuracy for the triplet and singlet potential energy surfaces of the propargyl alcohol reaction. The PEPs representing the established pathways (those found by Buettner)[28] for the propargyl alcohol reaction at the MP2/6-31++G(d,p), M06-2x/cc-pVTZ, and CCSD(T)/cc-pVTZ//M06-2x/cc-pVTZ levels of theory are shown in Figures 15-20. The importance of collecting CCSD(T) single-point energies is revealed with these PEPs. Figure 17 shows the established HCO radical formation pathway with energies computed at the M06-2x/cc-pVTZ level of theory. As seen in Figure 17, TS-1T violates the definition of a transition state as it is lower in energy than the starting material. Figure 15 shows the PEP for the established HCO radical pathway at the higher level of theory, CCSD(T), where TS-1T is 10.40 kJ/mol higher than the reactants, satisfying the definition of a transition state. The PEP shown in Figure 15 was generated by rerunning Buettner's MP2/6-311++G(d,p) structures at the M06-2x/cc-pVTZ level, followed by single-point energy calculations at the CCSD(T)/cc-pVTZ level of theory. Figure 16 shows the PEP of the established singlet surface, with single-point energies calculated at the CCSD(T)/cc-pVTZ level of theory. As mentioned previously, the singlet surface does not result in the formation of HCO radical. Structures of all intermediate, transition state, and product species are included in the Appendix.

www.manaraa.com

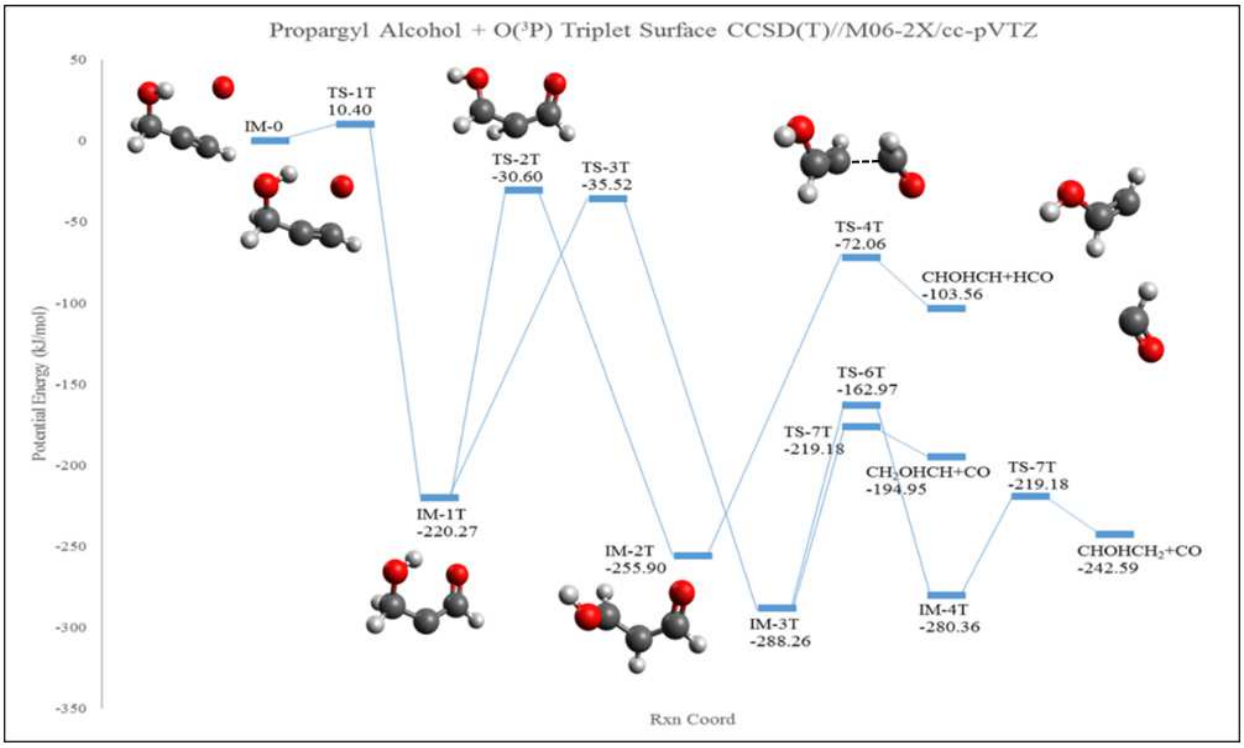

Figure 15. Established triplet surface pathways, CCSD(T)//M06-2x/cc-pVTZ level, key IM and TS structures shown.

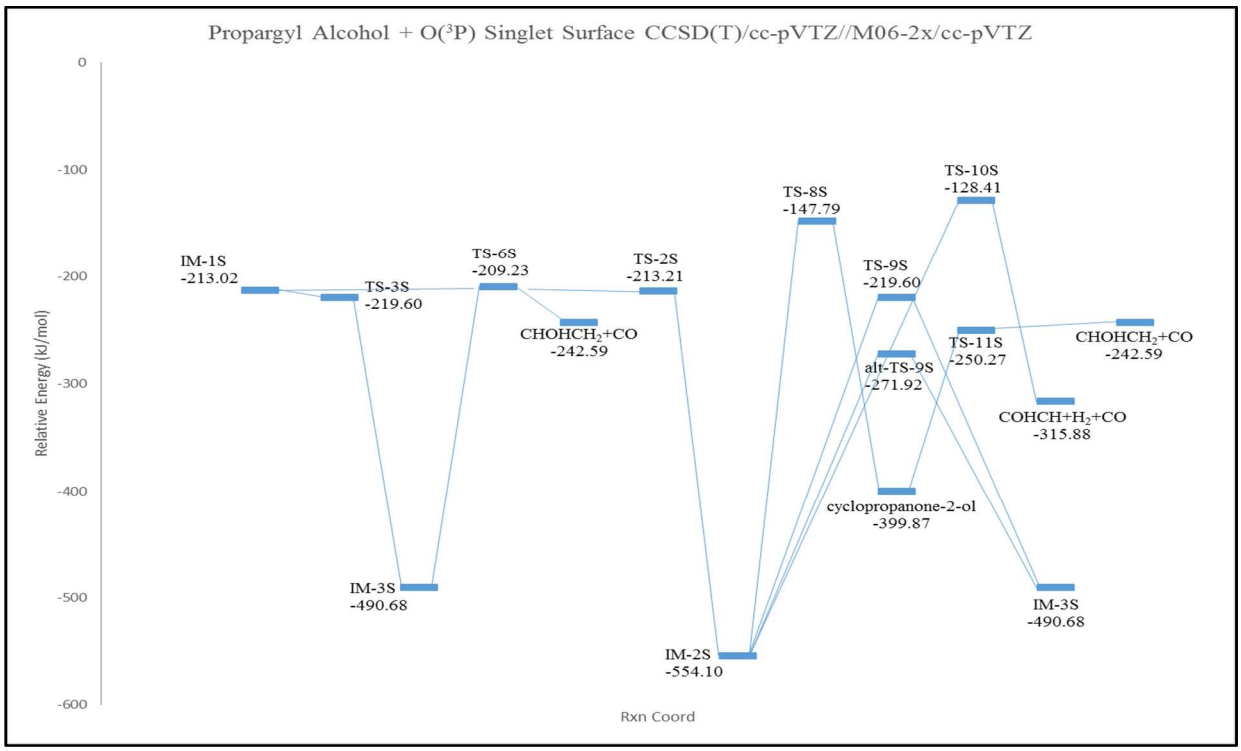

Figure 16. Established singlet surface pathways, CCSD(T)//M06-2x/cc-pVTZ level.

www.manaraa.com

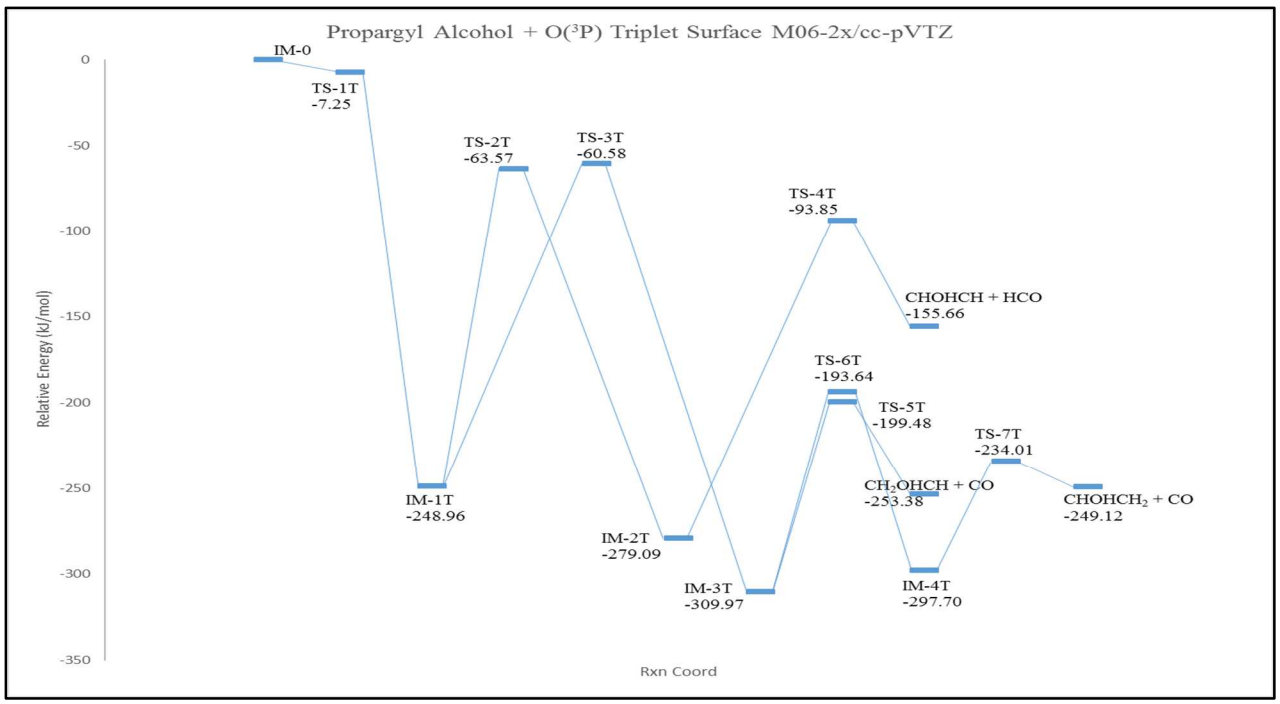

Figure 17. Established triplet surface pathways, M06-2x/cc-pVTZ level.

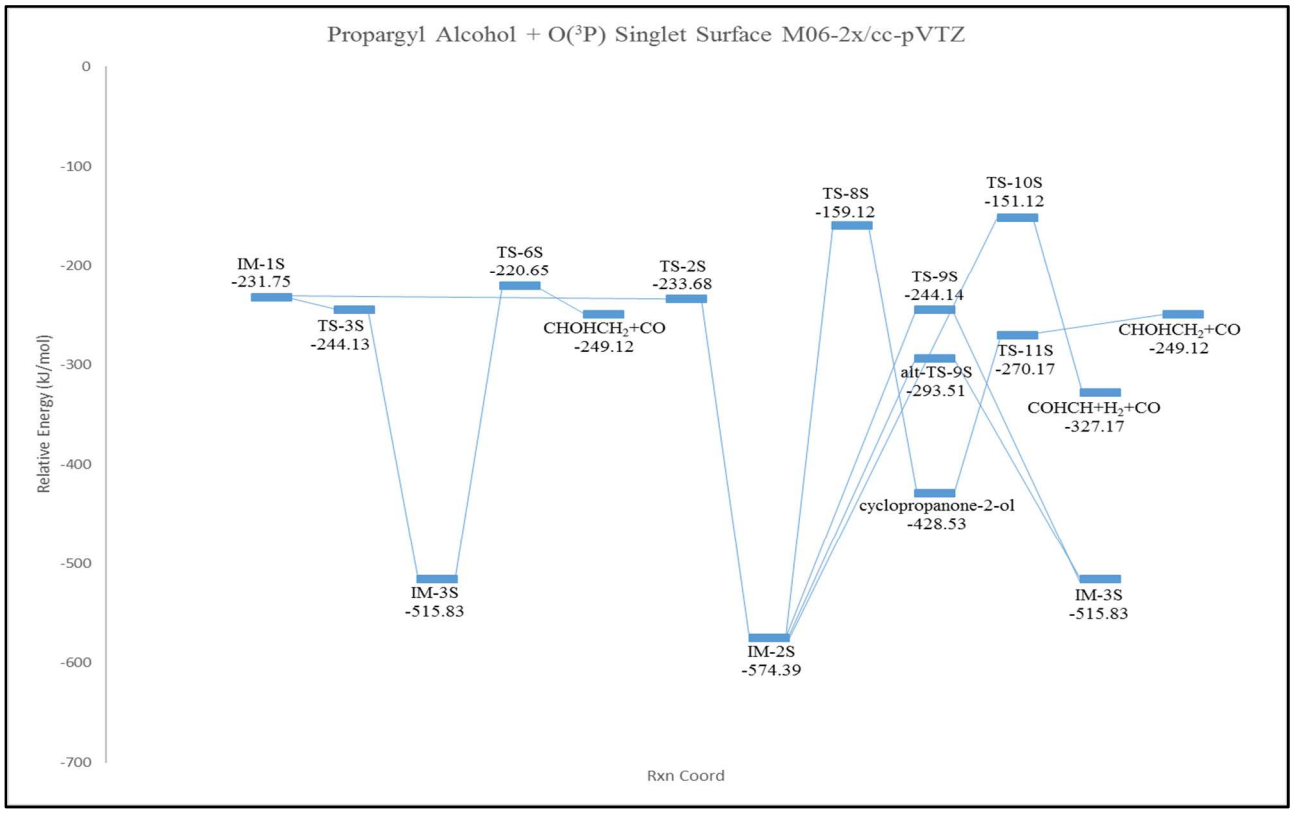

Figure 18. Established singlet surface pathways, M06-2x/cc-pVTZ level.

www.manaraa.com

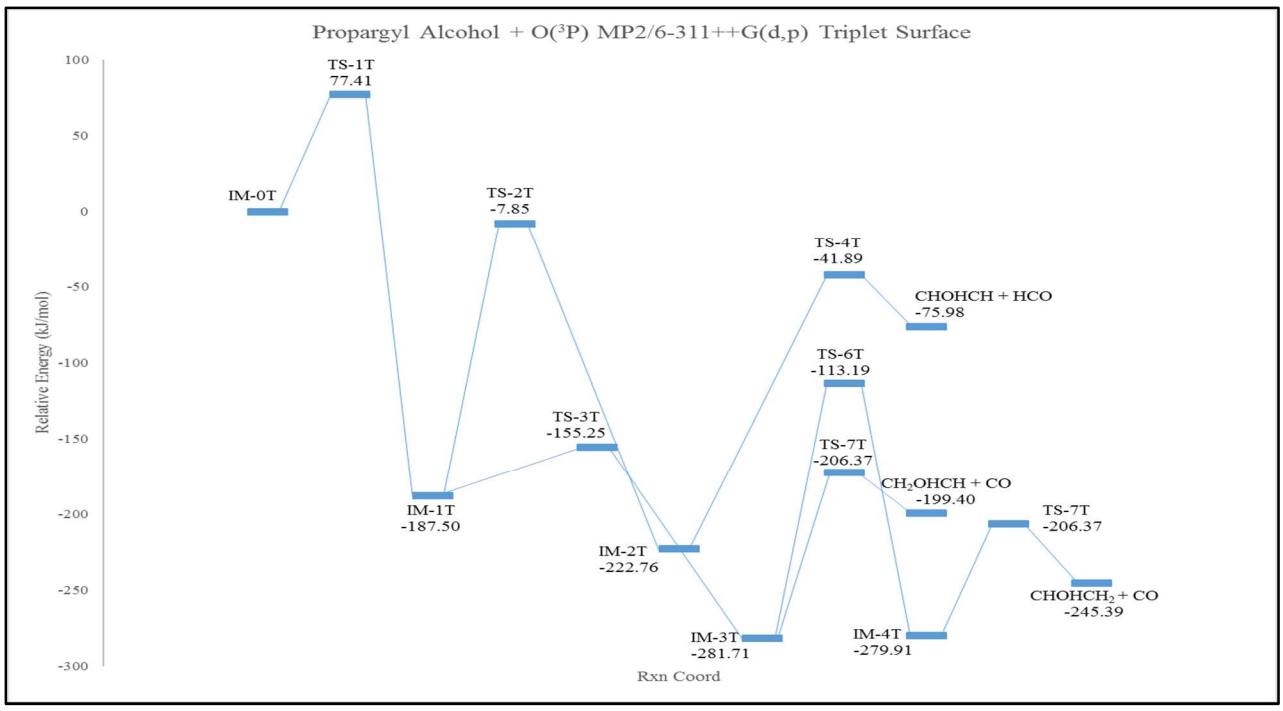

Figure 19. Established triplet surface pathways, MP2/6-311++G(d,p) level.

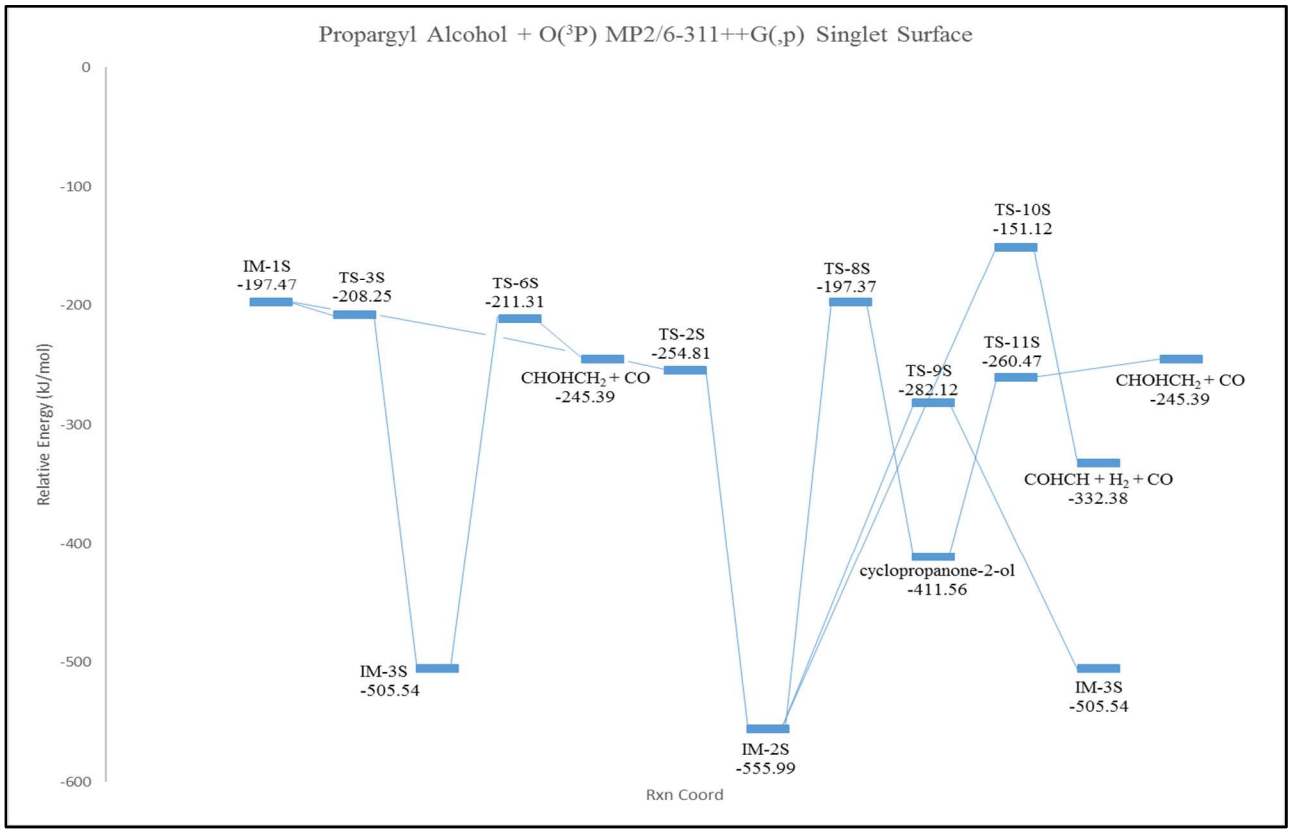

Figure 20. Established singlet surface pathways, MP2/6-311++G(d,p) level.

www.manaraa.com

Buettner found two pathways for HCO radical formation for the reaction of O(^{3}P) with propargyl alcohol.[28] This project expands upon Buettner's findings with three additional reaction pathways that result in HCO radical formation. The primary mechanism behind these novel HCO radical formation pathways is a hydrogen from the hydroxyl group, O9H5, shifting to the other oxygen atom of the molecule, O8 (see Figure 14 for atom numbering). Another important mechanism at play is the isomerization of HOC to HCO, making HOC radical formation pathways of interest. The PEP for the isomerization of the formyl radical is shown in Figure 21.

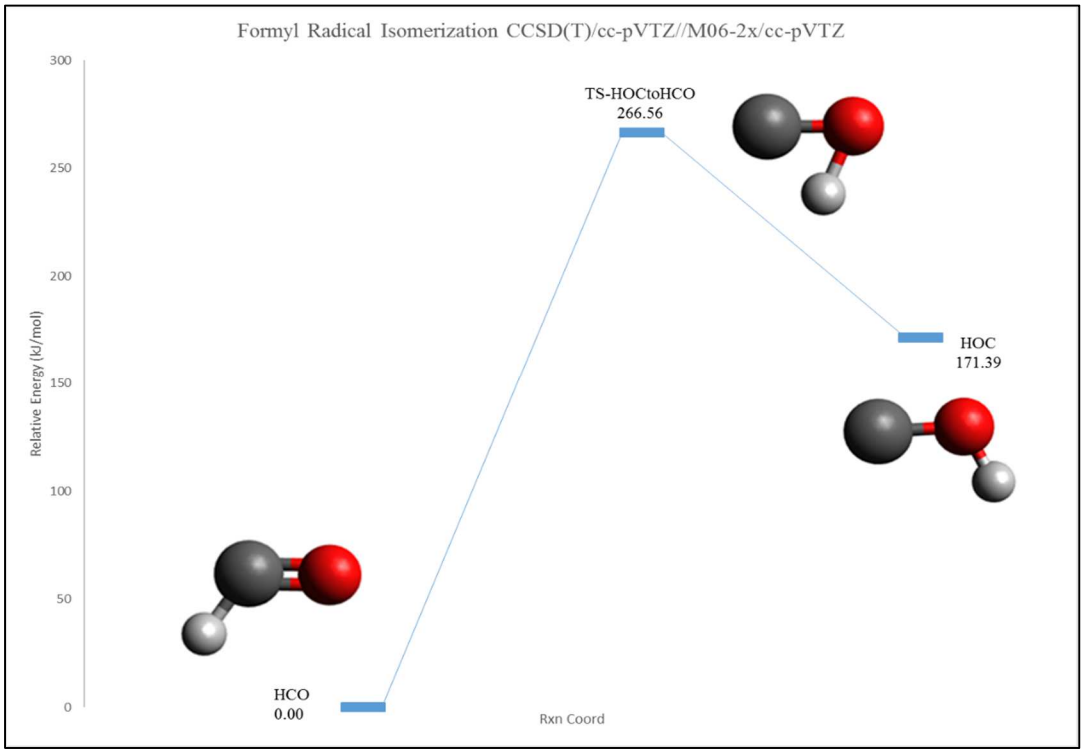

Figure 21. Isomerization of the formyl radical, computed at the CCSD(T)//M06-2x/cc-pVTZ level of theory.

www.manaraa.com

The PEPs for the novel HCO/HOC radical formation pathways are shown in Figures 22-24. At the MP2/6-311++G(d,p) level of theory, a stable structure for TS-8T could not be found, so the CCSD(T) single-point energy was used for constructing the PEP. It can also be seen that IM-5T is actually higher in energy than both of its adjacent transition states (TS-8T and TS-9T). However, M06-2x performed well and yielded PEPs that were more comparable to the CCSD(T) single-point energy PEPs. The novel HCO/HOC radical pathways presented here are predicted to be accessible due to the inherent conditions of a combustion reaction. Heats of combustion for alkyne compounds are an order of magnitude greater than the relative energy barriers present in all of the HCO/HOC radical pathways presented here. In addition to this, a lot of excess energy from the photolysis of SO_2 (the $O(^3P)$ source) provides the energy to overcome the relative energy barriers.

The first novel HCO radical formation pathway found in this study branches off from IM-1T in the $O(^3P)$ + propargyl alcohol established pathway. As seen in Figure 22, the pathway begins as H5 shifts from O9 to O8. The next step in the mechanism is a shift of H6 from C3 to C2. Finally, the C2-C3 bond breaks, resulting in the dissociation of the HCO fragment. It is worth noting that the novel HCO radical pathway that splits off from IM-1T has a lower initial relative energy (TS-8T, -81.84 kJ/mol) than the established HCO radical pathway (TS-2T, -30.60 kJ/mol), making the novel pathway a more thermodynamically viable pathway for HCO radical formation. The relative energies reported here are CCSD(T) single-point energies.

www.manaraa.com

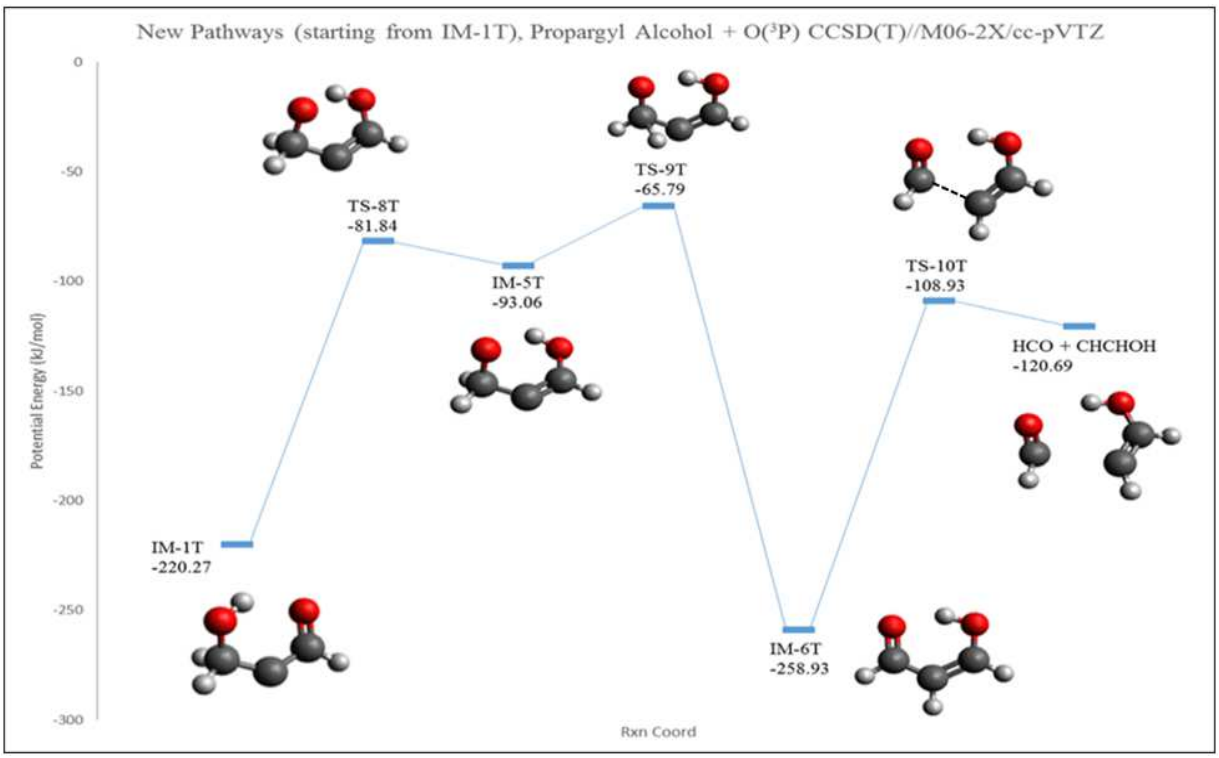

Figure 22. Novel HCO Pathway (branching off from IM-1T), CCSD(T)//M06-2x/cc-pVTZ level.

The second novel pathway for HCO radical production branches off from IM-2T. Figure 23 shows two novel pathways for the O(^{3}P) + propargyl alcohol reaction: one formaldehyde formation pathway and one HOC formation pathway. The first step in the HOC pathway is an H-shift from C3 to C2. The relative energy for this transition state is -44.51 kJ/mol (TS-11T), which is higher in energy than the established pathway relative energy of -72.06 kJ/mol (TS-4T). The established pathway is predicted to be the more likely mechanism to occur once the reaction coordinate reaches IM-2T due to it being the more thermodynamically preferred pathway.

www.manaraa.com

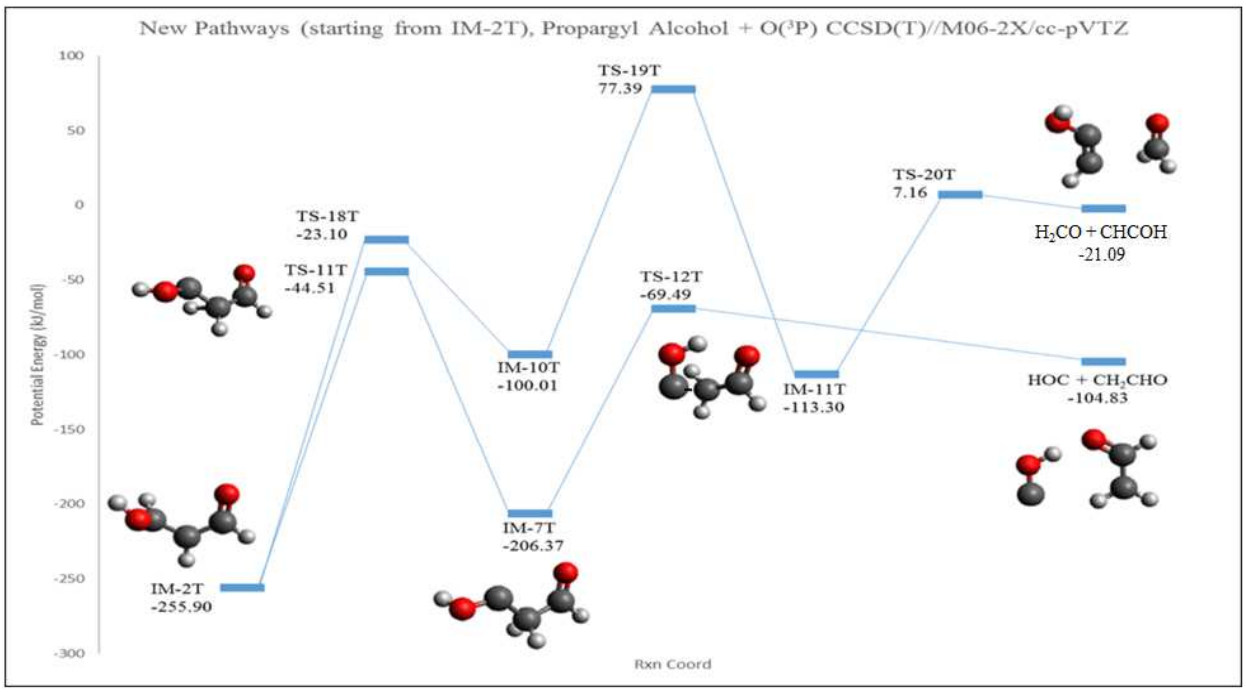

Figure 23. Novel HCO Pathway (branching off from IM-2T), CCSD(T)//M06-2x/cc-pVTZ level.

The third, fourth, and fifth novel pathways for HCO/HOC radical production all branch off from IM-4T. Figure 24 shows the mechanisms behind the novel pathways starting from IM-4T. First, IM-4T may undergo a hydrogen shift from O9 to O8 with a relative energy of -157.42 kJ/mol (TS-13T), which is higher in energy than TS-7T from the carbon monoxide formation channel (-219.18 kJ/mol). However, it is worth noting that the established PEP does not show HCO radical formation from IM-4T and so this work provides an entirely new avenue for formation of the formyl radical. The next structure in the reaction coordinate following TS-13T is IM-8T. The dissociation of HCO radical also occurs from IM-8T via TS-14T with a relative energy of -69.48 kJ/mol. In addition, the dissociation of HOC radical occurs at this point via TS-15T with a lower relative energy of -114.36 kJ/mol. The final novel pathway found is an HOC formation pathway that is significantly higher in energy than the other HCO/HOC radical

www.manaraa.com

pathways. IM-4T may undergo an H-shift from C2 to O8 via TS-16T with a relative energy of -1.64 kJ/mol. The following intermediate species, IM-9T, presents two possibilities for HOC dissociation. Once one dissociation occurs, a subsequent dissociation is not possible due to the energy required to break the C=C double bond. The relative energy for an HOC dissociation from IM-9T is 56.00 kJ/mol (TS-17T). This mechanism is thermodynamically unfavorable compared to the lower relative energy barriers of other HCO/HOC radical pathways in the O(^{3}P) + propargyl alcohol reaction.

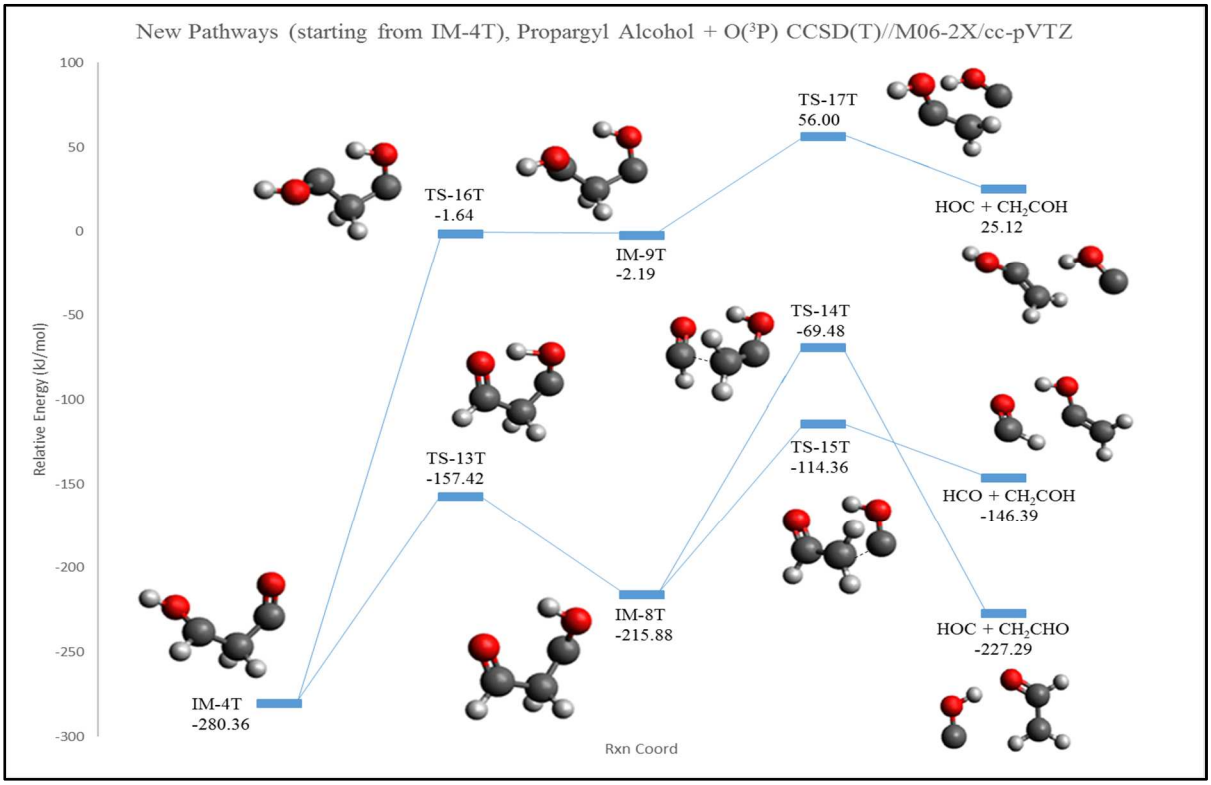

Figure 24. Novel HCO Pathway (branching off of IM-4T), CCSD(T)//M06-2x/cc-pVTZ level.

www.manaraa.com

Minimum Energy Crossing Point

Intersystem crossing occurs at the minimum energy crossing point (MECP), which was found using the MECP method by Harvey *et al.*[34] at the M06-2x level of theory. Intersystem crossing is an important phenomenon in chemistry as it allows a system to cross from one multiplicity potential energy surface to another. The reaction of $O(^3P)$ + propargyl alcohol always begins on the triplet surface as the reaction is always initiated with a triplet oxygen atom attacking the triple bond of a singlet alkyne species. Similar to the $O(^3P)$ + propyne reaction, intersystem crossing for $O(^3P)$ + propargyl alcohol takes place near the first IM in the reaction pathway. HCO radical can only form on the triplet surface as shown in previous studies,[18,28,29] but the singlet potential energy surface is still relevant as it is easily accessible due to a low energy crossing point structure between IM-1T and IM-1S with the potential energy difference between IM-1T and the MECP structure just 0.005%. The MECP lies just above IM-1S in energy by about 13 kJ/mol, and slightly higher than IM-1T by about 37 kJ/mol. Results of the MECP method are shown in Figure 25 and table 7. The results reveal that the geometry of the crossing-point structure is intermediate between IM-1T and IM-1S, with about half of the geometric parameters being closer to IM-1T and the other half being closer to IM-1S.

www.manaraa.com

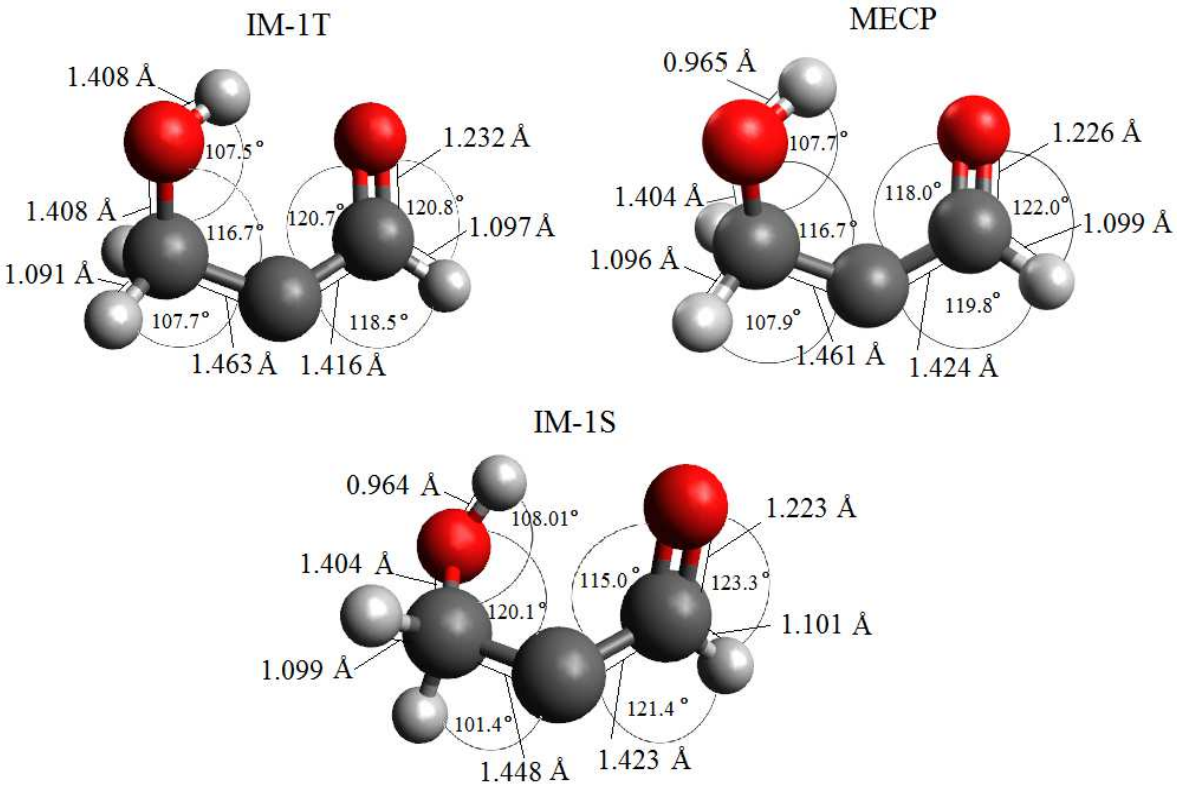

Figure 25. Structures for IM-1T (top left), MECP (top right), and IM-1S (bottom), calculated at the M06-2x/cc-pVTZ level.

Table 7. MECP results, calculated at the M06-2x/cc-pVTZ level of theory. Reported energies are not corrected for vibrational zero-point energies.

MECP (M06-2x)					
Parameter	**Crossing Point Value**	**IM-1T**	**IM-1S**	**% Diff. (triplet)**	**% Diff. (singlet)**
C1-H4 (Å)	1.099	1.097	1.101	-0.180	0.180
C1-C2 (Å)	1.424	1.416	1.423	-0.560	-0.070
C1-O8 (Å)	1.226	1.232	1.223	0.490	-0.240
C2-C3 (Å)	1.461	1.463	1.448	0.140	-0.890
C3-O9 (Å)	1.404	1.408	1.404	0.290	0.000
O9-H5 (Å)	0.965	0.966	0.964	0.100	-0.100
<O8-C1-H4 (°)	122.0	120.8	123.3	-1.0	1.1
<O8-C1-C2 (°)	118.0	120.7	115.0	2.3	-2.5
<C1-C2-C3 (°)	124.5	129.7	117.7	4.2	-5.5
<C2-C3-O9 (°)	116.7	112.1	120.1	-3.9	2.9
<C3-O9-H5 (°)	107.7	107.5	108.1	-0.2	0.4
Potential Energy (hartrees)	-267.0060	-267.0200	-267.0111	0.0052	0.0019

www.manaraa.com

NRT Analysis: O(^{3}P) + Propargyl Alcohol

Natural Resonance Theory (NRT)[36-40] analyses have been carried out on each stationary point in the O(^{3}P) + propargyl alcohol triplet state PEP in order to better understand how the movement of electron density dictates the reaction mechanisms at play. Natural spin density (NSD) and natural bond order (NBO) data are presented in Figures 26-37. For the sake of clarity, only the C and O atoms of the reaction are shown on the NSD and NBO plots, as the H atoms carry relatively low NSD values in the system. Natural spin densities are calculated as the difference between α spin state and β spin state populations on each atom. The NSD data for the established O(^{3}P) + propargyl alcohol pathway is shown in Figure 26, where the HCO radical product is composed of C1, O8, and H4.

www.manaraa.com

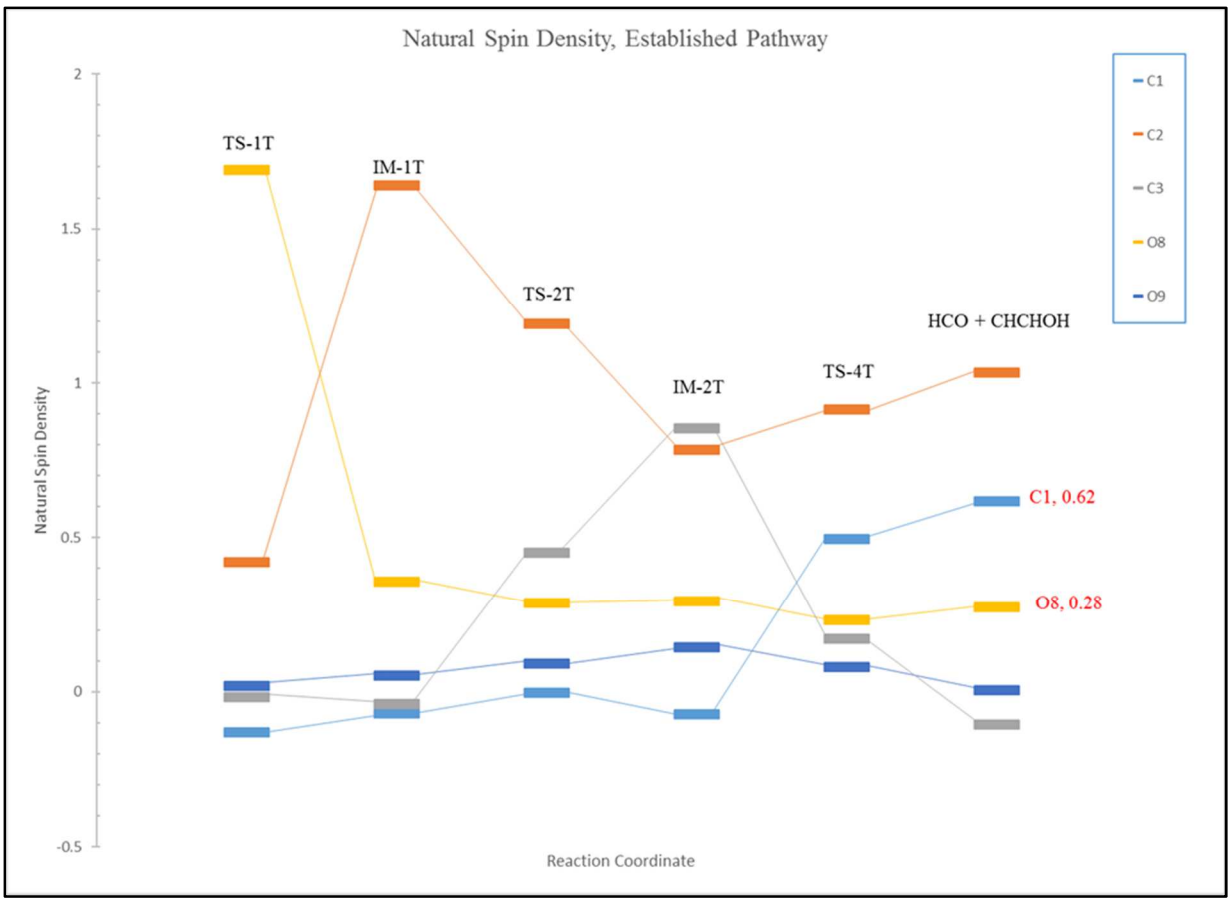

Figure 26. NSD Data for the Established HCO Pathway, calculated at the M06-2x/cc-pVTZ level of theory.

Figure 26 exemplifies the importance of conducting an NSD analysis as it reveals how the electron population shifts and confirms the dissociation of the radical species. For example, the HCO/HOC radical product should have a total NSD of 1 as it is a radical species and bears a single unpaired electron. Figure 26 shows that C1 has a NSD of 0.62 and O8 has a NSD of 0.28 at the end of the reaction coordinate, where formyl radical dissociation occurs. The total NSD of C1 and O8 is 0.90, with the remaining 0.10 NSD on H4 giving a total NSD of 1.0 for H4 C1 O8. The NSD also shows why HCO dissociation does not occur directly from IM-1T: the spin distribution would not allow for the production of a radical at that point in the reaction pathway.

www.manaraa.com

The NBO analysis, shown in Figure 27, also reveals important information as the bond orders of the system change drastically as the reaction progresses. Figure 27 shows that the C1-C2 bond order starts at 1.5 at the beginning of the established HCO radical pathway and ends at 0 as it is the C1-C2 bond that breaks during HCO dissociation. Similar NSD and NBO patterns are observed across all novel HCO/HOC radical pathways presented here.

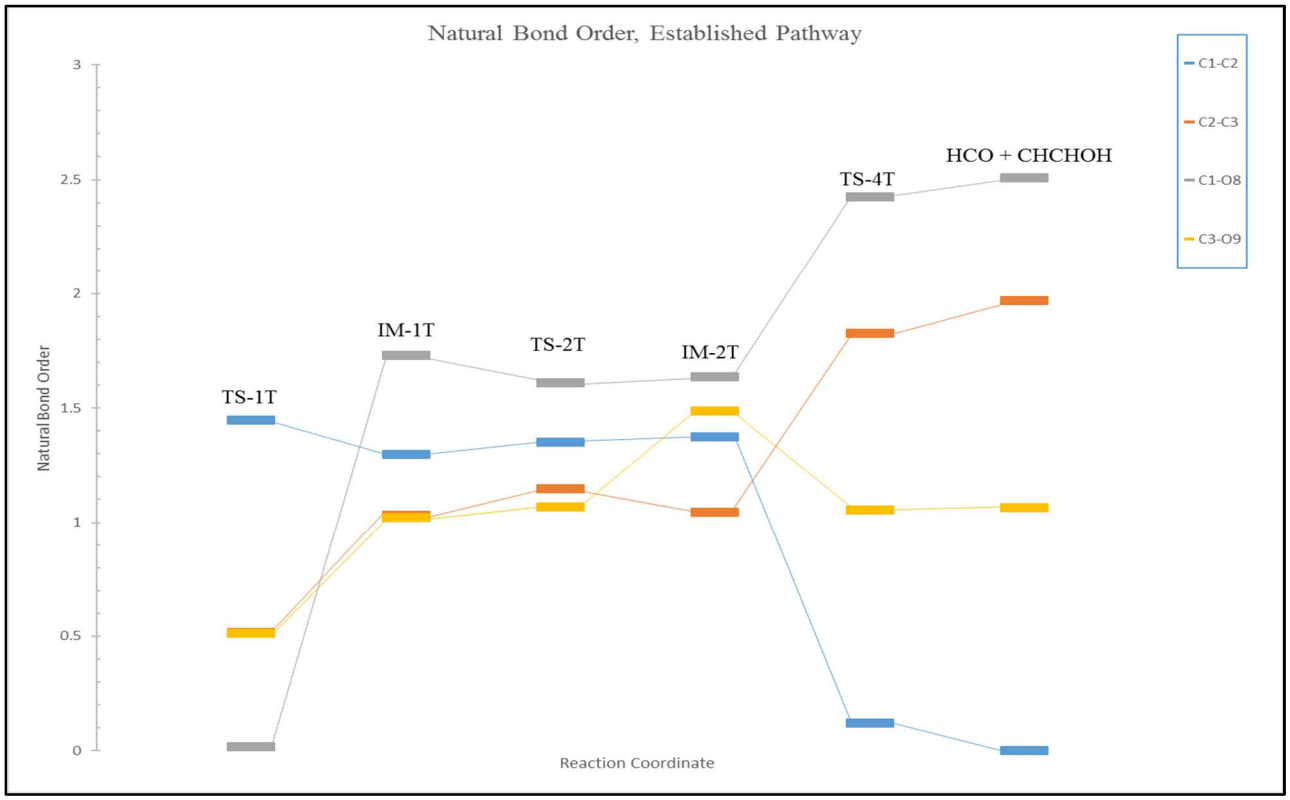

Figure 27. NBO Data for the Established HCO Pathway, calculated at the M06-2x/cc-pVTZ level of theory.

Figure 28 reveals a different shift in spin density in the O(^{3}P) + propargyl alcohol system. For the first novel pathway (from IM-1T), NSD will build up on different atoms in the system

www.manaraa.com

which ultimately leads to HCO dissociation. For this pathway, C3 and O9 make up the HCO radical and have a total NSD of 0.87, with the remaining 0.13 NSD on H7. This novel pathway involves breaking of the C2-C3 bond, a novel mechanism for the O(^{3}P) + propargyl alcohol reaction shown in Figure 29. At the beginning of this pathway, IM-1T exhibits a bond order of 1 between C2 and C3 that ultimately falls to 0 in the dissociation step of the pathway.

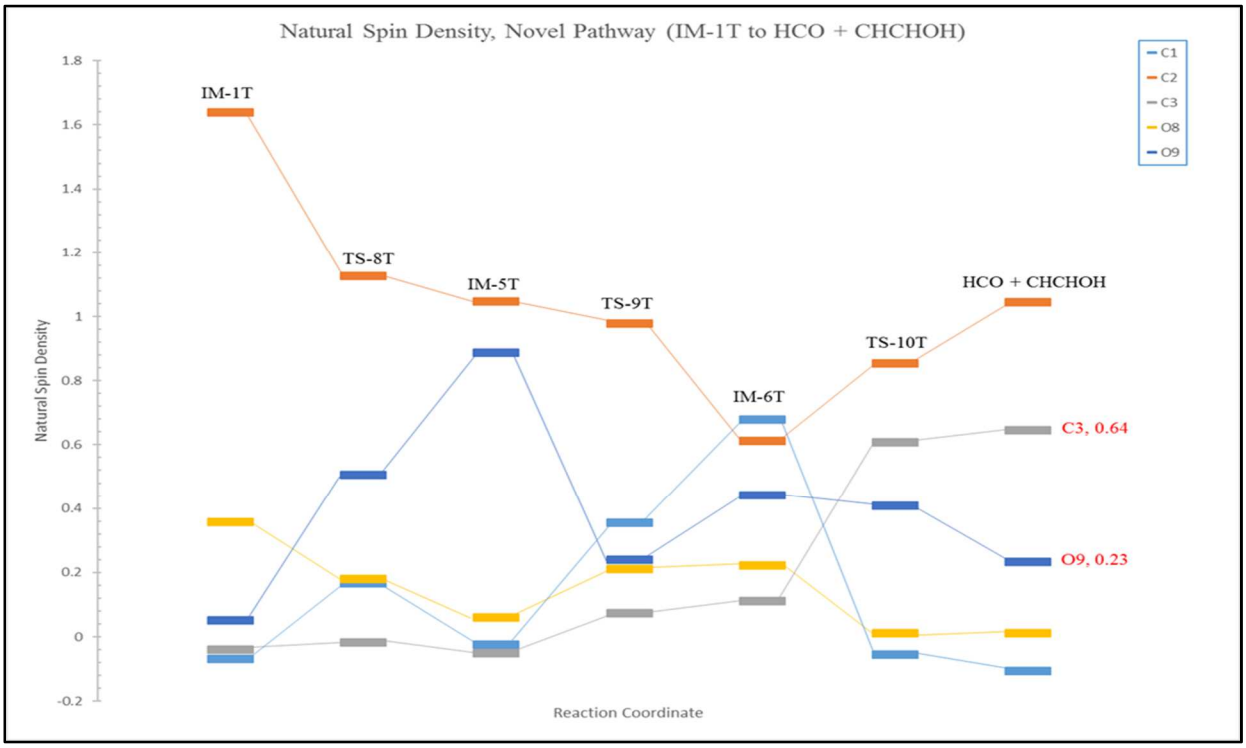

Figure 28. NSD Data for a novel HCO Pathway (IM-1T), calculated at the M06-2x/cc-pVTZ level of theory.

www.manaraa.com

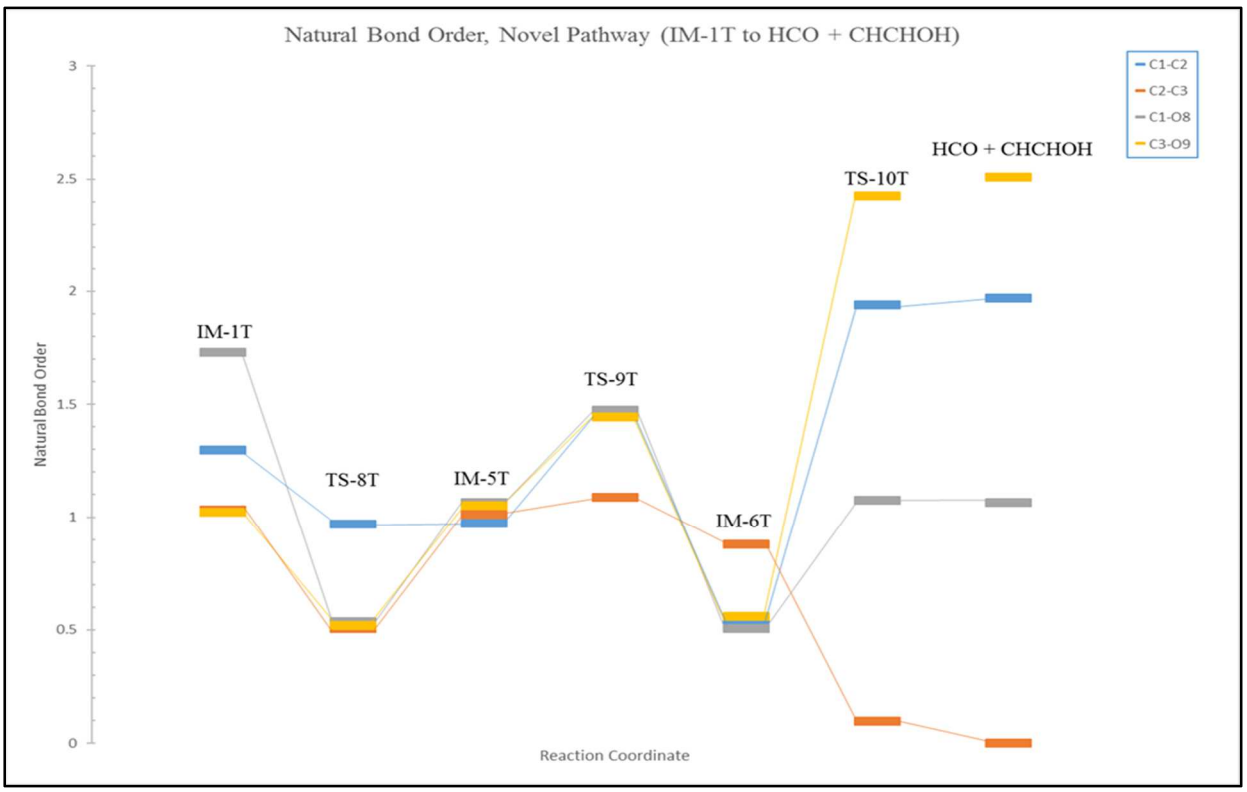

Figure 29. NBO Data for a novel HCO Pathway (IM-1T), calculated at the M06-2x/cc-pVTZ level of theory.

Different patterns in NSD are observed between HCO and HOC radical formation pathways. Generally, NSD is split across the C and O atoms of HCO radical in an approximately 1:3 (C:O) ratio. However, HOC formation pathways indicate something very different at play. The NSD distribution shows the unpaired electron is almost entirely located on the C atom in all HOC formation pathways as illustrated in Figure 30.

www.manaraa.com

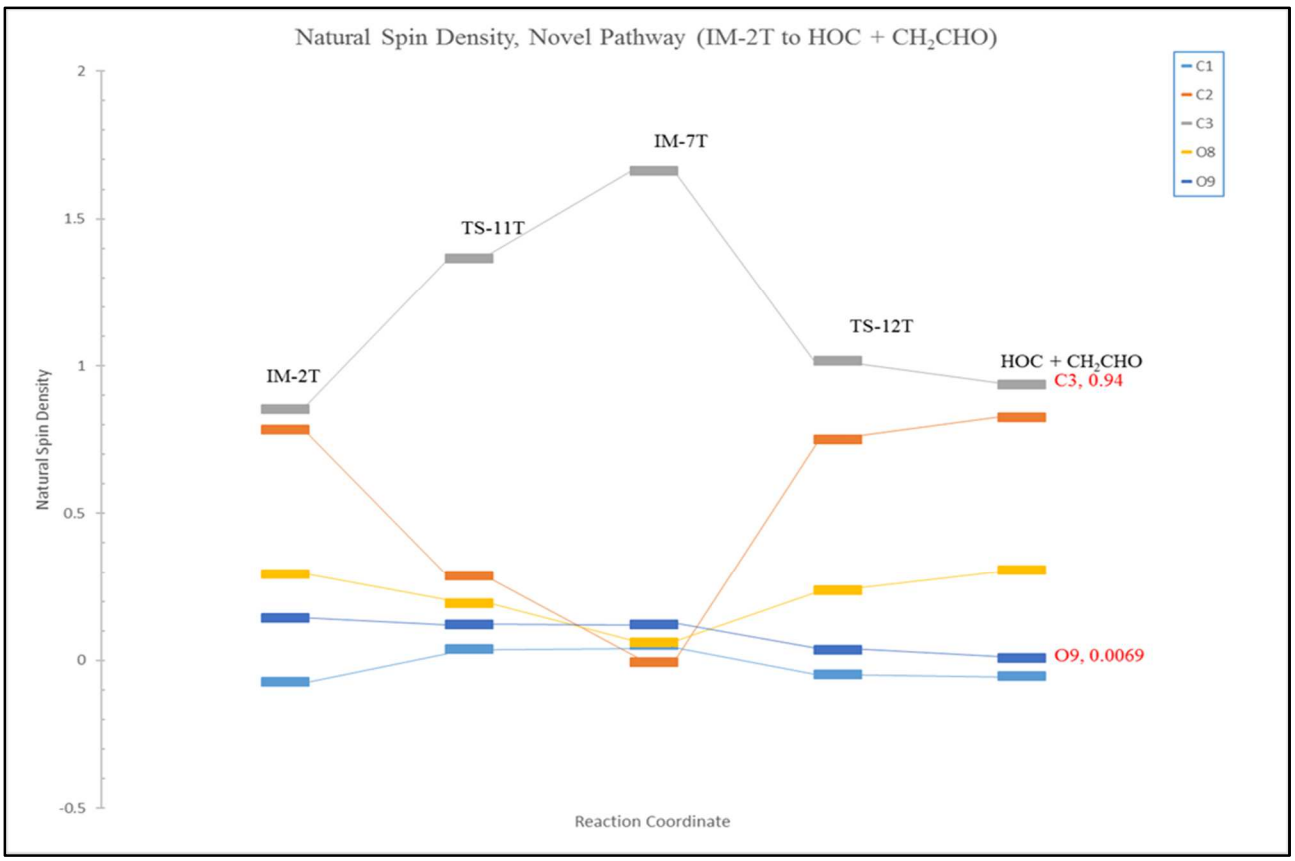

Figure 30. NSD Data for a novel HOC Pathway (IM-2T), calculated at the M06-2x/cc-pVTZ level of theory.

NBO data for the novel HOC pathway branching from IM-2T is shown in Figure 31. Again, the breaking of the C2-C3 bond is the key mechanism behind HOC dissociation in this pathway. NBO analysis for these novel pathways reveal that HCO/HOC dissociation may occur from either side of the molecule, as the HCO/HOC radical product may contain either the incoming O(^{3}P) atom from the first step in the pathway or the O atom from the hydroxyl substituent of propargyl alcohol.

www.manaraa.com

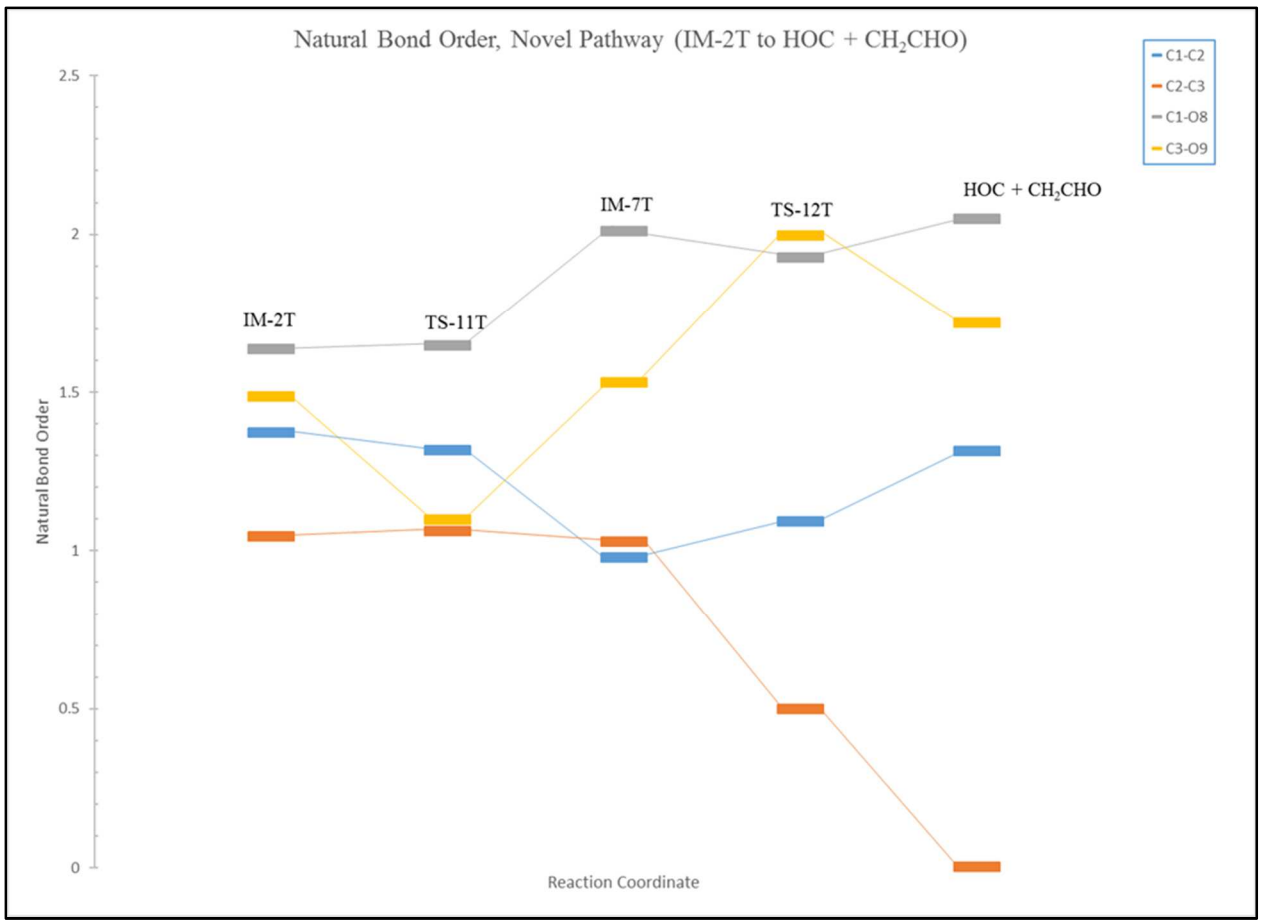

Figure 31. NBO Data for a novel HOC Pathway (IM-2T), calculated at the M06-2x/cc-pVTZ level of theory.

For completion, the NSD and NBO plots for the three novel HCO/HOC radical pathways that branch off of IM-4T are shown in Figures 32-37. In summary, the NSD plots reveal similar patterns as to what has been presented in Figures 26-31 so far. HOC dissociations involve almost all of the NSD aggregating around the C atom of the HOC, whereas the HCO dissociation reveals a 1:3 ratio (O:C) for NSD. Again, the NBO analysis confirms bond breakage for the dissociation steps in the reaction pathway.

www.manaraa.com

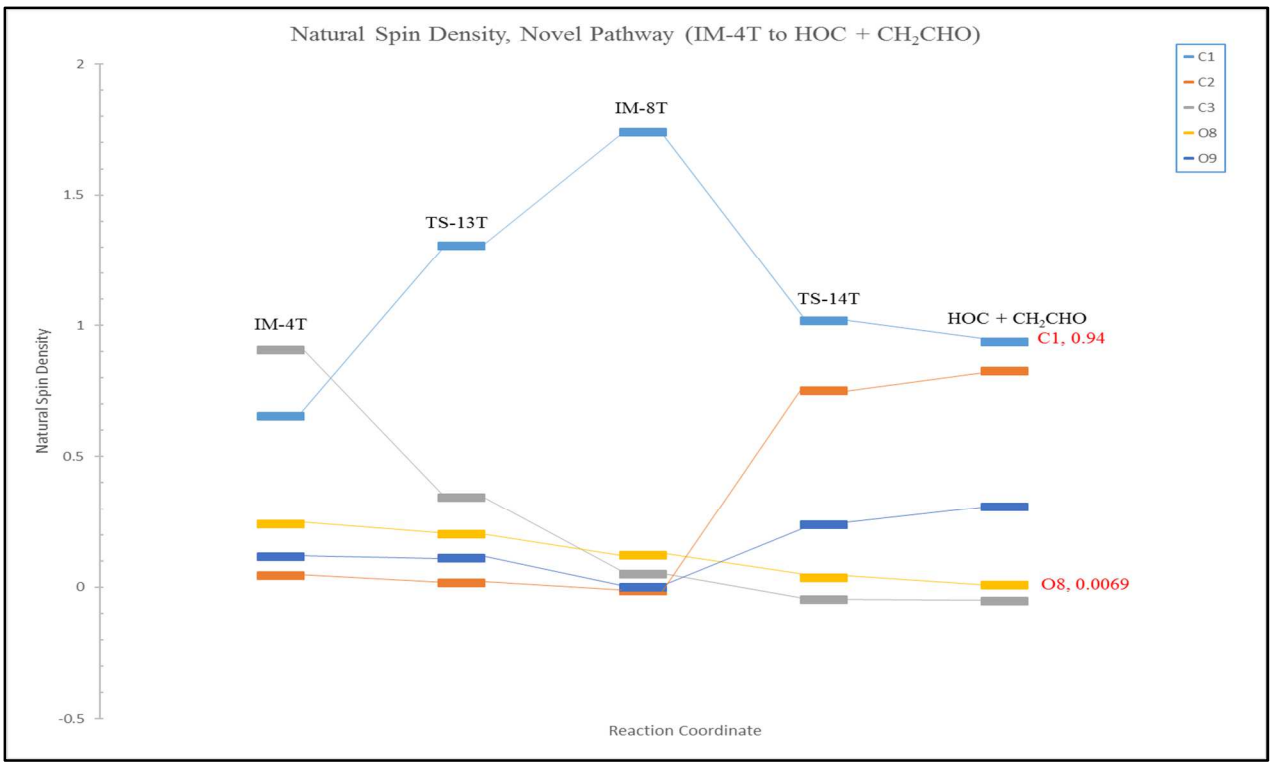

Figure 32. NSD Data for a novel HOC Pathway (IM-4T), calculated at the M06-2x/cc-pVTZ level of theory.

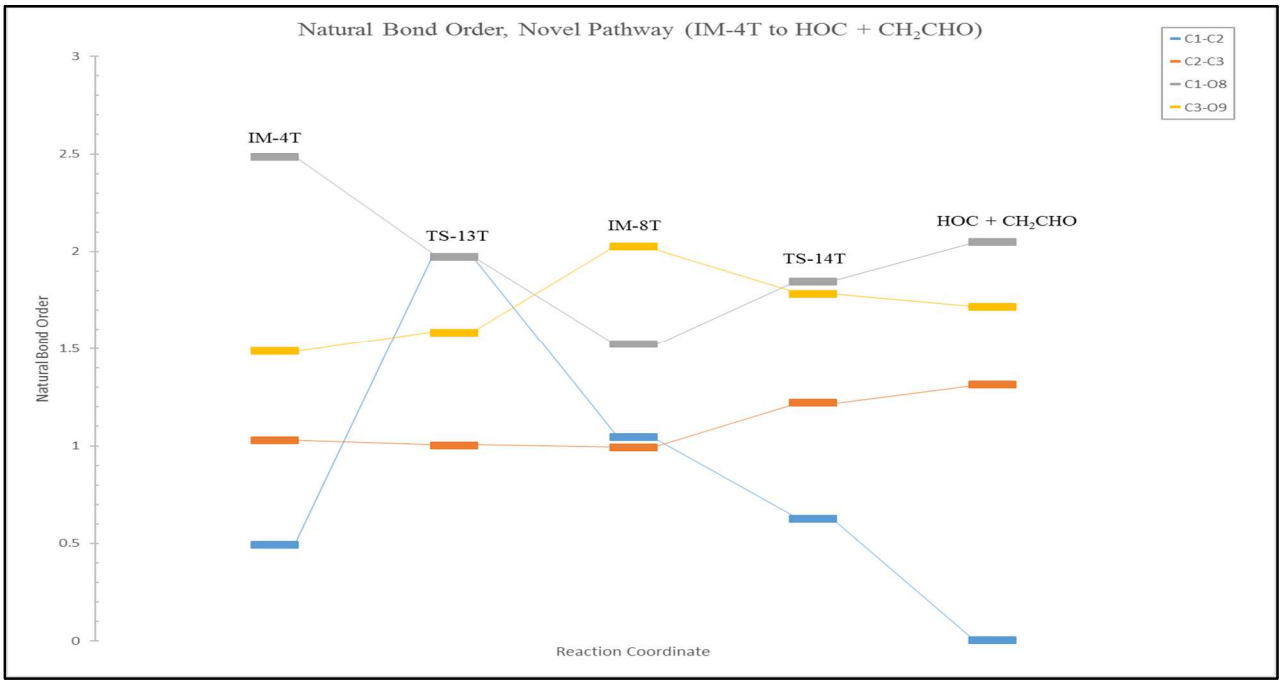

Figure 33. NBO Data for a novel HOC Pathway (IM-4T), calculated at the M06-2x/cc-pVTZ level of theory.

www.manaraa.com

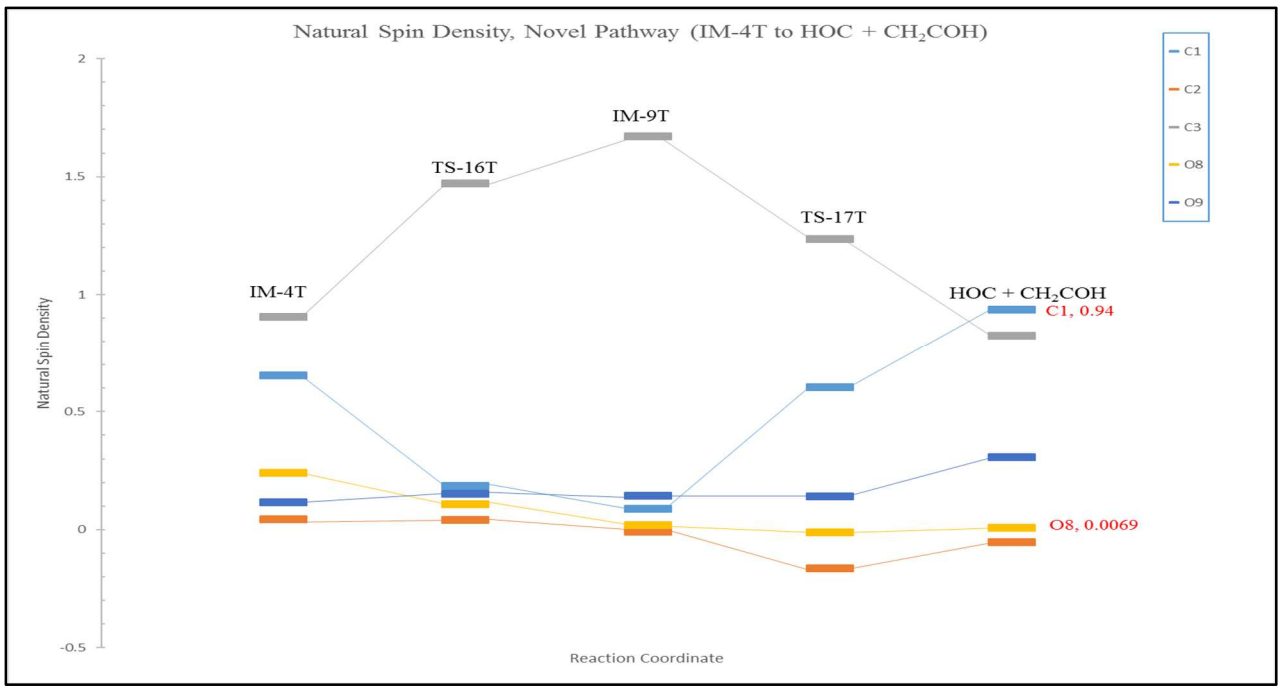

Figure 34. NSD Data for a novel HOC Pathway (IM-4T), calculated at the M06-2x/cc-pVTZ level of theory.

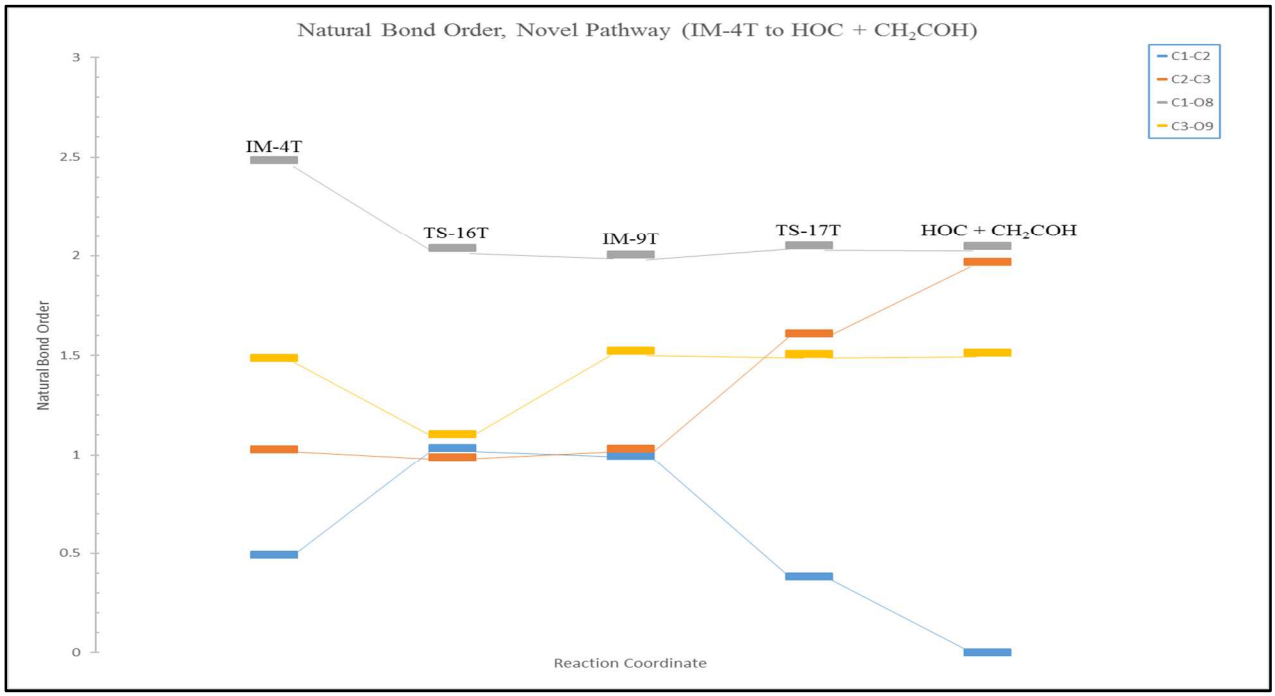

Figure 35. NBO Data for a novel HOC Pathway (IM-4T), calculated at the M06-2x/cc-pVTZ level of theory.

www.manaraa.com

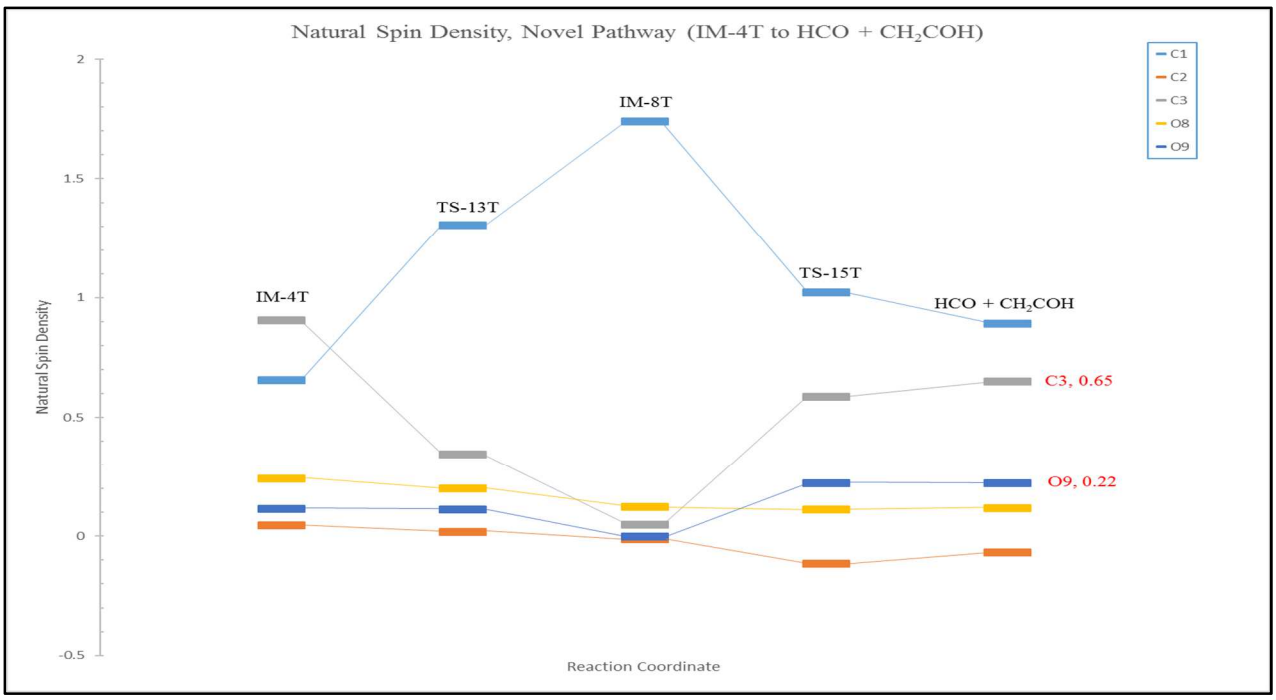

Figure 36. NSD Data for a novel HCO Pathway (IM-4T), calculated at the M06-2x/cc-pVTZ level of theory.

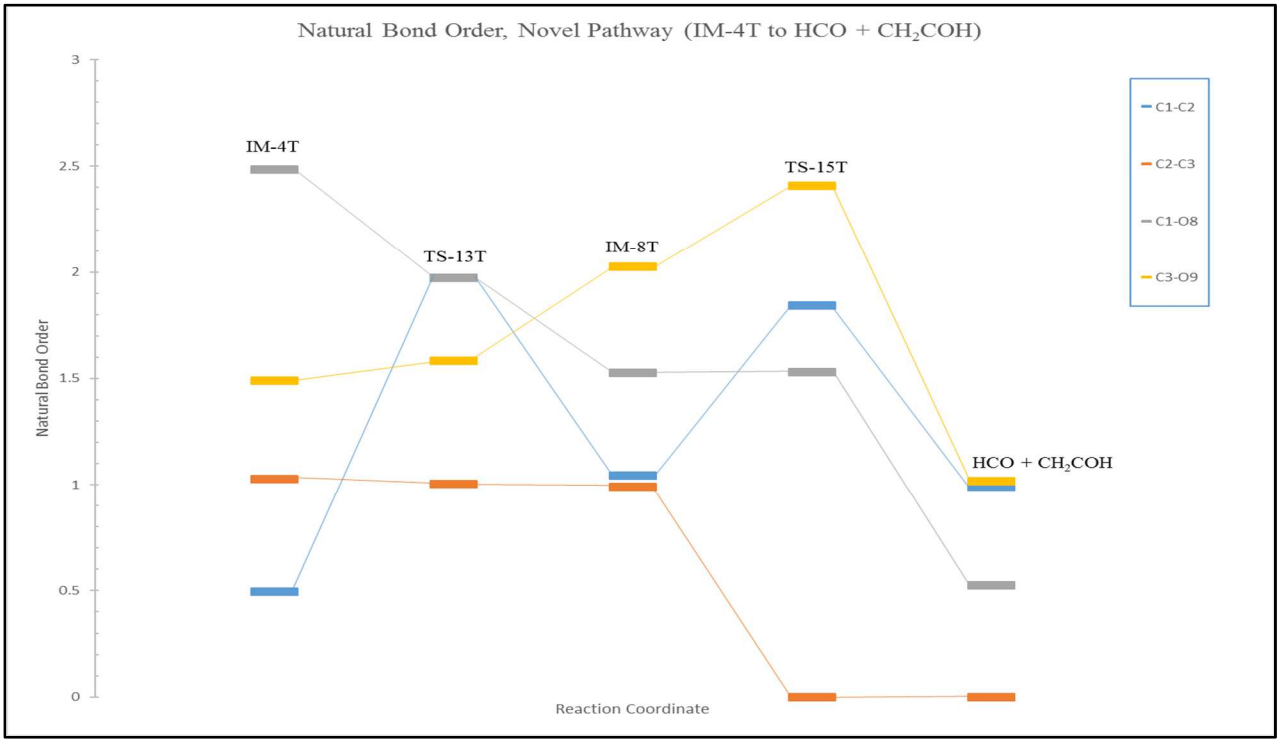

Figure 37. NBO Data for a novel HCO Pathway (IM-4T), calculated at the M06-2x/cc-pVTZ level of theory.

www.manaraa.com

Computational Results for $O(^3P)$ + 3-Butyn-1-ol

The other alkyne combustion reaction that has been investigated and presented here is the reaction of $O(^3P)$ + 3-butyn-1-ol. The numbering system for $O(^3P)$ + 3-butyn-1-ol is shown in Figure 38.

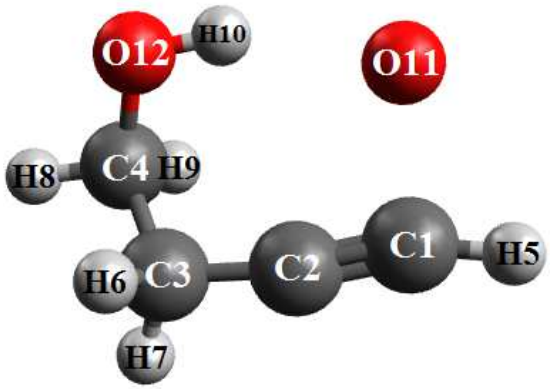

Figure 38. Numbering scheme for the $O(^3P)$ + 3-butyn-1-ol reaction.

Geometries: $O(^3P)$ + 3-Butyn-1-ol

Relevant bond lengths and angles for each IM and TS on the $O(^3P)$ + 3-butyn-1-ol triplet and singlet potential energy surfaces have been tabulated and are presented in tables 8 and 9. All geometries reported here are at the M06-2x/cc-pVTZ and MP2/6-311++G(d,p) levels of theory. As with the propargyl alcohol reaction discussed earlier, there is good agreement between the M06-2x and MP2 geometries with only a few deviations worth noting. First, the optimized structures for TS-3T show a difference of 20.4° between the M06-2x and MP2 results for the C2-C3-C4 bond angle. TS-7T shows a 10.6° difference between the M06-2x and MP2 results for the C1-C2-C3 bond angle. Again, the bond lengths for all structures across M06-2x and MP2 were in good agreement with minor differences on the order of 0.01 angstroms.

www.manaraa.com

Table 8. Selected bond lengths and angles for structures on the triplet potential energy surface of O(^{3}P) + 3-butyn-1-ol, calculated at the M06-2x/cc-pVTZ and MP2/6-311++G(d,p) levels of theory. The difference between the two levels, Δ, is also reported. The numbering scheme is shown in Figure 38.

Species	Level/Basis Set	C1-C2 (Å)	C2-C3 (Å)	C3-C4 (Å)	C1-O11 (Å)	C4-O12 (Å)	<C1-C2-C3 (°)	<C2-C3-C4 (°)	<O11-C1-C2 (°)	<C3-C4-O12 (°)
3-Butyn-1-ol	M06-2x/cc-pVTZ	1.198	1.461	1.531	-	1.407	176.300	110.500	-	111.900
	MP2/6-311++G(d,p)	1.220	1.463	1.532	-	1.416	176.000	110.700	-	111.900
	Δ	0.022	0.002	0.001	-	0.009	0.300	0.200	-	0.000
TS-1T	M06-2x/cc-pVTZ	1.217	1.453	1.541	2.008	1.398	170.800	110.900	99.900	112.100
	MP2/6-311++G(d,p)	1.213	1.454	1.541	1.860	1.405	170.200	112.200	101.600	112.200
	Δ	0.004	0.001	0.000	0.148	0.007	0.600	1.300	1.700	0.100
IM-1T	M06-2x/cc-pVTZ	1.413	1.462	1.542	1.234	1.398	137.700	114.100	123.500	112.300
	MP2/6-311++G(d,p)	1.452	1.474	1.543	1.205	1.405	134.800	114.600	124.000	112.800
	Δ	0.039	0.012	0.001	0.029	0.007	2.900	0.500	0.500	0.500
TS-2T	M06-2x/cc-pVTZ	1.423	1.430	1.516	1.235	1.403	134.900	119.700	121.700	111.100
	MP2/6-311++G(d,p)	1.450	1.441	1.518	1.216	1.411	132.500	119.800	123.000	111.500
	Δ	0.027	0.011	0.002	0.019	0.008	2.400	0.100	1.300	0.400
IM-2T	M06-2x/cc-pVTZ	1.435	1.454	1.501	1.227	1.415	121.400	120.800	122.900	110.600
	MP2/6-311++G(d,p)	1.470	1.459	1.505	1.201	1.422	120.300	120.200	123.700	110.700
	Δ	0.035	0.005	0.004	0.026	0.007	1.100	0.600	0.800	0.100
TS-3T	M06-2x/cc-pVTZ	1.447	1.448	1.485	1.227	1.407	123.300	112.200	124.800	112.200
	MP2/6-311++G(d,p)	1.456	1.456	1.493	1.226	1.413	122.100	132.600	125.100	112.600
	Δ	0.009	0.008	0.008	0.001	0.006	1.200	20.400	0.300	0.400
IM-3T	M06-2x/cc-pVTZ	1.517	1.467	1.474	1.200	1.418	114.600	130.800	124.800	111.400
	MP2/6-311++G(d,p)	1.515	1.482	1.484	1.215	1.425	116.400	133.900	125.400	112.900
	Δ	0.002	0.015	0.010	0.015	0.007	1.800	3.100	0.600	1.500
TS-4T	M06-2x/cc-pVTZ	2.184	1.332	1.481	1.185	1.412	90.600	133.100	116.300	111.500
	MP2/6-311++G(d,p)	2.130	1.329	1.486	1.200	1.419	90.800	133.700	116.900	111.800
	Δ	0.054	0.003	0.005	0.015	0.007	0.200	0.600	0.600	0.300
HCO + CH2CCH2OH	M06-2x/cc-pVTZ	-	1.307	1.480	1.173	1.415	-	136.600	-	112.200
	MP2/6-311++G(d,p)	-	1.292	1.482	1.186	1.421	-	138.700	-	112.800
	Δ	-	0.015	0.002	0.013	0.006	-	2.100	-	0.600
TS-5T	M06-2x/cc-pVTZ	2.148	1.302	1.515	1.191	1.408	117.600	124.800	109.800	111.200
	MP2/6-311++G(d,p)	2.029	1.284	1.516	1.194	1.415	117.500	126.200	115.200	111.300
	Δ	0.119	0.018	0.001	0.003	0.007	0.100	1.400	5.400	0.100
HCO + CHCHCH2OH	M06-2x/cc-pVTZ	-	1.303	1.509	1.171	1.409	-	124.800	-	111.800
	MP2/6-311++G(d,p)	-	1.284	1.516	1.194	1.415	-	126.200	-	111.300
	Δ	-	0.019	0.007	0.023	0.006	-	1.400	-	0.500
TS-6T	M06-2x/cc-pVTZ	1.379	1.482	1.540	1.217	1.401	135.300	111.500	135.800	111.800
	MP2/6-311++G(d,p)	1.393	1.487	1.543	1.214	1.406	134.100	111.500	137.400	112.200
	Δ	0.014	0.005	0.003	0.003	0.005	1.200	0.000	1.600	0.400
IM-4T	M06-2x/cc-pVTZ	1.436	1.491	1.523	1.194	1.408	126.600	116.900	130.300	112.200
	MP2/6-311++G(d,p)	1.456	1.497	1.526	1.198	1.416	126.600	117.300	130.100	112.500
	Δ	0.020	0.006	0.003	0.004	0.008	0.000	0.400	0.200	0.300
TS-7T	M06-2x/cc-pVTZ	2.227	1.472	1.529	1.135	1.409	124.700	114.300	114.700	112.500
	MP2/6-311++G(d,p)	2.143	1.481	1.534	1.149	1.418	114.100	113.200	113.400	112.300
	Δ	0.084	0.009	0.005	0.014	0.009	10.600	1.100	1.300	0.200
CO + CHCH2CH2OH	M06-2x/cc-pVTZ	-	1.468	1.530	1.123	1.409	-	111.600	-	112.200
	MP2/6-311++G(d,p)	-	1.480	1.530	1.140	1.418	-	112.600	-	112.300
	Δ	-	0.012	0.000	0.017	0.009	-	1.000	-	0.100
TS-8T	M06-2x/cc-pVTZ	1.438	1.481	1.499	1.196	1.413	123.900	121.700	130.300	112.000
	MP2/6-311++G(d,p)	1.449	1.484	1.501	1.205	1.423	124.000	122.100	129.900	112.200
	Δ	0.011	0.003	0.002	0.009	0.010	0.100	0.400	0.400	0.200

www.manaraa.com

Table 9. Continued selected bond lengths and angles for structures on the triplet potential energy surface of O(^{3}P) + 3-butyn-1-ol, calculated at the M06-2x/cc-pVTZ and MP2/6-311++G(d,p) levels of theory. The difference between the two levels, Δ, is also reported. The numbering scheme is shown in Figure 38.

Species	Level/Basis Set	C1-C2 (Å)	C2-C3 (Å)	C3-C4 (Å)	C1-O11 (Å)	C4-O12 (Å)	<C1-C2-C3 (°)	<C2-C3-C4 (°)	<O11-C1-C2 (°)	<C3-C4-O12 (°)
IM-5T	M06-2x/cc-pVTZ	1.512	1.497	1.490	1.177	1.421	114.400	122.200	127.900	112.400
	MP2/6-311++G(d,p)	1.516	1.501	1.495	1.189	1.429	114.500	121.800	127.900	112.800
	Δ	0.004	0.004	0.005	0.012	0.008	0.100	0.400	0.000	0.400
TS-9T	M06-2x/cc-pVTZ	2.142	1.458	1.492	1.137	1.412	109.200	123.400	113.500	112.400
	MP2/6-311++G(d,p)	2.100	1.469	1.496	1.152	1.422	110.600	123.300	114.700	112.200
	Δ	0.042	0.011	0.004	0.015	0.010	1.400	0.100	1.200	0.200
CO + CH2CHCH2OH	M06-2x/cc-pVTZ	-	1.451	1.493	1.122	1.413	-	121.800	-	112.800
	MP2/6-311++G(d,p)	-	1.460	1.498	1.139	1.422	-	121.500	-	112.700
	Δ	-	0.009	0.005	0.017	0.009	-	0.300	-	0.100
TS-10T	M06-2x/cc-pVTZ	1.522	1.501	1.477	1.175	1.368	112.300	119.400	126.300	120.200
	MP2/6-311++G(d,p)	1.524	1.504	1.482	1.187	1.376	113.300	119.100	126.800	119.800
	Δ	0.002	0.003	0.005	0.012	0.008	1.000	0.300	0.500	0.400
IM-6T	M06-2x/cc-pVTZ	1.511	1.536	1.494	1.178	1.356	114.400	114.900	128.800	120.600
	MP2/6-311++G(d,p)	1.514	1.538	1.501	1.191	1.364	115.000	115.100	128.800	120.200
	Δ	0.003	0.002	0.007	0.013	0.008	0.600	0.200	0.000	0.400
TS-11T	M06-2x/cc-pVTZ	2.173	1.503	1.490	1.141	1.360	107.500	115.100	112.700	120.700
	MP2/6-311++G(d,p)	2.128	1.508	1.497	1.155	1.367	109.900	115.500	114.600	120.400
	Δ	0.045	0.005	0.007	0.014	0.007	2.400	0.400	1.900	0.300
CO + CH2CH2CHOH	M06-2x/cc-pVTZ	M06-2x did not converge.								
	MP2/6-311++G(d,p)	-	1.496	1.499	1.140	1.370	-	112.900	-	118.000
	Δ	M06-2x did not converge.								
TS-12T	M06-2x/cc-pVTZ	1.431	1.449	1.496	1.226	1.364	121.000	118.500	123.100	120.900
	MP2/6-311++G(d,p)	1.470	1.451	1.499	1.197	1.373	119.400	118.200	124.100	120.100
	Δ	0.039	0.002	0.003	0.029	0.009	1.600	0.300	1.000	0.800
IM-7T	M06-2x/cc-pVTZ	1.425	1.491	1.507	1.231	1.350	121.900	114.400	123.100	119.100
	MP2/6-311++G(d,p)	1.456	1.493	1.514	1.207	1.355	121.000	114.700	123.800	119.000
	Δ	0.031	0.002	0.007	0.024	0.005	0.900	0.300	0.700	0.100
IM-8T	M06-2x/cc-pVTZ	1.513	1.490	1.460	1.203	1.362	113.800	120.900	124.800	119.300
	MP2/6-311++G(d,p)	1.516	1.495	1.468	1.217	1.370	113.800	121.000	124.900	118.500
	Δ	0.003	0.005	0.008	0.014	0.008	0.000	0.100	0.100	0.800
TS-14T	M06-2x/cc-pVTZ	2.238	1.354	1.470	1.175	1.365	104.100	122.300	119.300	118.500
	MP2/6-311++G(d,p)	MP2 did not converge.								
	Δ									
HCO + CH2CHCHOH	M06-2x/cc-pVTZ	-	1.375	1.382	1.171	1.343	-	126.300	-	125.400
	MP2/6-311++G(d,p)	-	1.381	1.377	1.184	1.348	-	126.400	-	126.000
	Δ	-	0.006	0.005	0.013	0.005	-	0.100	-	0.600
TS-15T	M06-2x/cc-pVTZ	1.552	1.476	1.486	1.274	1.396	119.500	120.300	116.300	111.700
	MP2/6-311++G(d,p)	MP2 did not converge.								
	Δ									
IM-9T	M06-2x/cc-pVTZ	1.560	1.478	1.483	1.289	1.384	119.100	122.300	113.100	114.800
	MP2/6-311++G(d,p)	MP2 did not converge.								
	Δ									
TS-16T	M06-2x/cc-pVTZ	1.512	1.503	1.436	1.202	1.342	111.200	119.600	124.400	132.600
	MP2/6-311++G(d,p)	1.517	1.506	1.441	1.217	1.352	111.200	120.300	124.400	132.400
	Δ	0.005	0.003	0.005	0.015	0.010	0.000	0.700	0.000	0.200
IM-10T	M06-2x/cc-pVTZ	1.499	1.532	1.487	1.205	1.330	114.600	113.600	125.200	126.000
	MP2/6-311++G(d,p)	1.504	1.534	1.496	1.219	1.339	114.900	114.000	125.200	125.400
	Δ	0.005	0.002	0.009	0.014	0.009	0.300	0.400	0.000	0.600

www.manaraa.com

Potential Energy Profiles: O(^{3}P) + 3-Butyn-1-ol

All potential energies presented in this section are referenced relative to the reactants of the reaction, 3-butyn-1-ol and O(^{3}P). This reaction has not been investigated computationally prior to this project. All of the PEPs presented here are determined at the M06-2x/cc-pVTZ and CCSD(T)/cc-pVTZ//M06-2x/cc-pVTZ levels of theory because, as discussed earlier, the MP2/6-311++G(d,p) level of theory gave potential energies that were consistently further off from the higher level CCSD(T) results than were the M06-2x results. Again, all single-point energies presented here were calculated at the CCSD(T)/cc-pVTZ level of theory which were carried out on the M06-2x/cc-pVTZ optimized geometries. Figure 39 shows the PEP for two HCO radical formation pathways at the M06-2x/cc-pVTZ level of theory which, again, demonstrates the importance of collecting single-point energies via CCSD(T) as TS-1T violates the definition of a transition state by being lower in energy than IM-0 at the M06-2x/cc-pVTZ level.

www.manaraa.com

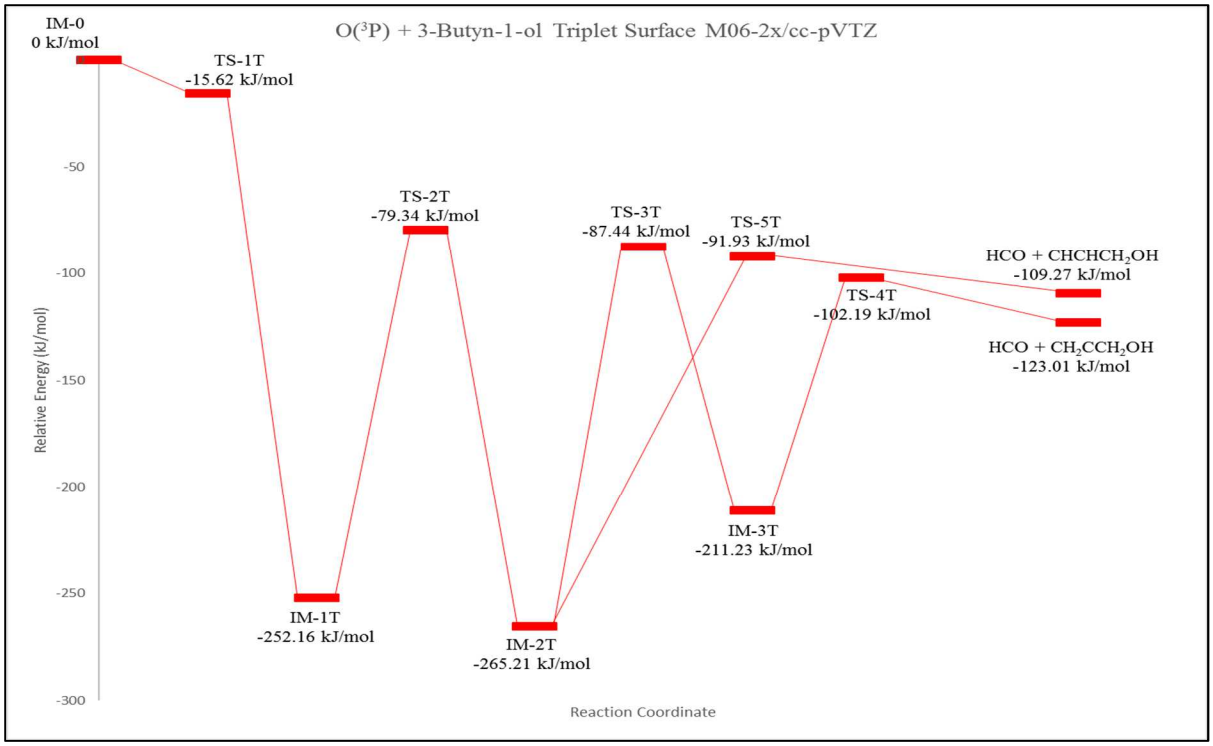

Figure 39. Two HCO formation pathways for O(^{3}P) + 3-butyn-1-ol, M06-2x/cc-pVTZ level.

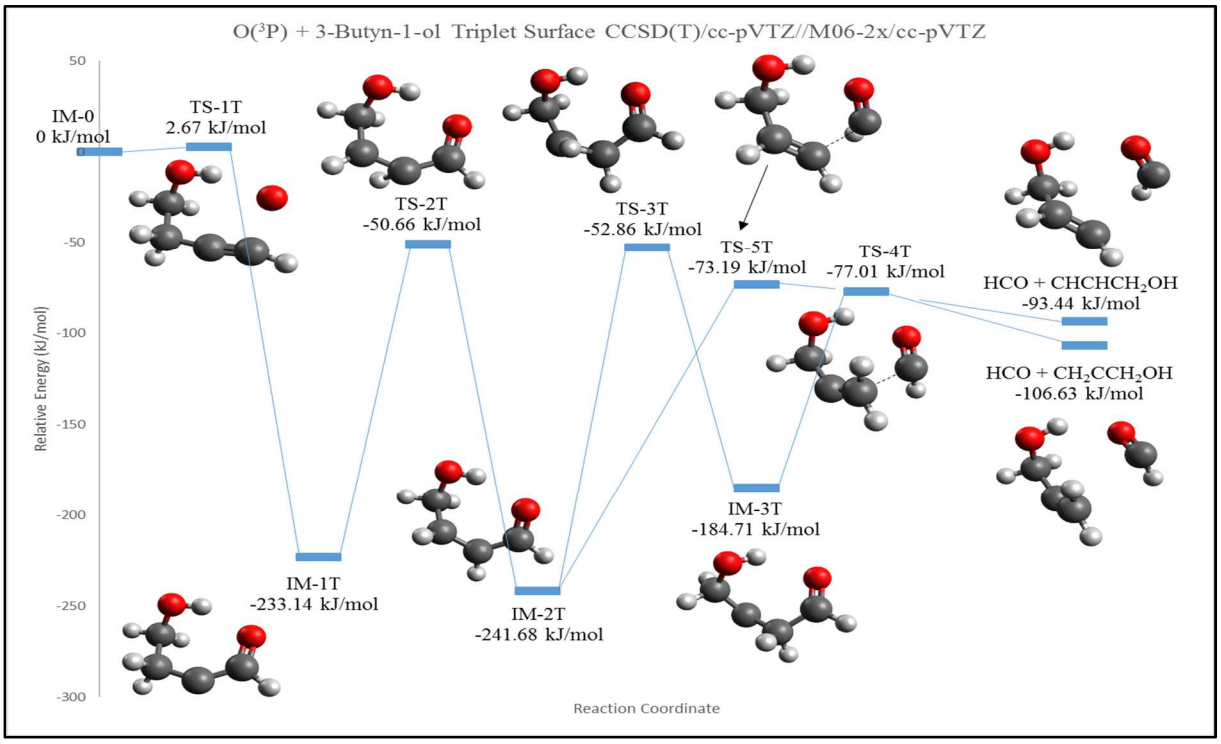

Figure 40. Two HCO formation pathways for O(^{3}P) + 3-butyn-1-ol, CCSD(T)//M06-2x/cc-pVTZ level.

www.manaraa.com

As seen in Figure 40, the lowest energy pathway for HCO dissociation involves two H-shifts taking place. After the formation of the adduct (IM-1T), a hydrogen shift takes place from C3 to C2, forming IM-2T. From IM-2T, HCO dissociation occurs via TS-5T at a relative energy of -73.19 kJ/mol. However, IM-2T may undergo a second hydrogen shift from C3 to C2 via TS-3T which then results in HCO dissociation at a relative energy of -106.63 kJ/mol. Figure 41 shows another PEP for two additional pathways: one HCO radical pathway and one HOC radical pathway. It is worth noting that TS-13T did not converge at the M06-2x/cc-pVTZ level of theory, and so the MP2/6-311++G(d,p) structure and relative energy were used to construct this PEP.

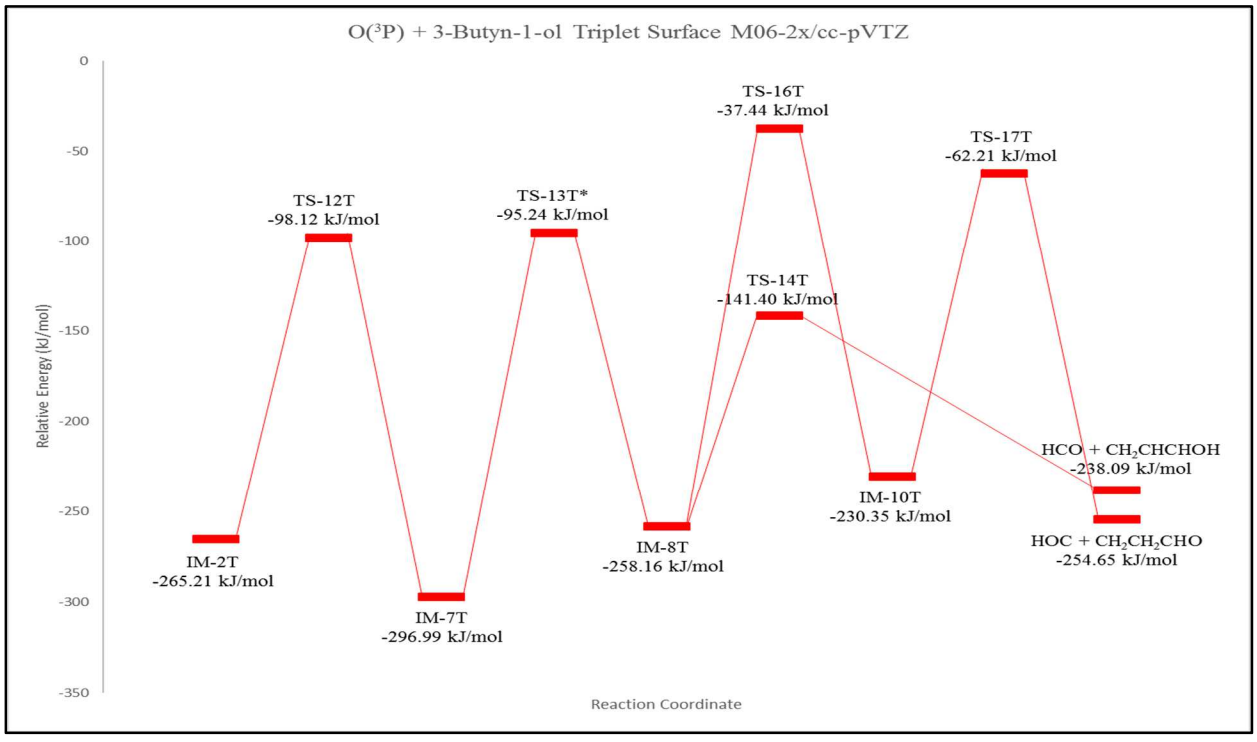

Figure 41. Additional HCO/HOC formation pathways for O(^{3}P) + 3-butyn-1-ol, M06-2x/cc-pVTZ level.

www.manaraa.com

Figure 42 shows the CCSD(T)//M06-2x/cc-pVTZ energies of the HCO and HOC radical production pathways shown in Figure 41. Figure 42 reveals the two lowest energy pathways that result in HCO radical formation, based upon the isomerization of HOC as discussed earlier. Both pathways split off from IM-2T (Figure 40). Similar mechanisms are observed for the O(^{3}P) + 3-butyn-1-ol reaction as were obtained for the O(^{3}P) + propargyl alcohol reaction, namely the role of the hydroxyl substituent engaging in the reaction mechanism. As seen in Figure 41, the hydroxyl group on C4 eventually forms the HOC product via TS-17T. The final pathway presented here is another HOC dissociation pathway and is shown in Figures 43 and 44.

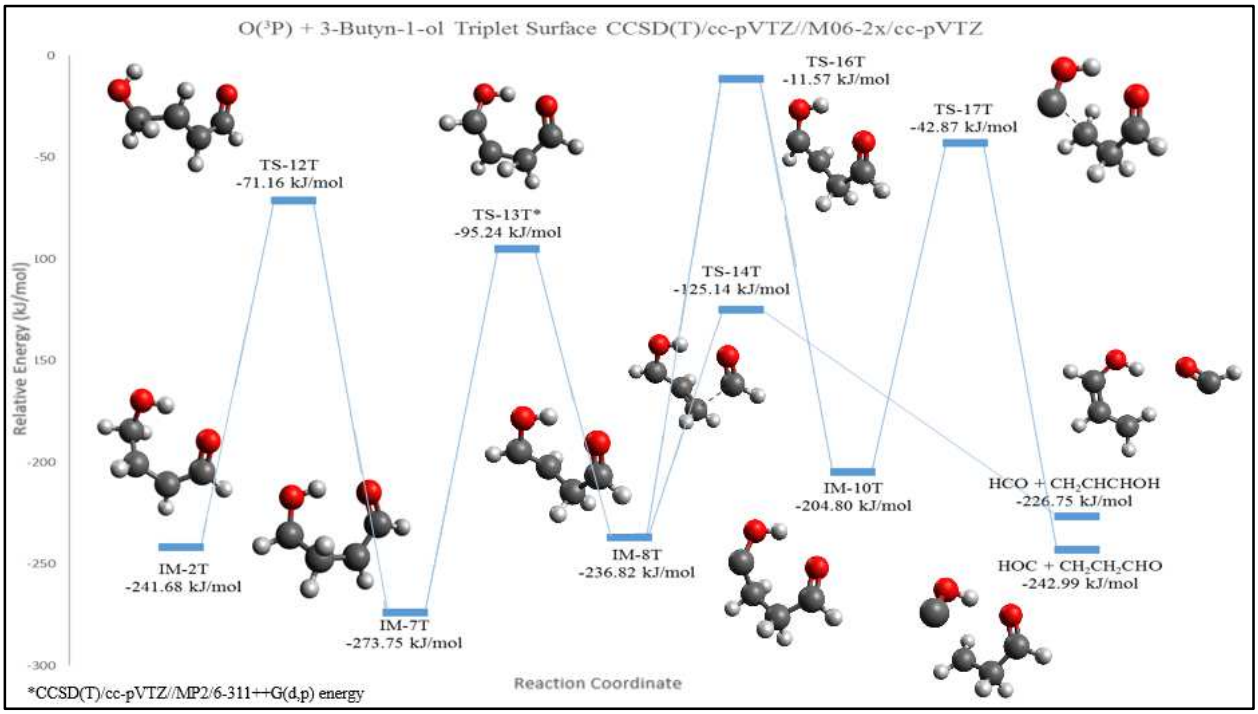

Figure 42. Additional HCO/HOC formation pathways for O(^{3}P) + 3-butyn-1-ol, CCSD(T)//M06-2x/cc-pVTZ level.

www.manaraa.com

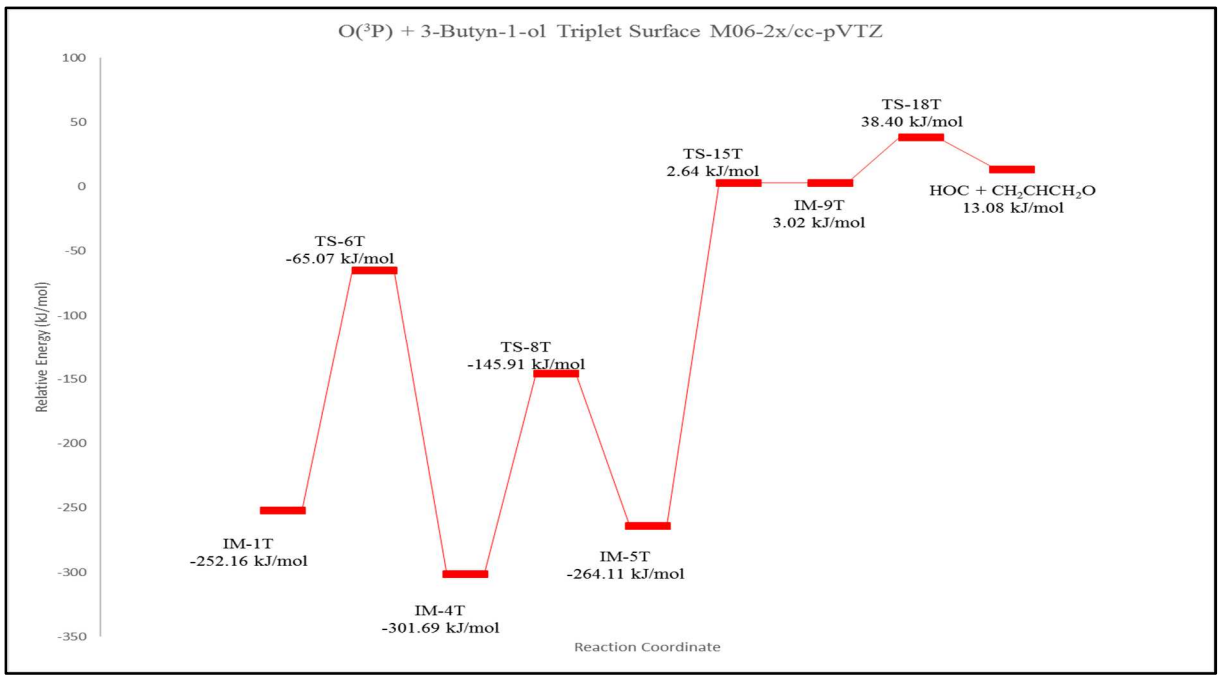

Figure 43. Final HOC dissociation pathway found for O(^{3}P) + 3-butyn-1-ol, M06-2x/cc-pVTZ level.

www.manaraa.com

Figure 44 reveals that the hydroxyl group plays an important role in the formation of HOC. Similar to a couple of the novel pathways for the propargyl alcohol reaction, a hydrogen atom shifts from O12 to O11 via TS-15T, which is followed by the dissociation of HOC via TS-18T.

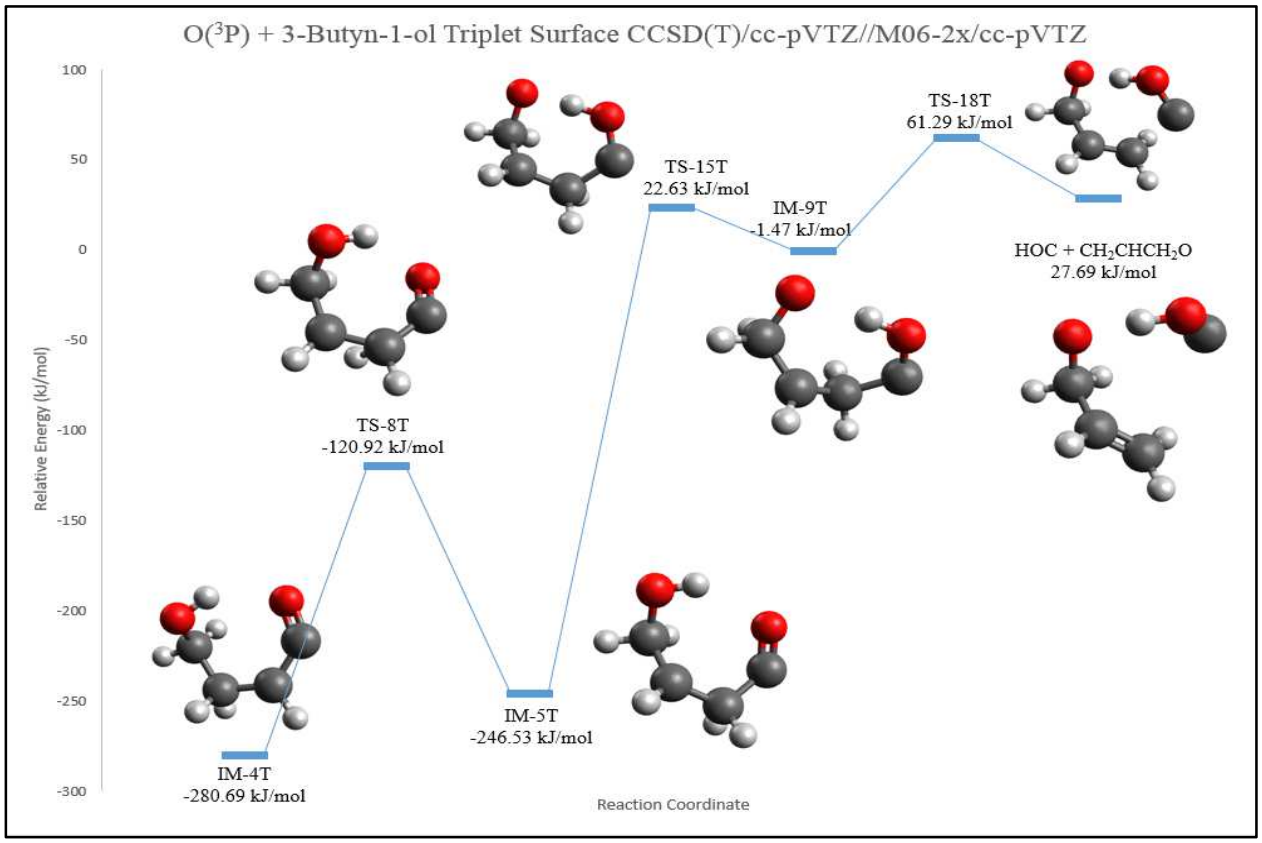

Figure 44. Final HOC dissociation pathway found for O(^{3}P) + 3-butyn-1-ol, CCSD(T)//M06-2x/cc-pVTZ.

www.manaraa.com

NRT Analysis: O(^{3}P) + 3-Butyn-1-ol

NSD and NBO data for the reaction of O(^{3}P) + 3-butyn-1-ol is shown in Figures 45-54. Again, only the C and O atoms are shown on the plots to keep them from being too cluttered. NSD and NBO plots for the first HCO dissociation pathway (Figure 39) are shown in Figures 45 and 46, respectively. Each individual pathway for HCO/HOC radical has its own NSD and NBO plots.

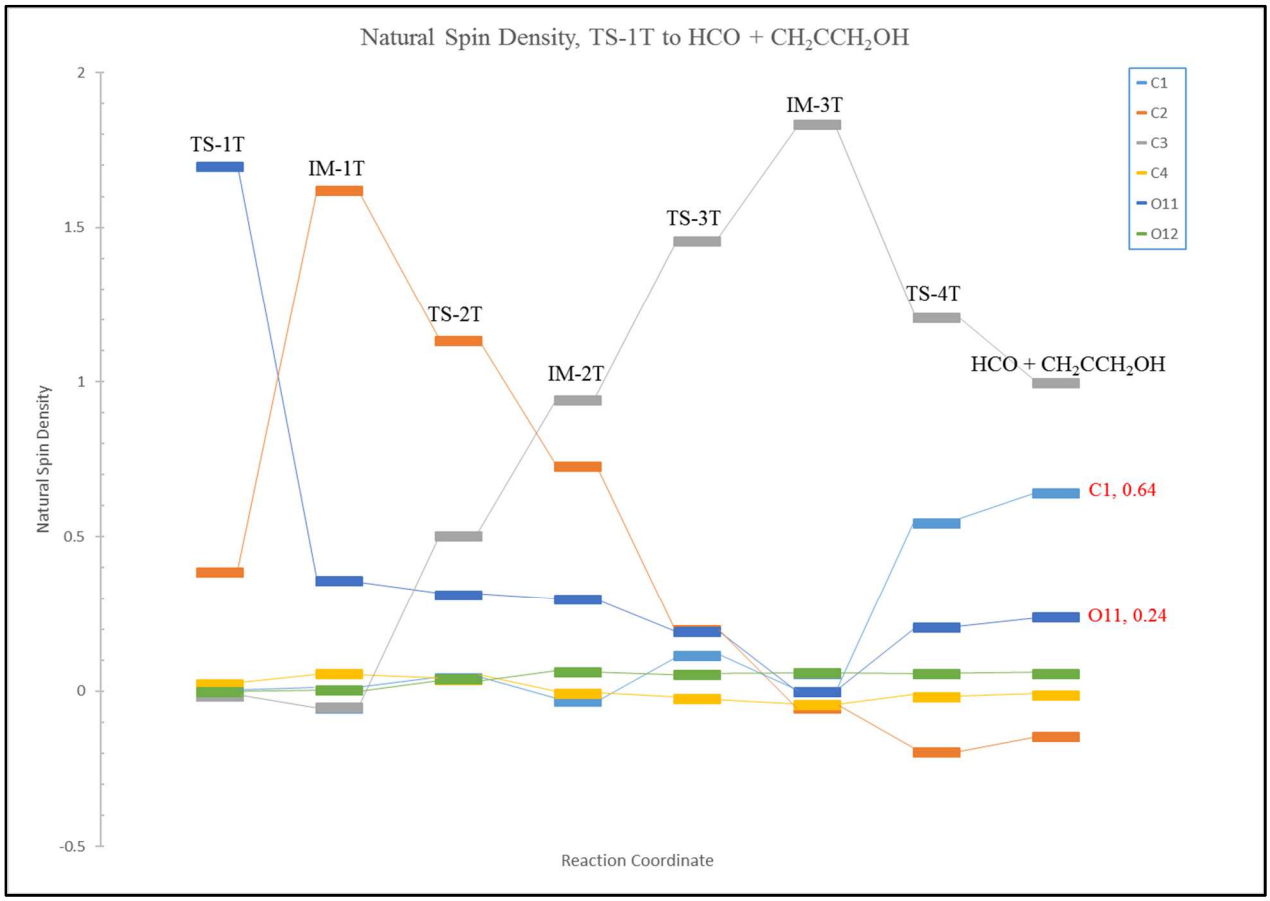

Figure 45. NSD Data for the HCO pathway shown in Figure 40, calculated at the M06-2x/cc-pVTZ level of theory.

www.manaraa.com

As seen in Figure 45, similar trends are observed for the HCO dissociation from 3-butyn-1-ol and from propargyl alcohol. The reaction begins with almost all of the NSD on the incoming triplet oxygen atom, O11, which then quickly transfers to C2 of the system after the formation of the adduct (IM-1T). After the dissociation step for HCO radical formation takes place, NSD is distributed in a similar 1:3 (O:C) ratio giving the HCO radical a total NSD of 1 (including the NSD of H5, not shown here). Figure 46 confirms the bond orders expected for HCO radical, with a C1-O11 NBO of about 2.5.

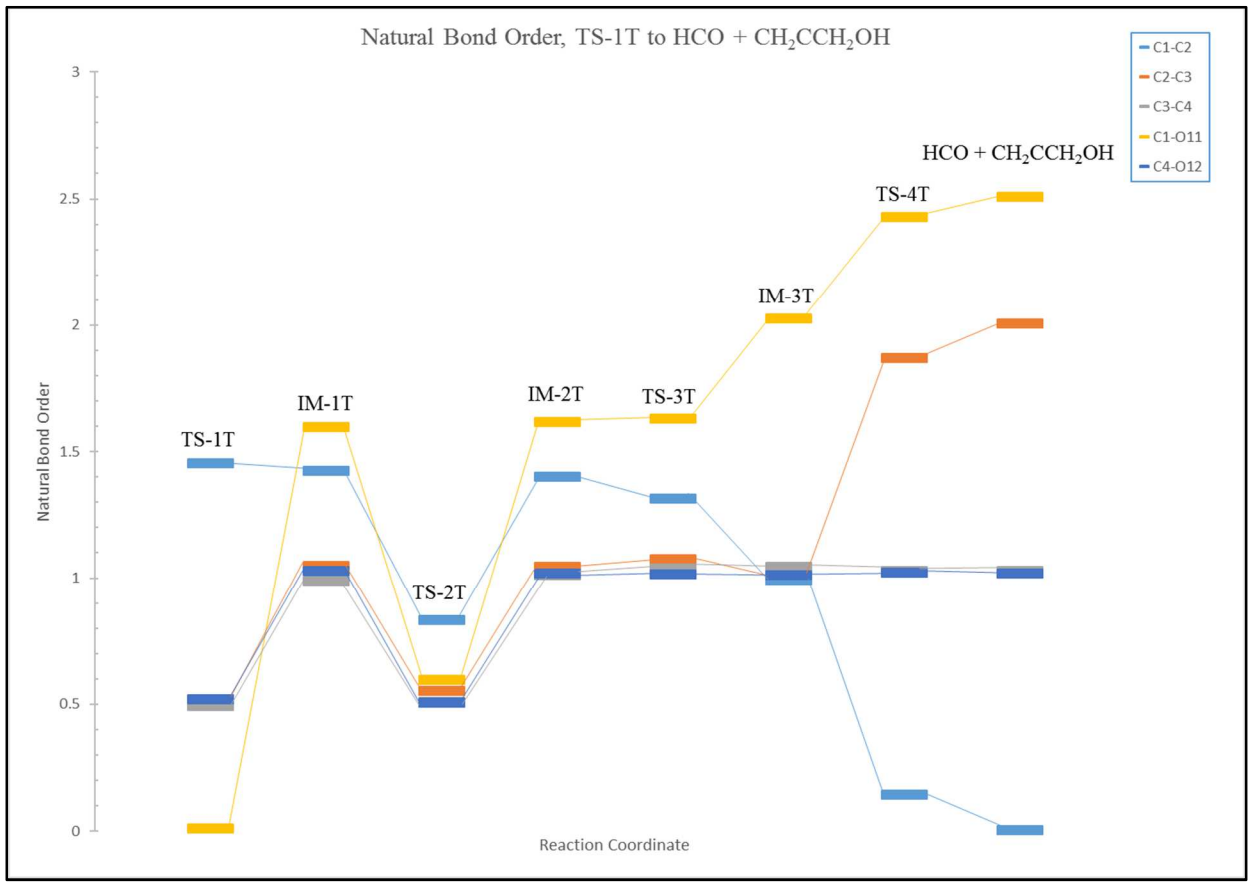

Figure 46. NBO Data for the HCO pathway shown in Figure 40, calculated at the M06-2x/cc-pVTZ level of theory.

www.manaraa.com

The NRT results of all the other O(^{3}P) + 3-butyn-1-ol reaction pathways are presented in figures 47-54. Similar trends are observed in these figures as were observed in the NRT results for the O(^{3}P) + propargyl alcohol, namely the 1:3 (O:C) NSD distribution ratio on the HCO radical product and an NSD of ~1 on the carbon atom of HOC radical products.

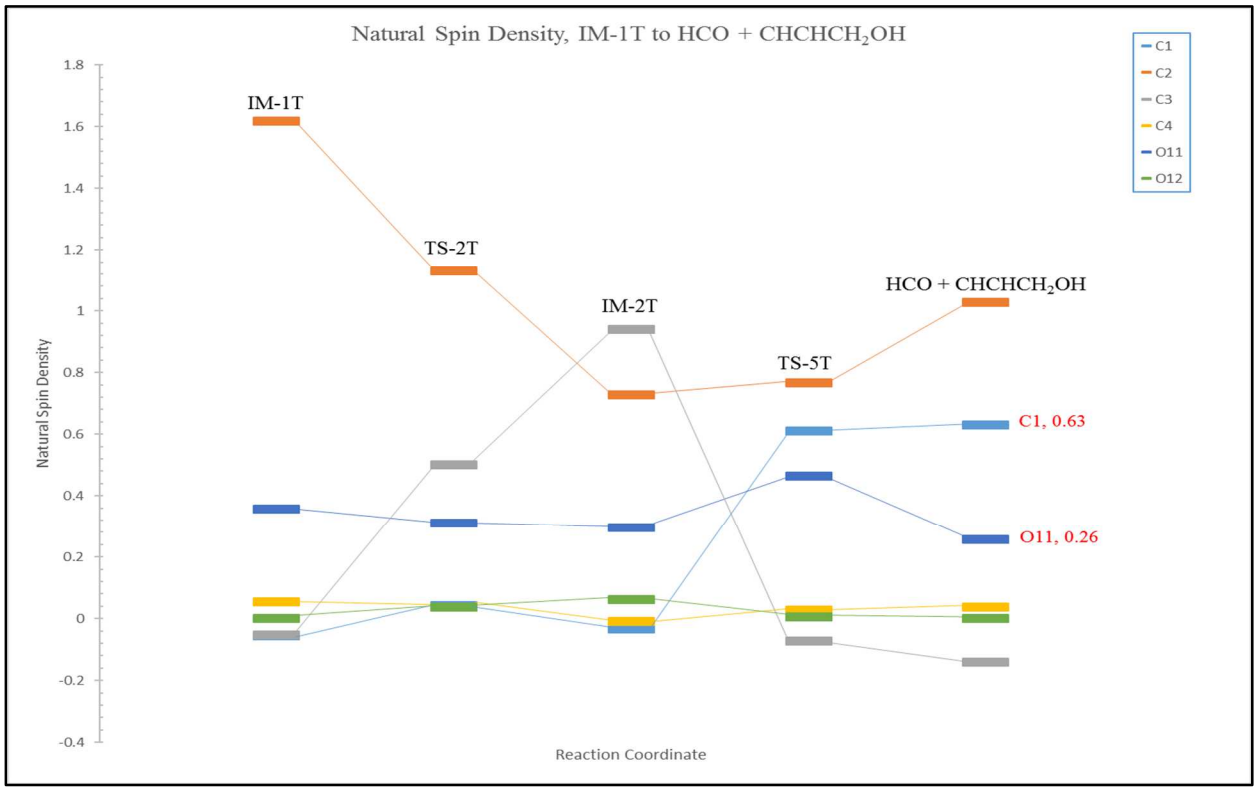

Figure 47. NSD Data for the other HCO pathway shown in Figure 40, calculated at the M06-2x/cc-pVTZ level of theory.

www.manaraa.com

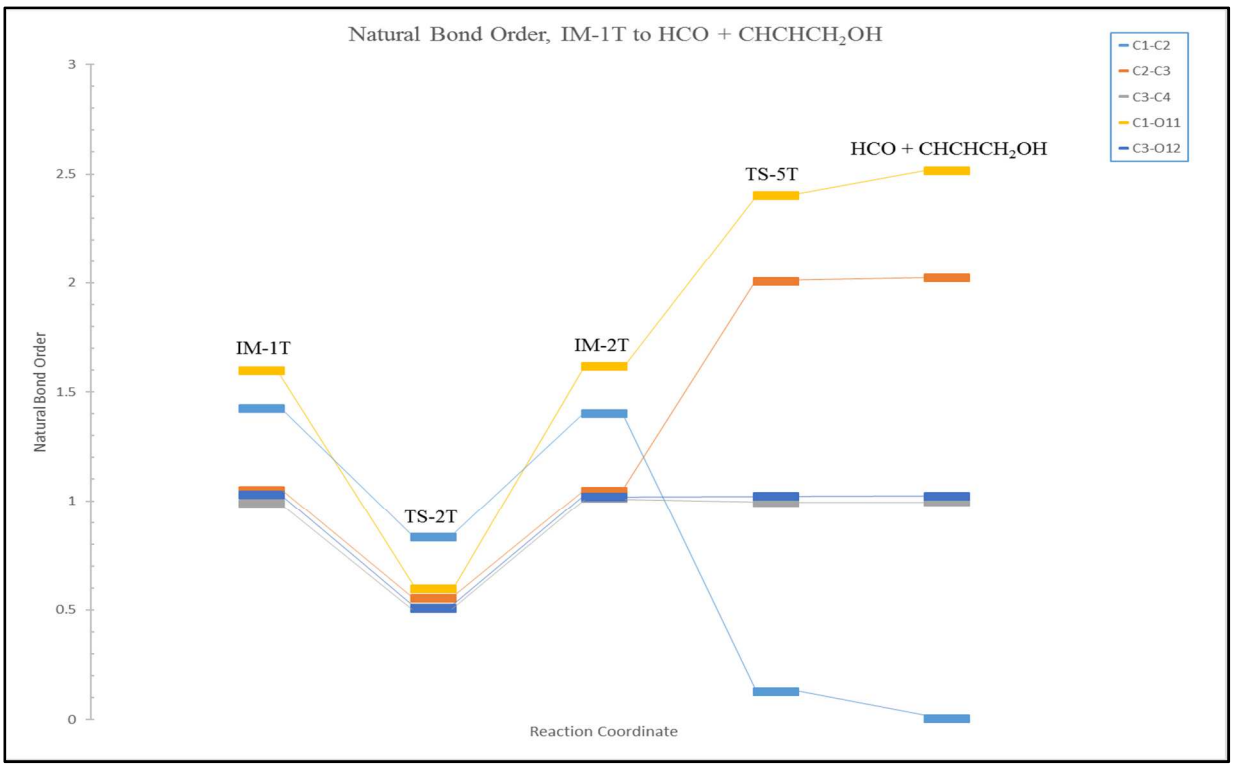

Figure 48. NBO Data for the other HCO pathway shown in Figure 40, calculated at the M06-2x/cc-pVTZ level of theory.

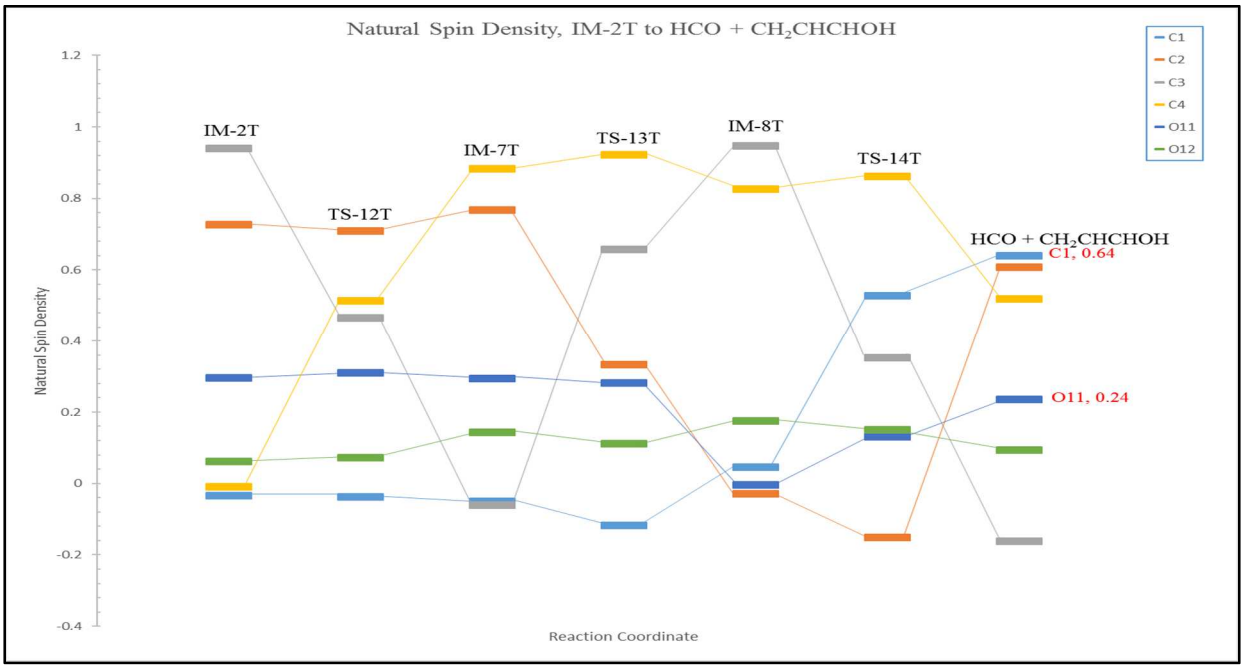

Figure 49. NSD Data for the HCO pathway shown in Figure 42, calculated at the M06-2x/cc-pVTZ level of theory.

www.manaraa.com

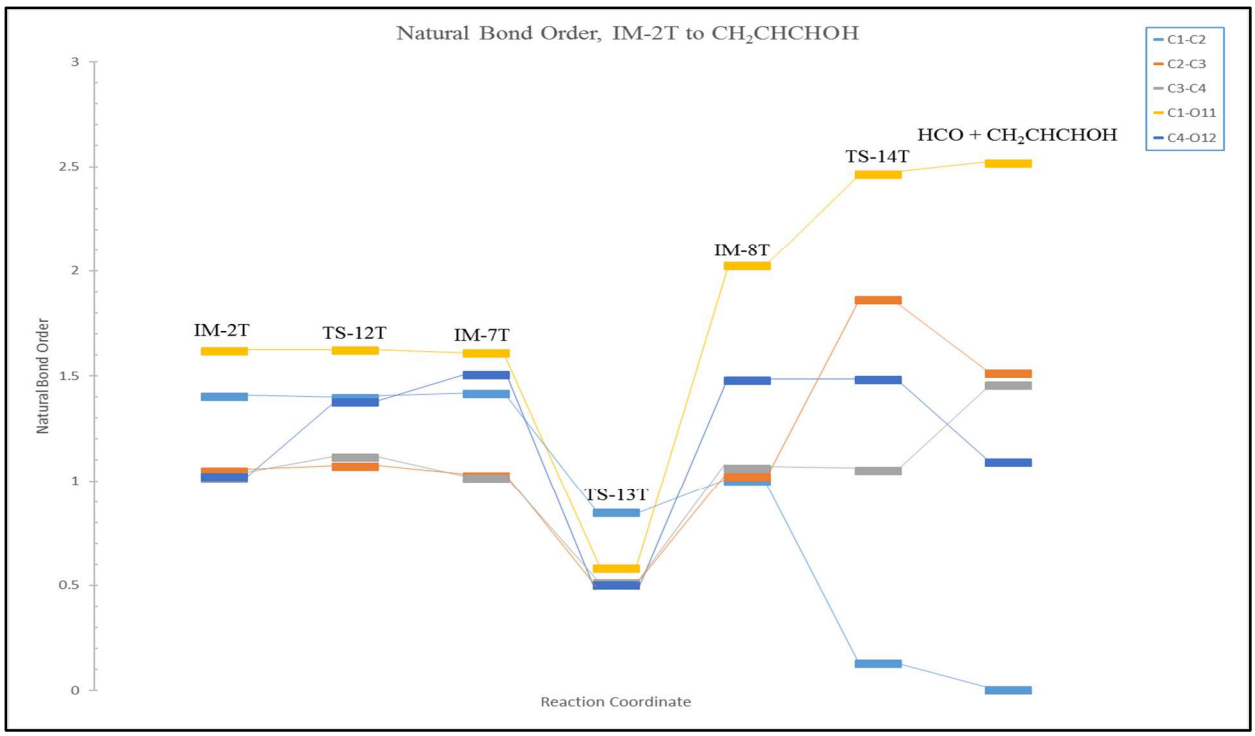

Figure 50. NBO Data for the HCO pathway shown in Figure 42, calculated at the M06-2x/cc-pVTZ level of theory.

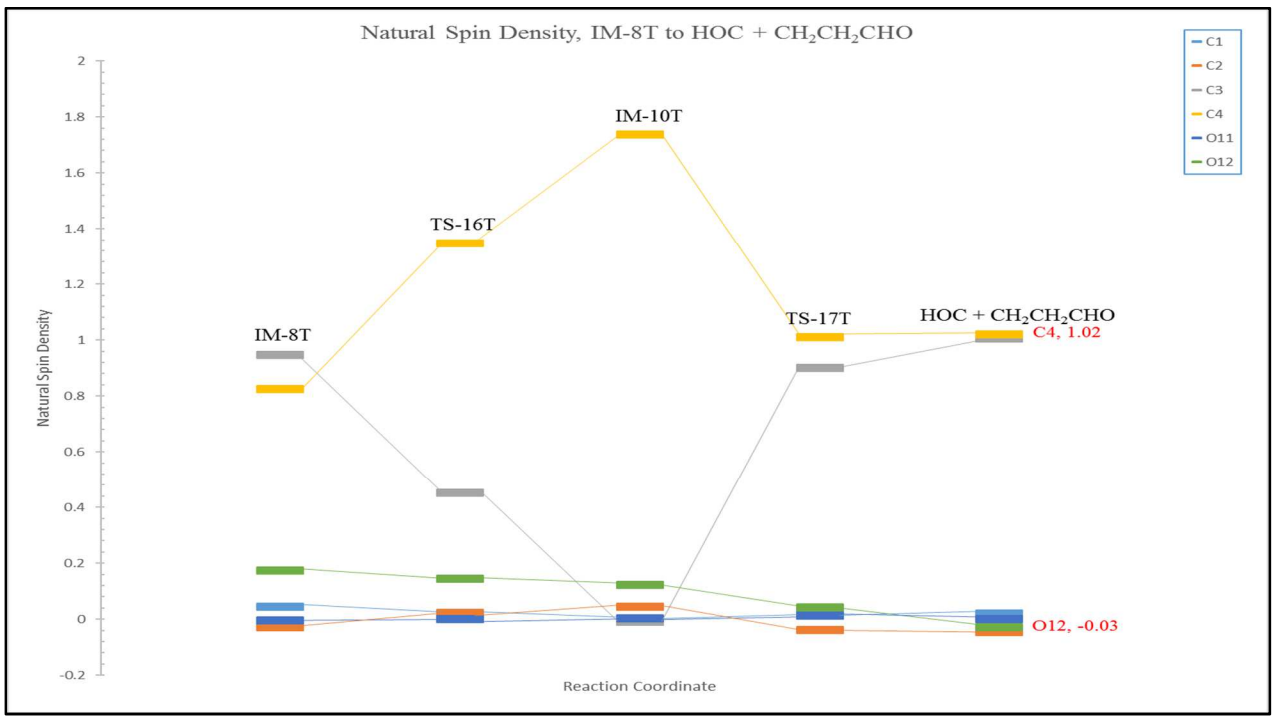

Figure 51. NSD Data for the HOC pathway shown in Figure 42, calculated at the M06-2x/cc-pVTZ level of theory.

www.manaraa.com

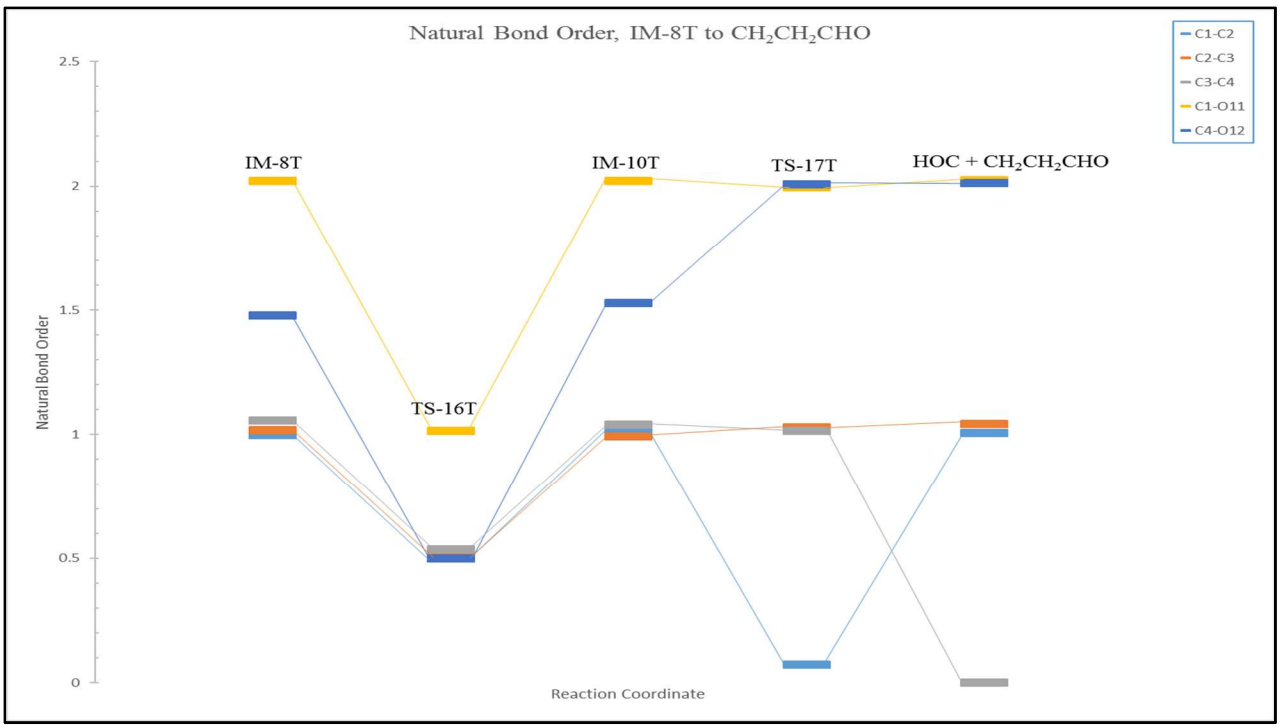

Figure 52. NBO Data for the HOC pathway shown in Figure 42, calculated at the M06-2x/cc-pVTZ level of theory.

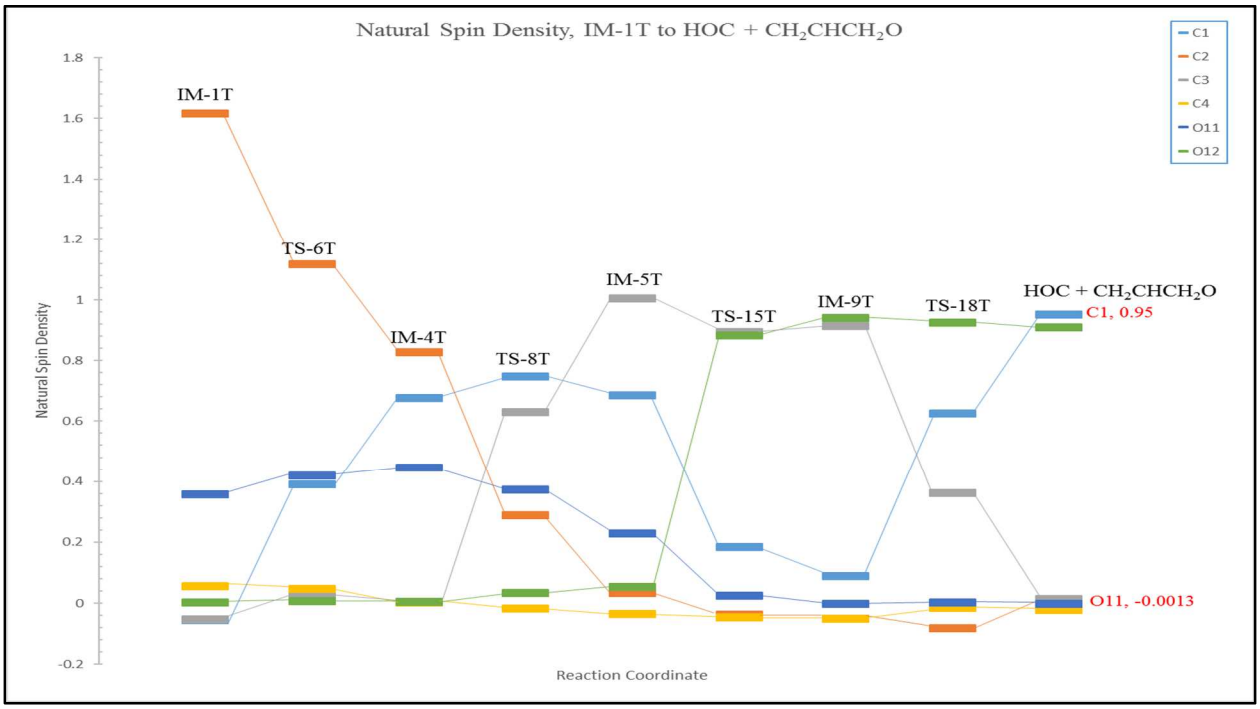

Figure 53. NSD Data for the HOC pathway shown in Figure 44, calculated at the M06-2x/cc-pVTZ level of theory.

www.manaraa.com

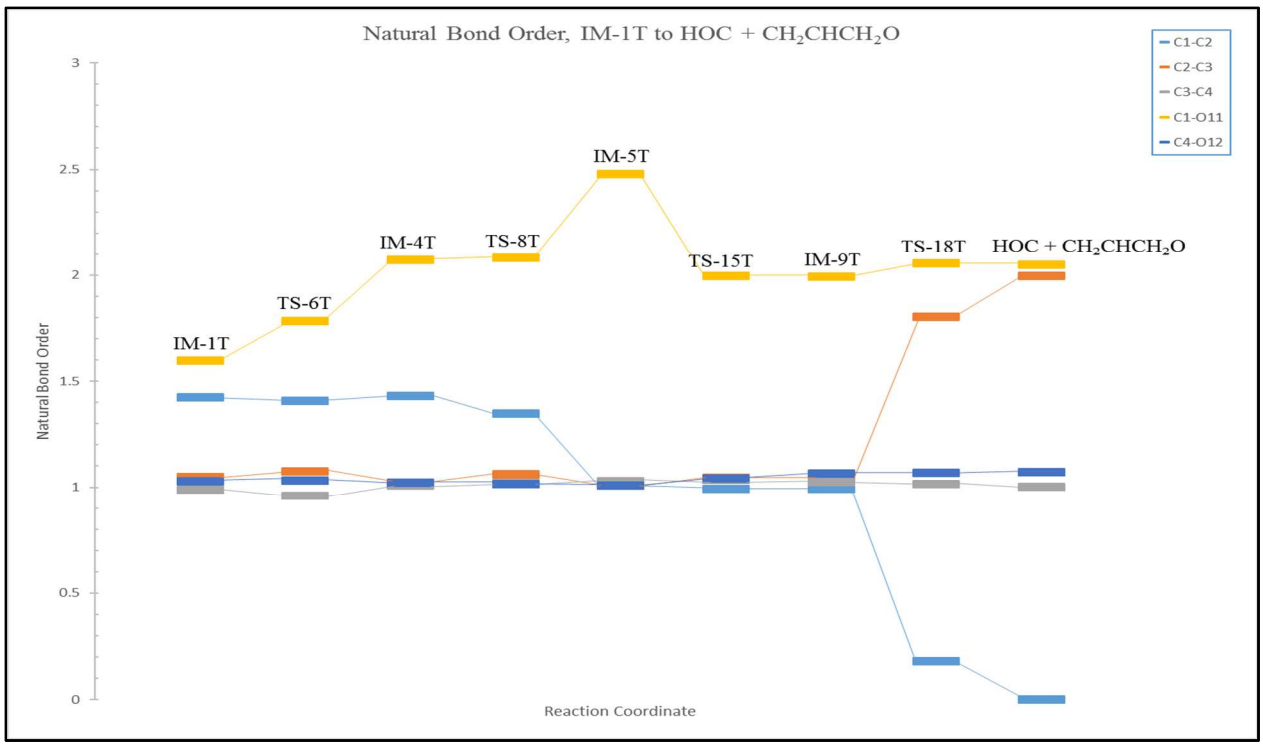

Figure 54. NBO Data for the HOC pathway shown in Figure 44, calculated at the M06-2x/cc-pVTZ level of theory.

Following the trends observed in the propargyl alcohol reaction, the HOC formation pathways for O(^{3}P) + 3-butyn-1-ol reaction reveal that nearly all of the NSD is on the C and H atoms of the HOC product, with almost none present on the O atom. The bond orders in HOC are also consistently lower than they are for HCO, with an NBO of about 2 between the C and O atoms in HOC and an NBO of about 2.5 between the C and O atoms in HCO.

www.manaraa.com

Subsequent Pathways

The final set of results for this project revolves around the formation of additional HCO/HOC radical products after one dissociation of HCO/HOC radical has already occurred. Of the $O(^3P)$ + alkyne reactions studied to date, these "subsequent" pathways are totally unique to the reaction of $O(^3P)$ + 3-butyn-1-ol and may also aid in explaining the variations of HCO radical absorption intensity observed in the CRDLAS data. The PEPs shown here were generated by obtaining optimized structures at the M06-2x/cc-pVTZ level and then running single-point energy calculations at the CCSD(T)/cc-pVTZ level. All energies shown here are measured relative to the reactant; i.e., the fragment radical from which HCO/HOC radical subsequently dissociates. The first subsequent pathway revealed here branches off from the first PEP shown for $O(^3P)$ + 3-butyn-1-ol (Figure 39). After HCO dissociates, a fragment CH_2CCH_2OH radical is left over. The reaction pathway for CH_2CCH_2OH radical to form HOC + ethylene is shown in Figure 55. The next subsequent pathway branches off from the other fragment product shown in Figure 39. $CHCHCH_2OH$ radical may also follow a reaction pathway that results in the formation of HOC + ethylene, which is shown in Figure 56. The final subsequent pathway branches off from the product fragment in Figure 41. The CH_2CH_2CHO radical may follow a one-step reaction pathway to form HCO + ethylene, as shown in Figure 57.

www.manaraa.com

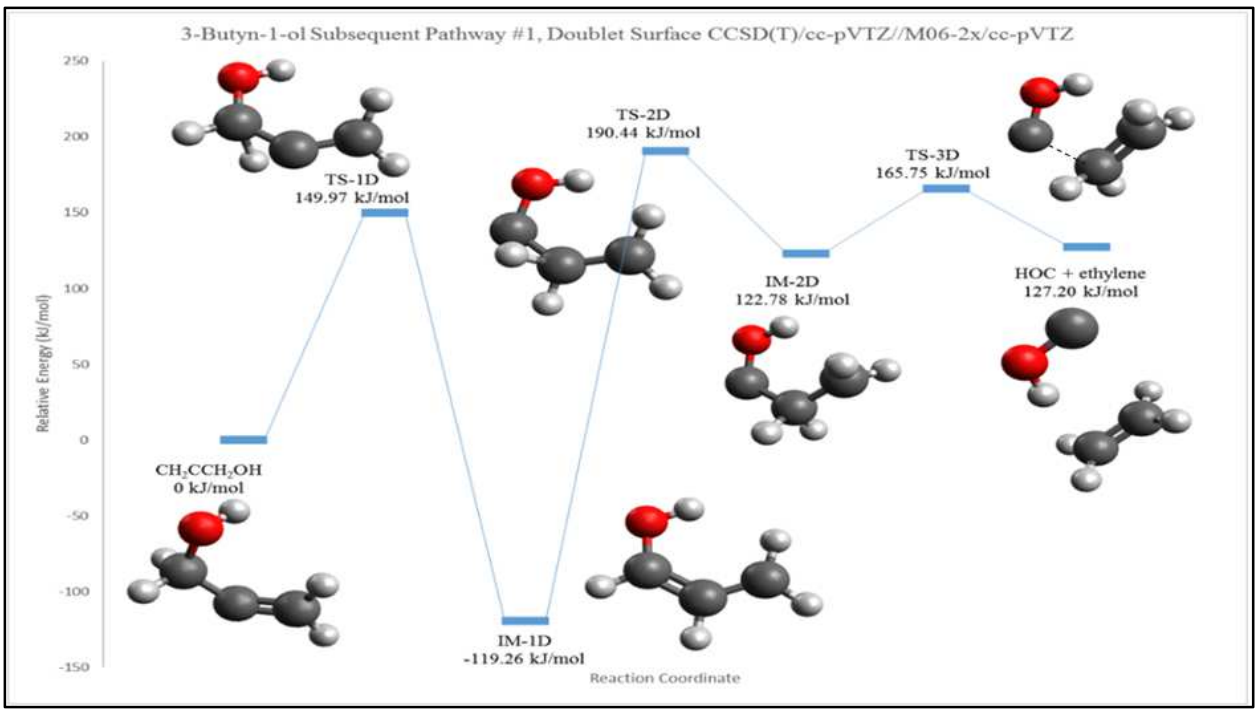

Figure 55. Subsequent dissociation pathway for HOC, CCSD(T)//M06-2x/cc-pVTZ level.

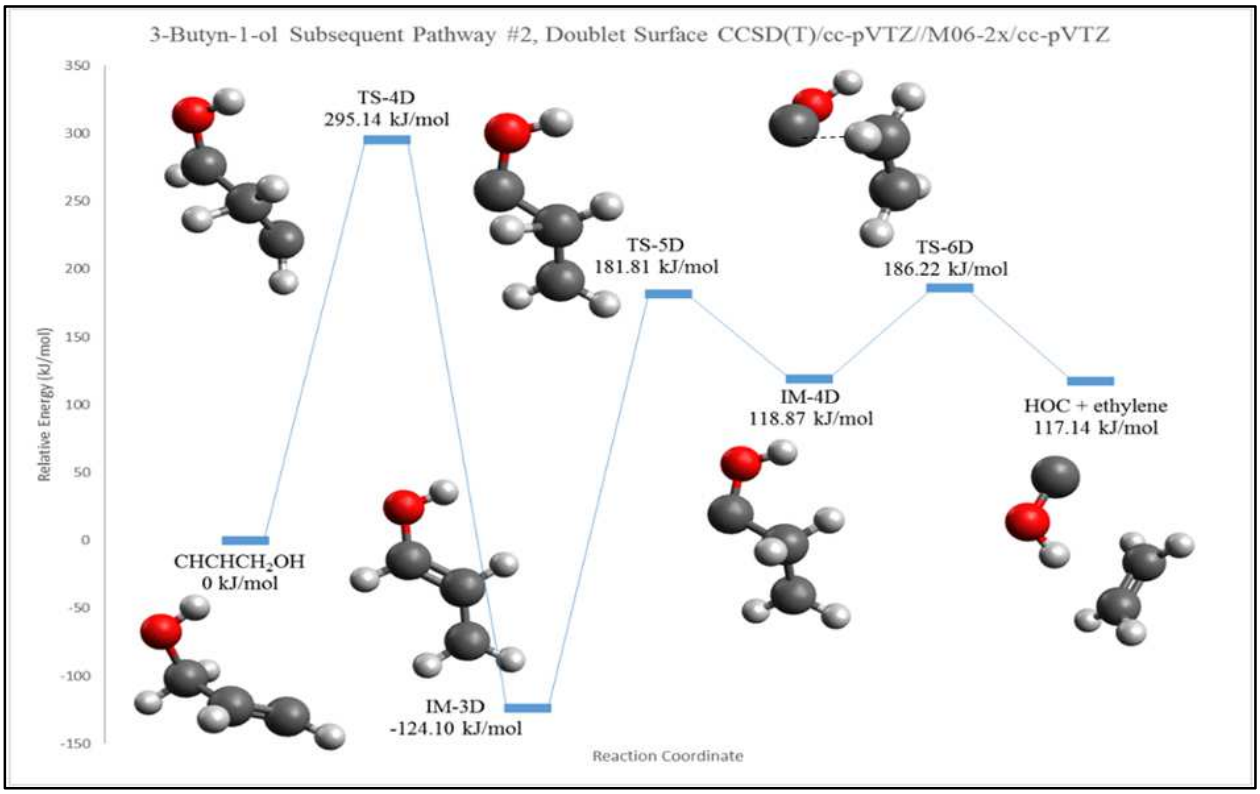

Figure 56. Subsequent dissociation pathway for HOC, CCSD(T)//M06-2x/cc-pVTZ level.

www.manaraa.com

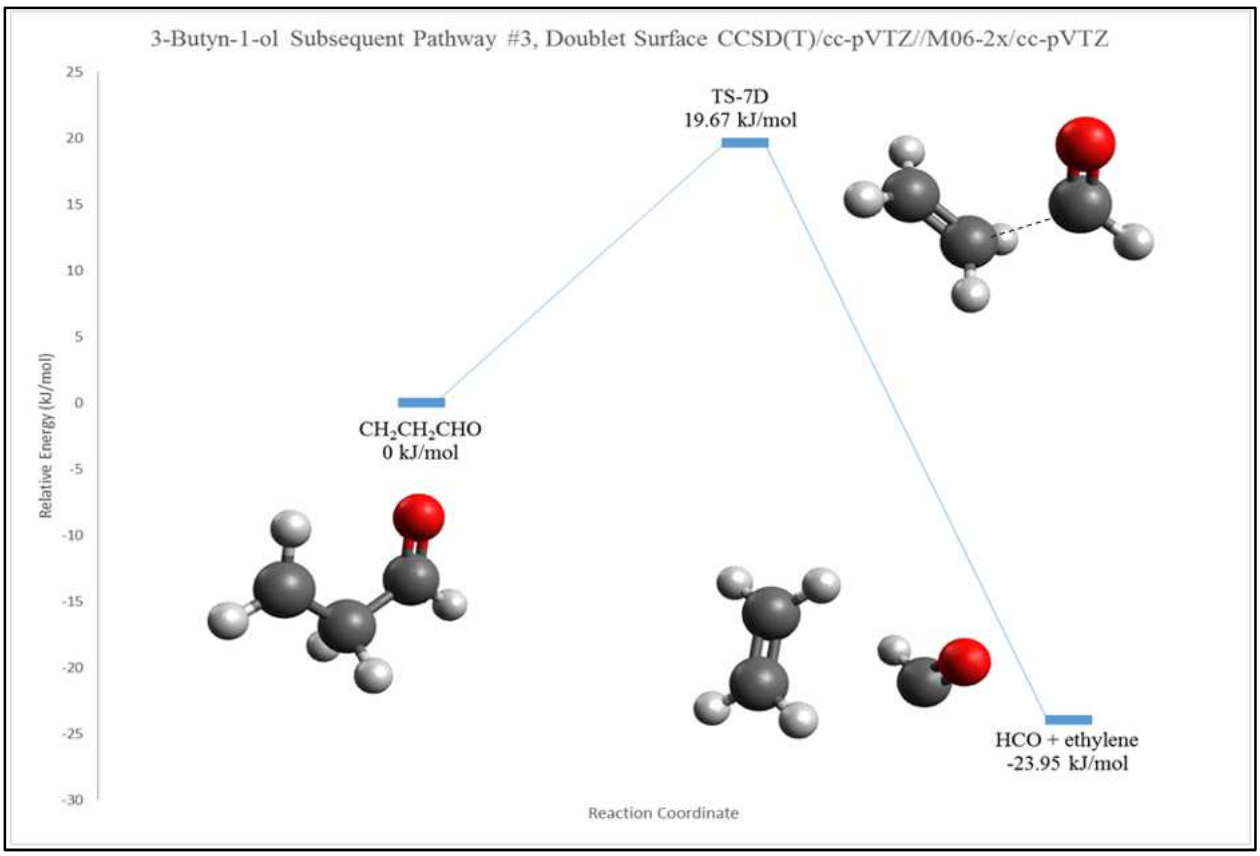

Figure 57. Subsequent dissociation pathway for HCO, CCSD(T)//M06-2x/cc-pVTZ level.

Shown in Figure 57, the subsequent dissociation of HCO radical from CH_2CH_2CHO is thermodynamically favorable as the reaction has to overcome a small relative energy barrier of 19.67 kJ/mol and results in products that are 23.95 kJ/mol lower than the reactant. This subsequent pathway is predicted to be favorable as it has the fewest number of steps, lowest relative energy barrier, and products that are lower in energy than the fragment radical reactant. The subsequent dissociation pathway shown in Figure 57 may very well contribute to the strong HCO radical absorption signal detected for $O(^3P)$ + 3-butyn-1-ol during the CRDLAS studies conducted by Buettner.[28]

www.manaraa.com

CHAPTER V

CONCLUSION

There are many consistencies worth discussing between the reactions of $O(^3P)$ + propargyl alcohol and $O(^3P)$ + 3-butyn-1-ol. With regards to the PEPs presented in this thesis, similar mechanisms are at play in both reactions involving the hydroxyl substituent. The presence of two oxygen atoms in these systems allows for more avenues of formyl radical production, as illustrated in the PEPs. The hydroxyl group has proven to take part in reaction mechanisms that lead to HCO and HOC radical formation for both the incoming $O(^3P)$ atom (O8 for propargyl alcohol and O11 for 3-butyn-1-ol) and for the hydroxyl oxygen itself (O9 for propargyl alcohol and O12 for 3-butyn-1-ol). Both formyl radical and isoformyl radical formation may occur via bond breakage at either end of the molecule because of the involvement of the hydroxyl group in these mechanisms.

In addition to the unique HCO/HOC radical formation pathways for hydroxyl-substituted alkynes, subsequent HCO/HOC dissociations have been demonstrated for the reaction of $O(^3P)$ + 3-butyn-1-ol. These subsequent dissociations have also been investigated for $O(^3P)$ + propargyl alcohol, but were never found. The first steps of a possible subsequent HCO/HOC dissociation pathway for $O(^3P)$ + propargyl alcohol were found, but the relative energy barrier for the dissociation step was too great, therefore making subsequent HCO/HOC radical formation unviable.

The reaction mechanisms between $O(^3P)$ + propargyl alcohol and $O(^3P)$ + 3-butyn-1-ol are proven to be similar through NRT analysis. For both reactions, NSD is distributed at a 1:3 (O:C) ratio for HCO radical formation and accumulates almost entirely on the C atom for HOC

www.manaraa.com

formation. In addition, the NBO between C and O for HCO radical is about 2.5, whereas the NBO between C and O for HOC is around 2.

Future work on the topic of substituted alkyne combustion includes further studies into the subsequent dissociation pathways of HCO/HOC radical from all intermediate products formed after the initial dissociation in the reaction of $O(^3P)$ + 3-butyn-1-ol. In addition, a full NRT analysis of the subsequent dissociation pathways in the $O(^3P)$ + 3-butyn-1-ol reaction is also desirable to confirm the presence of an unpaired electron on the dissociated radical as well as bond breakage during the subsequent dissociation step.

The computational data presented in this project may offer some insight into the variations observed during the CRLAS studies. First, the reaction of $O(^3P)$ + propyne showed a relatively low intensity for the signature of HCO radical, whereas $O(^3P)$ + propargyl alcohol showed a strong signal. Buettner described two pathways for HCO radical formation in the $O(^3P)$ + propyne reaction,[28] whereas this project reveals six pathways for HCO/HOC radical formation in the $O(^3P)$ + propargyl alcohol reaction. The hypothesis given here may be described as a "statistical" explanation for the stronger HCO radical signal observed in the propargyl alcohol reaction. More possibilities for HCO radical formation in the propargyl alcohol reaction means that HCO radical is forming in higher abundance than in the propyne reaction. Second, the reaction of $O(^3P)$ + butyne showed a signal for HCO radical that was stronger than propyne, yet weaker than 3-butyn-1-ol. Buettner described two HCO radical formation pathways for the reaction of $O(^3P)$ + butyne, whereas this project shows six HCO/HOC radical pathways for the reaction of $O(^3P)$ + 3-butyn-1-ol (including the viable subsequent HCO pathway). The combination of more possibilities for HCO dissociation and the presence of a viable subsequent HCO radical formation pathway may explain the stronger HCO radical signal observed for 3-

www.manaraa.com

butyn-1-ol over butyne during the CRDLAS experiments. Building upon the work conducted by Buettner and Dilday has revealed new insights into the formation of HCO radical from the combustion of hydroxyl-substituted alkynes.

www.manaraa.com

REFERENCES

1) U.S. Energy Information Administration / Primary Energy Consumption by Source and Sector, http://www.eia.gov/totalenergy/data/monthly/pdf/flow/primary_energy.pdf (accessed 10/9/16).

2) Total Energy Data Browser, https://www.eia.gov/totalenergy/data/browser/#/?f=A&start=1949&end=2016&charted=4-6-7-14 (accessed 10/9/16).

3) NASA Climate Change, http://climate.nasa.gov/ (accessed 10/9/16).

4) Andresen, P.; Luntz, A. C. The chemical dynamics of the reactions of $O(^3P)$ with saturated hydrocarbons. I. Experiment. *J. Chem. Phys.* **72**, 5842-5850 (1980).

5) Herron, J. T. Evaluated Chemical Kinetic Data for the Reactions of Atomic Oxygen $O(^3P)$ with Saturated Organic Compounds in the Gas Phase. *J. Phys. Chem.* **17**, 967-1026 (1988).

6) Ausfelder, F.; McKendrick, K. G. The dynamics of reactions of $O(^3P)$ atoms with saturated hydrocarbons and related compounds. *Science Reviews* **25**, 299-370 (2000).

7) Fu, B.; Han, Y.; Bowman, J. M.; Leonori, F.; Balucani, N.; Angelucci, L.; Occhiogrosso, A.; Petrucci, R.; Casavecchia, P. Experimental and theoretical studies of the $O(^3P) + C_2H_4$ reaction dynamics: collision energy dependence of branching ratios and extent of intersystem crossing. *J. Chem. Phys.* **137**, 22A532 (2012).

8) West, A. C.; Kretchmer, J. S.; Sellner, B.; Park, K.; Hase, W. L.; Lischka, H.; Windus, T. L. $O(^3P) + C_2H_4$ potential energy surface: study at the multireference level. *J. Phys. Chem. A* **113**, 12663-12674 (2009).

www.manaraa.com

9) Saito, T.; Nishihara, S.; Kataoka, Y.; Nakanishi, Y.; Kitagawa, Y.; Kawakami, T.; Yamanaka, S.; Okumura, M.; Yamaguchi, K. Reinvestigation of the reaction of ethylene and singlet oxygen by the approximate spin projection model. Comparison with multireference coupled-cluster calculations. *J. Phys. Chem. A* **114,** 7967-7974 (2010).

10) Leonori, F.; Balucani, N.; Nevrly, V.; Bergeat, A.; Falcinelli, S.; Vanuzzo, G.; Casavecchia, P. Experimental and theoretical studies on the dynamics of the O(^{3}P) + propene reaction: primary products, branching ratios, and role of intersystem crossing. *J. Phys. Chem. A* **119,** 14632-14652 (2015).

11) Cavallotti, C. Relevance of the channel leading to formaldehyde + triplet ethylidene in the O(^{3}P) + propene reaction under combustion conditions. *J. Phys. Chem. A* **5**, 4213-4218 (2014).

12) Zhang, W.; Du, B.; Feng, C. An ab initio dynamics study on the reaction of O(^{3}P) with $CH_3CH{=}CH_2$ (^{1}A'). *J. Mol. Struc.:THEOCHEM* **806,** 121-129 (2007).

13) Huang, X.; Xing, G.; Bersohn, R. Dynamics of the reaction of O(^{3}P) atoms with acetylene. *J. Phys. Chem.* **101,** 5818-5823 (1992).

14) Rajak, K.; Maiti, B. Communcations: direct dynamics study of the O(^{3}P) + C_2H_4 reaction: contribution from spin nonconserving route. *J. Chem. Phys.* **133,** 011101 (2010).

15) Harding, L. B. Theoretical studies on the reaction of atomic oxygen (^{3}P) with acetylene. *J. Phys. Chem.* **85**, 10-11 (1981).

16) Girard, Y.; Chaquin, P. Addition reaction of ^{1}D and ^{3}P atomic oxygen with acetylene. Potential energy surfaces and stability of the primary products. Is oxirene only a triplet molecule? A theoretical study. *J. Phys. Chem.* **107,** 10462-10470 (2003).

www.manaraa.com

17) Nguyen, T. L.; Vereechken, L.; Peeters, J. Quantum chemical and theoretical kinetics study of the $O(^3P) + C_2H_4$ reaction: a multistate process. *J. Phys. Chem.* **110,** 6696-6706 (2006).

18) Zhao, S.; Wu, W.; Zhao, H.; Wang, H.; Yang, C.; Liu, K.; Su, H. Adiabatic and nonadiabatic reaction pathways of the $O(^3P)$ with propyne. *J. Phys. Chem. A* **113,** 23-24 (2009).

19) Savee, J. D.; Borkar, S.; Welz, O.; Sztáray, B.; Taatjes, C.; Osborn, D. L. Multiplexed photoionization mass spectrometry investigation of the $O(^3P)$ + propyne reaction. *J. Phys. Chem. A.* **119,** 7388-7403 (2015).

20) Vanuzzo, G.; Balucani, N.; Leonori, F.; Stranges, D.; Falcinelli, S.; Bergeat, A.; Casavecchia, P.; Gimondi, I.; Cavallotti, C. Isomer-specific chemistry in the proyne and allene reaction with oxygen atoms: CH_3CH + CO versus CH_2CH_2 + CO products. *J. Phys. Chem. Lett.* **7,** 1010-1015 (2016).

21) Singleton, D. L.; Cvetanović. Temperature dependence of the reactions of oxygen atoms with olefins. *J. Am. Chem. Soc.* **98**, 6812-19 (1976).

22) Neeb, P.; Horie, O.; Moortgat, G. The ethane-ozone reaction in the gas phase. *J. Phys. Chem.* **102**, 6778-6785 (1998).

23) Quandt, R.; Min, Z.; Wang, X.; Bersohn, R. Reactions of O (^3P) with alkenes: H, CH_2CHO, CO, and OH channels. *J. Phys. Chem. A* **102**, 60-64 (1998).

24) Vaidya, W. M. Spectrum of the flame of ethylene. *Proc. R. Soc. London, Ser. A* **147***,* 513-521 (1934).

25) Min, Z.; Wong, T.; Quandt, R.; Bersohn R. The reactions of O (^3P) with alkenes: The formyl radical channel. *J. Phys. Chem.* **103**, 10451-10453 (1999).

www.manaraa.com

26) Serrano-Andrés, L.; Forsberg, N.; Malmqvist, P. Vibronic structure in triatomic molecules: the hydrocarbon flame bands of the formyl radical (HCO). A theoretical study. *J. Chem. Phys.* **108**, 7202-16 (1998).

27) Kinsey, J. L. Laser-induced fluorescence. *Ann. Rev. Phys. Chem.* **28,** 349-372 (1977).

28) Buettner, A. D. M.S. Thesis, Illinois State University, 2010.

29) Dilday, B. J. M.S. Thesis, Illinois State University, 2014.

30) Casavecchia, P.; Leonori, F.; Balucani, N. Reaction dynamics of oxygen atoms with unsaturated hydrocarbons from crossed molecular beam studies: primary products, branching ratios and role of intersystem crossing. *Int. Rev. Phys. Chem.* **34**, 161-204 (2015).

31) Scherer, J. J.; Paul, J. B.; O'Keefe, A.; Saykally, R. J. Cavity ringdown laser absorption spectroscopy: history, development, and application to pulsed molecular beams. *Chem. Rev.* **97**, 25-51 (1997).

32) R, Statistical Language Program, https://www.r-project.org (accessed 10/25/16).

33) Gaussian 09, Frisch, M. J.; Trucks, G. W.; Schlegel, H. B.; Scuseria, G. E.; Robb, M. A.; Cheeseman, J. R.; Scalmani, G.; Barone, V.; Mennucci, B.; Petersson, G. A.; Nakatsuji, H.; Caricato, M.; Li, X.; Hratchian, H. P.; Izmaylov, A. F.; Bloino, J.; Zheng, G.; Sonnenberg, J. L.; Hada, M.; Ehara, M.; Toyota, K.; Fukuda, R.; Hasegawa, J.; Ishida, M.; Nakajima, T.; Honda, Y.; Kitao, O.; Nakai, H.; Vreven, T.; Montgomery, J. A., Jr.; Peralta, J. E.; Ogliaro, F.; Bearpark, M.; Heyd, J. J.; Brothers, E.; Kudin, K. N.; Staroverov, V. N.; Kobayashi, R.; Normand, J.; Raghavachari, K.; Rendell, A.; Burant, J. C.; Iyengar, S. S.; Tomasi, J.; Cossi, M.; Rega, N.; Millam, N. J.; Klene, M.; Knox, J. E.; Cross, J. B.; Bakken, V.; Adamo, C.; Jaramillo, J.; Gomperts, R.; Stratmann, R. E.;

www.manaraa.com

Yazyev, O.; Austin, A. J.; Cammi, R.; Pomelli, C.; Ochterski, J. W.; Martin, R. L.; Morokuma, K.; Zakrzewski, V. G.; Voth, G. A.; Salvador, P.; Dannenberg, J. J.; Dapprich, S.; Daniels, A. D.; Farkas, Ö.; Foresman, J. B.; Ortiz, J. V.; Cioslowski, J.; Fox, D. J. Gaussian, Inc., Wallingford CT, 2009.

34) Harvey, J. N.; Aschi, M.; Schwarz, H.; Koch, W. The singlet and triplet states of phenyl cation. A hybrid approach for locating minimum energy crossing points between non-interacting potential energy surfaces. *Theor. Chem. Acc.* **99**, 95-99 (1998).

35) Chachiyo, T.; Rodriguez, J. H. A direct method for locating minimum-energy crossing points (MECPs) in spin-forbidden transistions and nonadiabatic reactions. *J. Chem. Phys.* **123,** 094711 (2005).

36) Foster, J. P.; Weinhold, F. Natural hybrid orbitals. *J. Am. Chem. Soc.* **102,** 7211-7218 (1980).

37) Reed, A. E.; Weinhold, F. Natural bond orbital analysis of near-Hartree-Fock water dimer. *J. Chem. Phys.* **78**, 4066-4073 (1983).

38) Reed, A. E.; Weinstock, R. B.; Weinhold, F. Natural population analysis. *J. Chem. Phys.* **83,** 735-746 (1985).

39) Glendening, E. D.; Weinhold, F. Natural resonance theory: I. general formalism. *J. Comp. Chem.* **19,** 593-609 (1998).

40) Carpenter, J. E.; Weinhold, F. Analysis of the geometry of the hydroxymethyl radical by the "different hybrids for different spins" natural bond orbital procedure. *J. Mol. Struc.:THEOCHEM.* **169,** 41-62 (1988).

41) Kerr, J. A. Bond dissociation energies by kinetic methods. *Chem. Rev.* **66**, 465-500 (1966).

www.manaraa.com

42) Quandt, R.; Min, Z.; Wang, X.; Bersohn, R. Reactions of $O(^3P)$ with alkenes: H, CH_2CHO, CO, and OH channels. *J. Phys. Chem.* **102**, 60-64 (1998).

43) Xing G.; Huang, X.; Wang, X. Bersohn, R. Reactions of $O(^3P)$ with alkynes: the CO and H atom channels. *J. Chem. Phys.* **105**, 488-95 (1996).

www.manaraa.com

APPENDIX A: ALL OPTIMIZED STRUCTURES FOR O(^{3}P) + PROPARGYL ALCOHOL AND O(^{3}P) + 3-BUTYN-1-OL AT THE M06-2X/CC-PVTZ LEVEL

All structures from the O(^{3}P) + propargyl alcohol and O(^{3}P) + 3-butyn-1-ol reactions are presented here with potential energies listed in hartrees. All structures presented here were optimized at the M06-2x/cc-pVTZ level of theory. Energies listed here were collected via single-point calculations at the CCSD(T)/cc-pVTZ level of theory, corrected with vibrational zero-point energies found at the M06-2x/cc-pVTZ level. Several species have multiple conformers listed; the lowest energy conformer was chosen for constructing the PEP and was kept consistent throughout the pathway. For example, IM-1T from the established HCO radical pathway for O(^{3}P) + propargyl alcohol has 5 different conformers, with "cis-b" being the lowest in energy. So, isomer cis-b was chosen for IM-1T and each following species in the pathway has the "cis-b" conformation. Each panel in Appendix A shows a transition state in the center with reactants, products, or intermediates on either side to which the transition state connects.

www.manaraa.com

M06-2x/cc-pVTZ Structures for the Triplet State Surface of O(^{3}P) + Propargyl Alcohol

IM-0T, Propargyl Alcohol + O(^{3}P)	TS-1T	IM-1T
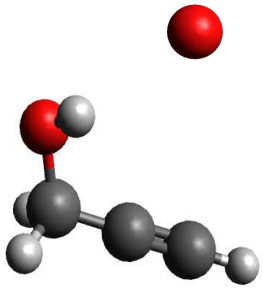 -266.8591241	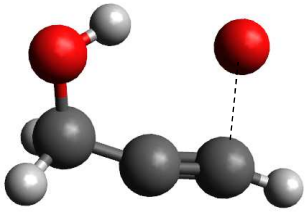 -266.8618870	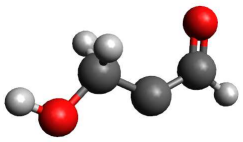 cis a -266.9493519 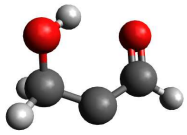 cis b -266.9539469 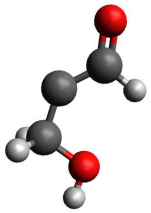 trans a -266.9478242 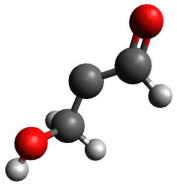 trans b -266.9459440 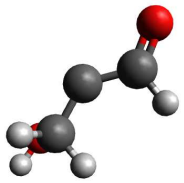 trans c -266.9460338

www.manaraa.com

IM-1T	TS-2T	IM-2T
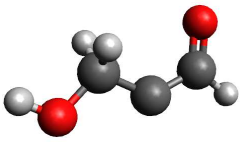 cis a -266.9493519	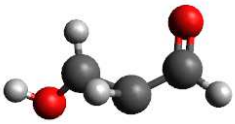 cis isomer a -266.8860872	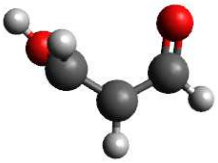 cis a -266.9651347
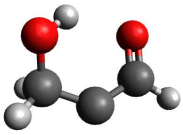 cis b -266.9539469	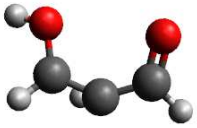 cis isomer b -266.8832447	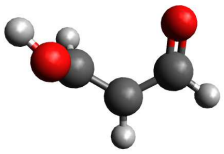 cis b -266.9651287
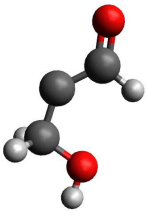 trans a -266.9478242	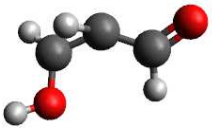 trans isomer a -266.8833371	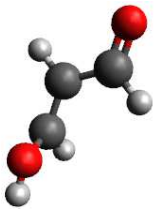 trans a -266.9654235
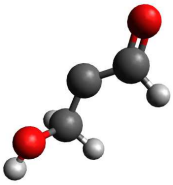 trans b -266.9459440	trans isomer b -266.8822934	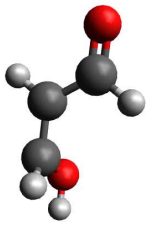 trans b -266.9654224
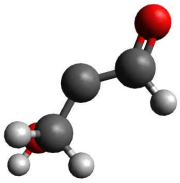 trans c -266.9460338		

www.manaraa.com

IM-1T	TS-3T	IM-3T
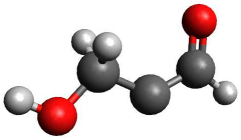 cis a -266.9493519	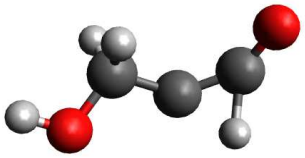 isomer a -266.9410758	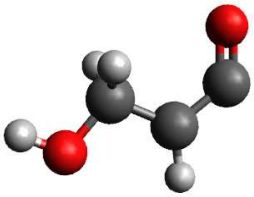 cis a -266.9760899
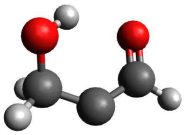 cis b -266.9539469		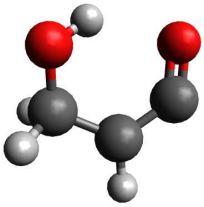 cis b -266.9771845
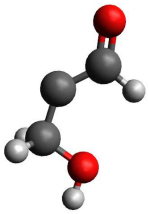 trans a -266.9478242	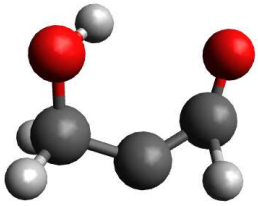 isomer b -266.8821970	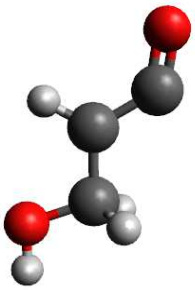 trans a -266.9757781
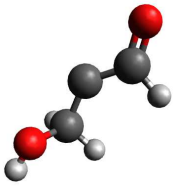 trans b -266.9459440		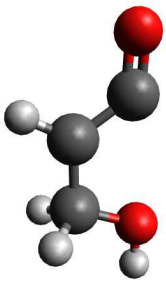 trans b -266.9731641
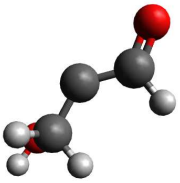 trans c -266.9460338		

www.manaraa.com

IM-2T	TS-4T	CHOHCH + HCO
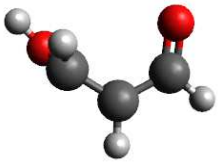 cis a -266.9651347		
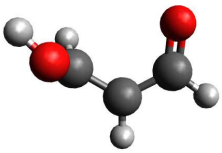 cis b -266.9651287		
trans a -266.9654235		
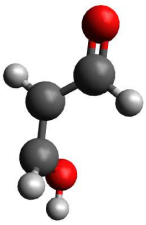 trans b -266.9654224	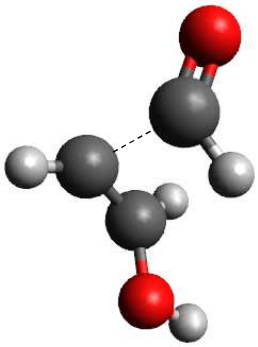 -266.8948699	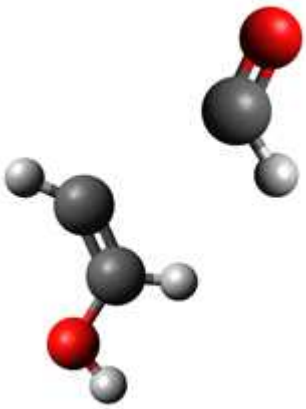 -266.9031782

www.manaraa.com

IM-3T	TS-5T	$CH_2OHCH + CO$
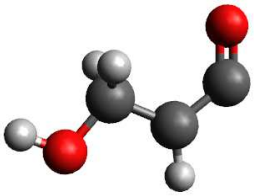 cis a -266.9760899	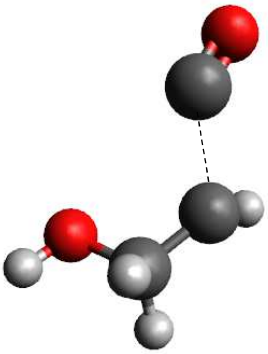 out -266.9351006	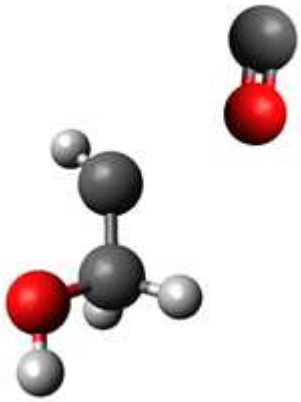 -266.9556318
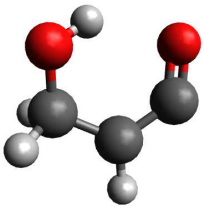 cis b -266.9771845		
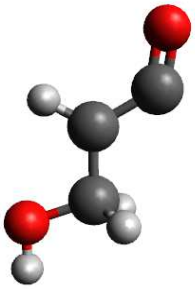 trans a -266.9757781	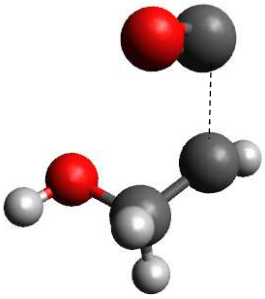 in -266.9346053	
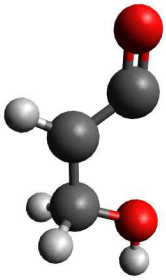 trans b -266.9731641		

www.manaraa.com

IM-3T	TS-6T	IM-4T
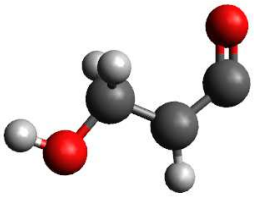	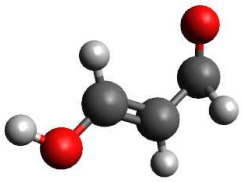	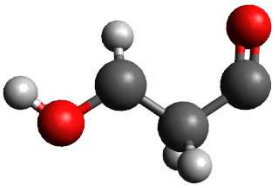
cis a -266.9760899	cis a -266.9224242	cis a -266.9725106
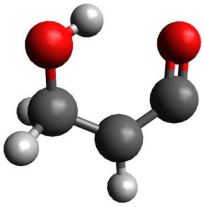	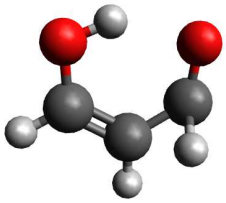	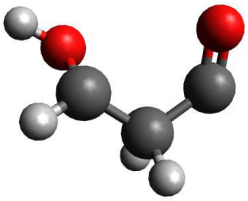
cis b -266.9771845	cis b -266.9328771	cis b -266.9699719
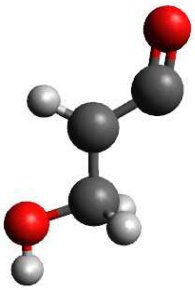	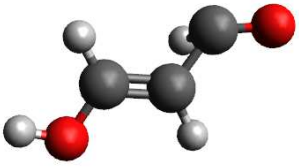	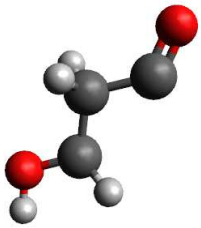
trans a -266.9757781	trans a -266.9177598	trans a -266.9717873
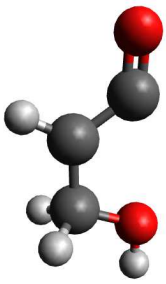	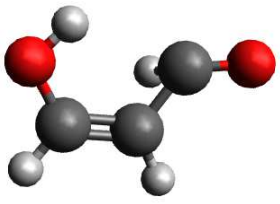	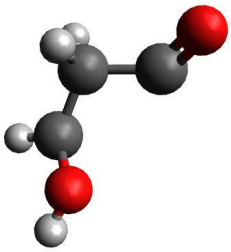
trans b -266.9731641	trans b -266.9254706	trans b -266.9705895

www.manaraa.com

IM-4T	TS-7T	$CHOHCH_2 + CO$
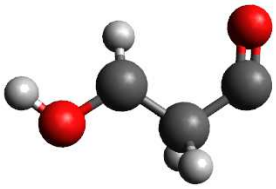 cis a -266.9725106	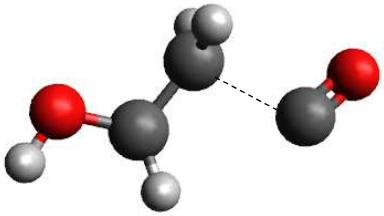 isomer a -266.9482544	-266.9540082
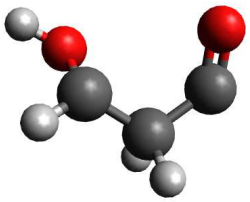 cis b -266.9699719		
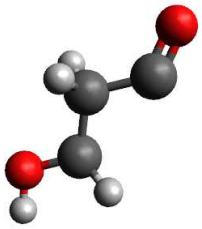 trans a -266.9717873	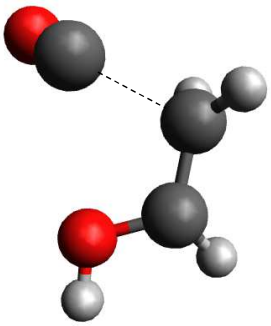 isomer b -266.9465438	
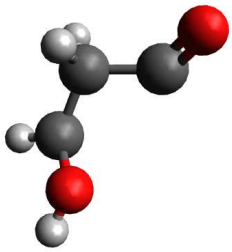 trans b -266.9705895		

www.manaraa.com

M06-2x/cc-pVTZ Structures for the Singlet State Surface of O(^{3}P) + Propargyl Alcohol

IM-1S	TS-2S	IM-2S
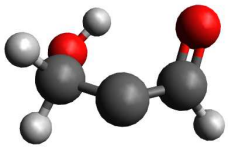 noncyclic -266.9473912	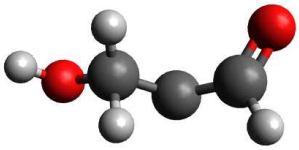 isomer a -266.9448858	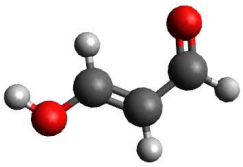 cis a -267.0643292
		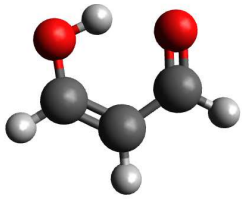 cis b -267.0778960
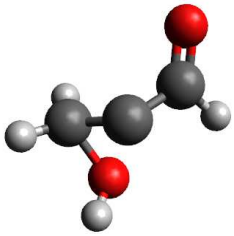 cyclic structure -266.9375599	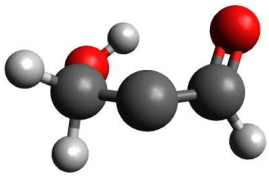 isomer b -266.9481275	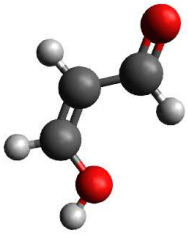 trans a -267.0627604
		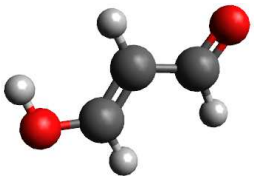 trans b -267.0676352

www.manaraa.com

IM-1S	TS-3S	IM-3S
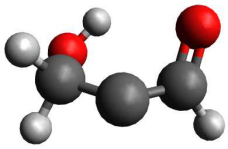 noncyclic -266.9473912	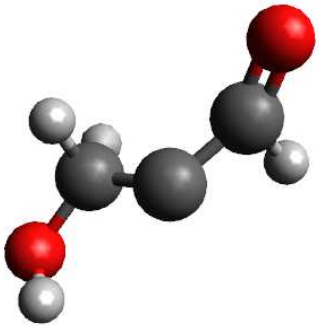 isomer a -266.9521073	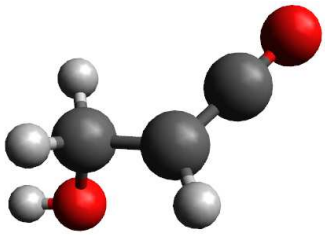 isomer a -267.0543533
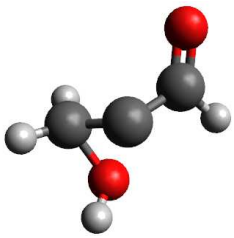 cyclic structure -266.9375599	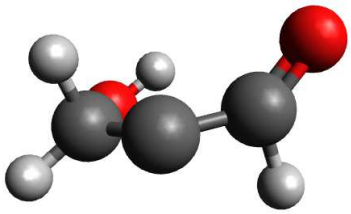 isomer b -266.9504614	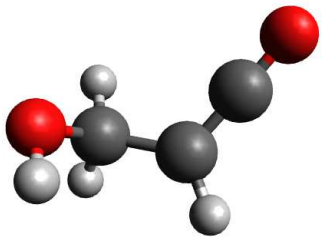 isomer b -267.0555924
	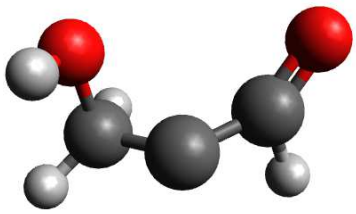 isomer c -266.9361058	

www.manaraa.com

IM-3S	TS-6S	$CHOHCH_2 + CO$
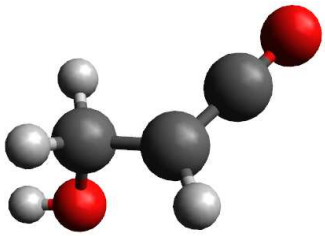 isomer a -267.0543533	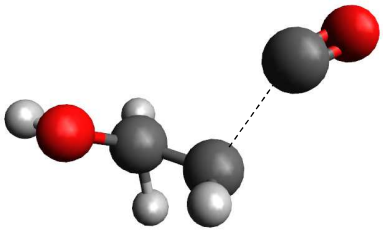 -266.9431655	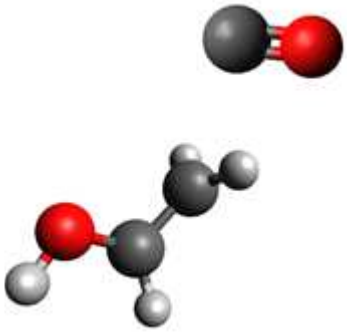 -266.9540082
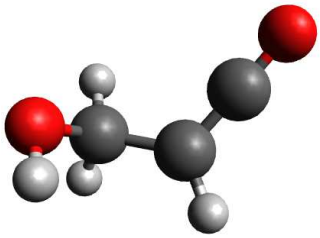 isomer b -267.0555924		

www.manaraa.com

IM-2S	TS-8S	Cyclopropanone-2-ol
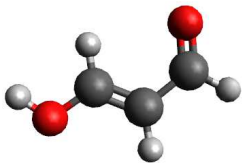 cis a -267.0643292	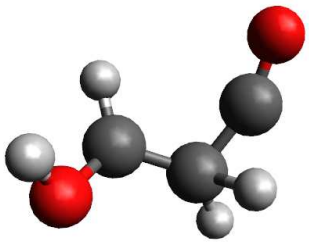 -266.9197282	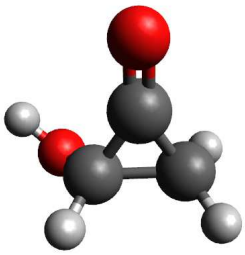 -267.0223423
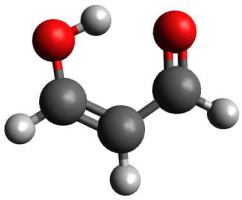 cis b -267.0778960		
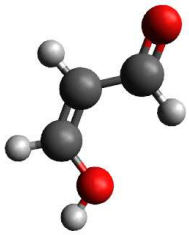 trans a -267.0627604		
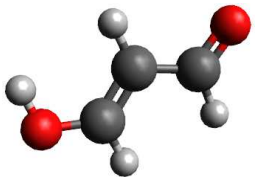 trans b -267.0676352		

www.manaraa.com

IM-2S	TS-9S	IM-3S
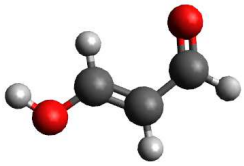 cis a -267.0643292	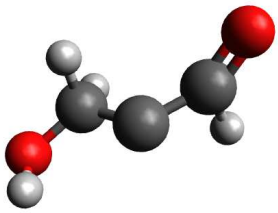 -266.9521111	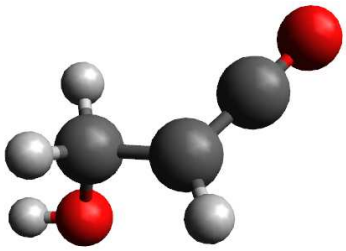 isomer a -267.0543533
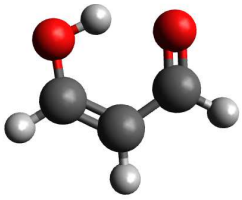 cis b -267.0778960		
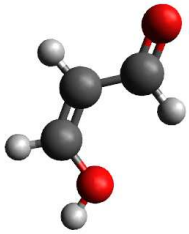 trans a -267.0627604	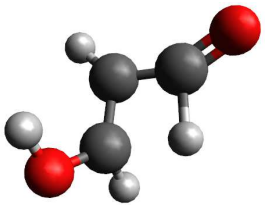 alt -266.9709177	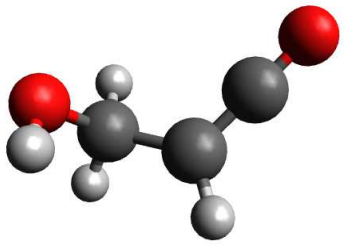 isomer b -267.0555924
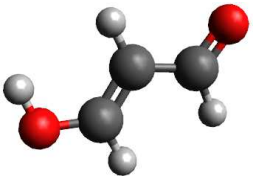 trans b -267.0676352		

www.manaraa.com

IM-2S	TS-10S	COHCH + H_2 + CO
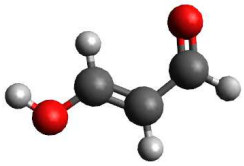 cis a -267.0643292	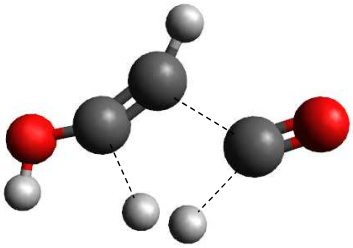 -266.9166816	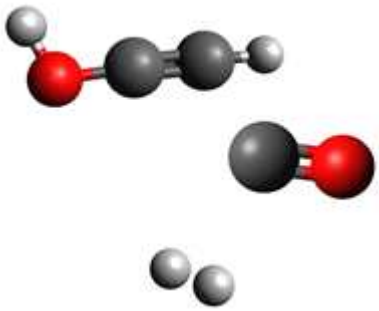 -266.9837346
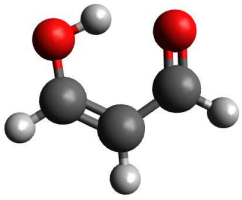 cis b -267.0778960		
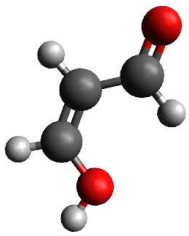 trans a -267.0627604		
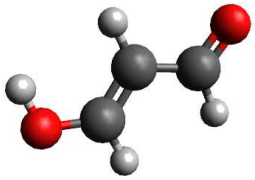 trans b -267.0676352		

www.manaraa.com

Cyclopropanone-2-ol	TS-11S	$CHOHCH_2 + CO$
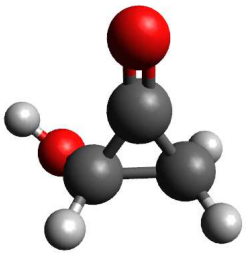	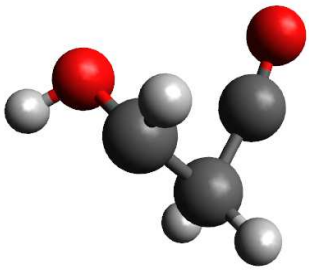	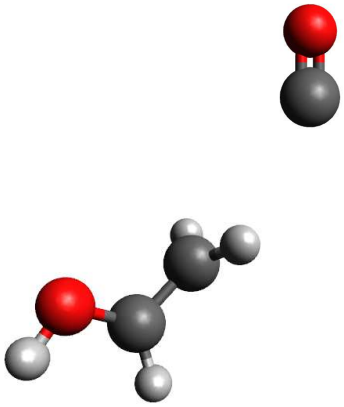
-267.0223423	isomer a -266.9595882	-266.9540082
	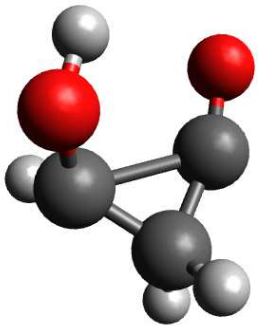	
	isomer b -266.9620263	

www.manaraa.com

M06-2x/cc-pVTZ Structures for the Novel HCO/HOC Pathways, Triplet Surface of O(^{3}P) + Propargyl Alcohol

IM-2T	TS-11T	IM-7T
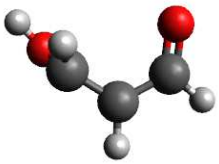	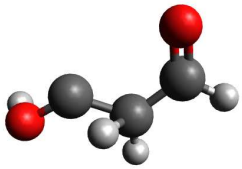	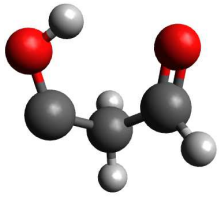
cis a -266.9651347	cis a -266.8899442	cis a -266.9480623
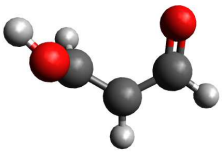	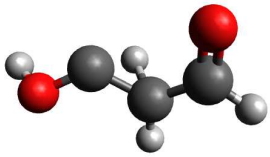	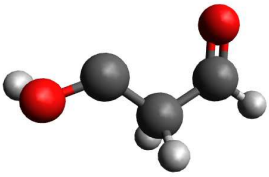
cis b -266.9651287	cis b -266.8890255	cis b -266.9453539
	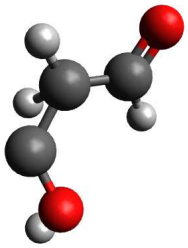	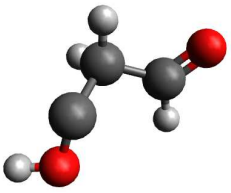
trans a -266.9654235	trans a -266.8877299	trans a -266.9460350
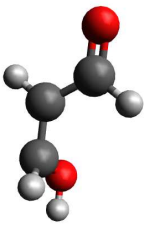	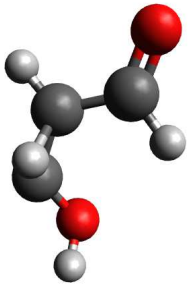	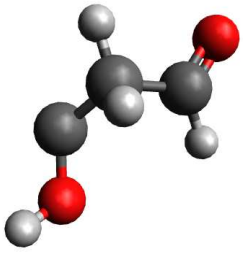
trans b -266.9654224	trans b -266.8877299	trans b -266.9460347

www.manaraa.com

IM-7T	TS-12T	HOC + CH_2CHO
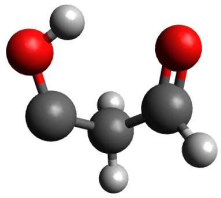 cis a -266.9480623	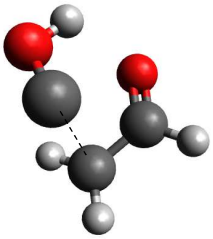 -266.8931969	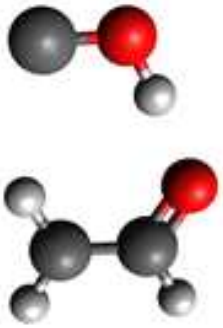 -266.9050821
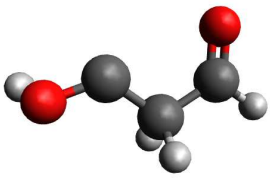 cis b -266.9453539		
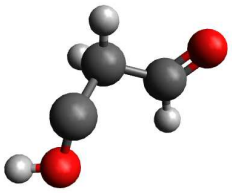 trans a -266.9460350		
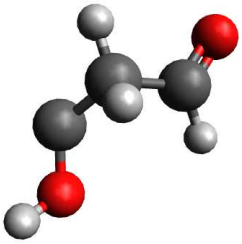 trans b -266.9460347		

www.manaraa.com

HCO	TS-HCOtoHOC	HOC
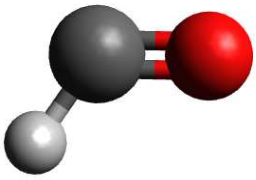	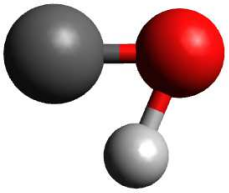	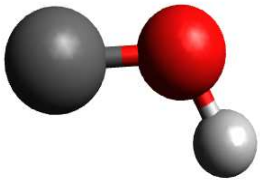
-113.8340068	-113.7337104	-113.7704440

www.manaraa.com

IM-1T	TS-8T	IM-5T
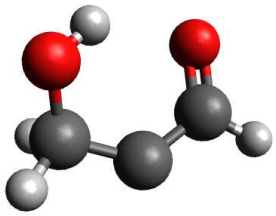	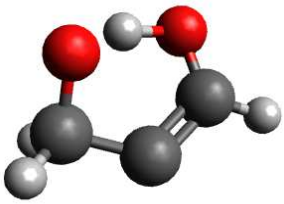	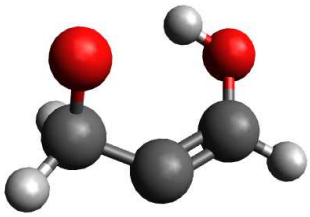
cis b -266.9539469	-266.9034689 (run irc)	-266.9053594

www.manaraa.com

IM-5T 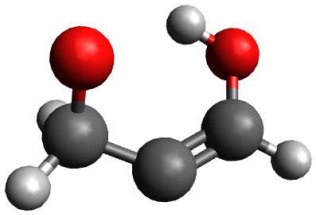 -266.9053594	TS-9T 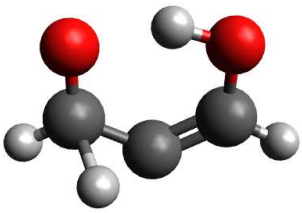 -266.8954087	IM-6T 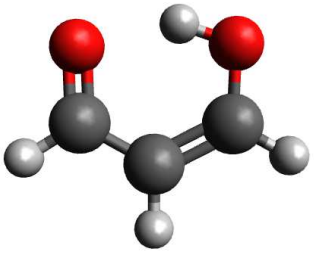 -266.9680024
IM-6T 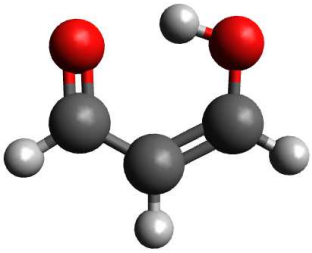 -266.9680024	TS-10T 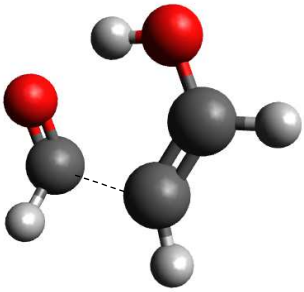 -266.9086851	$HCO + (CH)_2OH$ 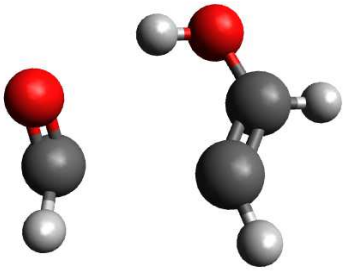 -266.9127285

www.manaraa.com

IM-4T 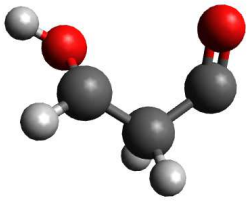 cis b -266.9699719	TS-13T 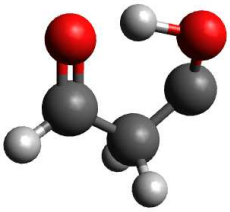 -266.9297035	IM-8T 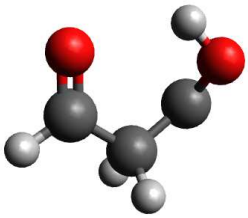 -266.9510305
IM-8T 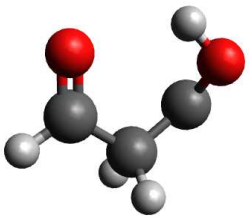 -266.9510305	TS-14T 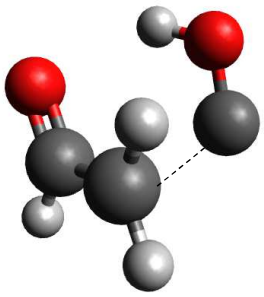 -266.8931959	HOC + CH_2CHO 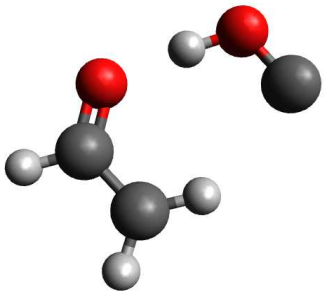 -266.9050823

www.manaraa.com

IM-8T 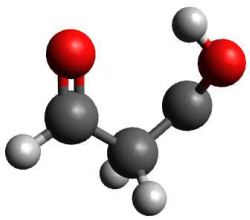 -266.9510305	TS-15T 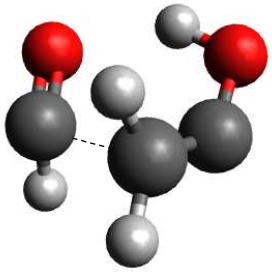 -266.9129135	$HCO + CH_2COH$ 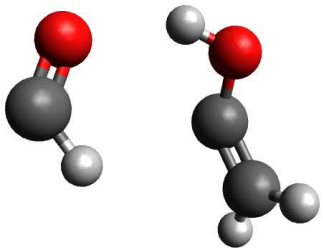 -266.9212739
IM-4T 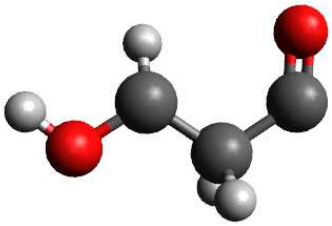 cis a -266.9725106	TS-16T 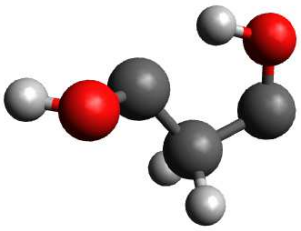 -266.8696642	IM-9T 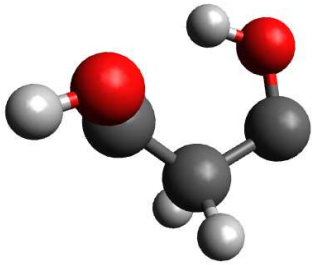 -266.8695996

www.manaraa.com

IM-9T 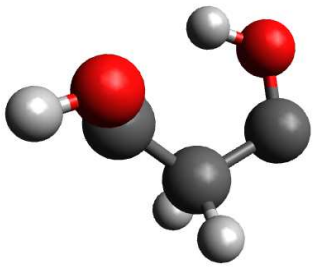 -266.8695996	TS-17T 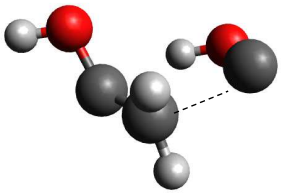 product a -266.8456978 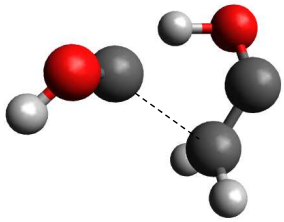 product b -266.8474018	HOC + CH_2COH 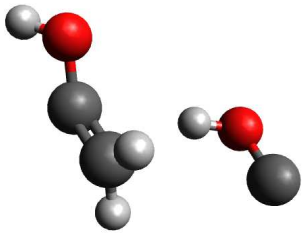 product a -266.8589759 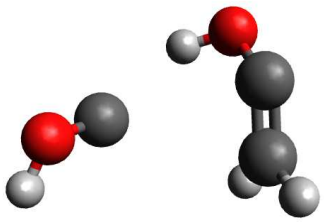 product b -266.8581729
IM-2T 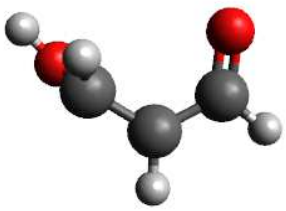 cis a -266.9651347	TS-18T 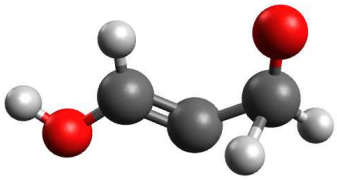 -266.8793503	IM-10T 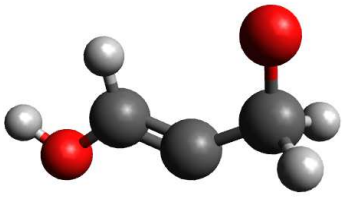 -266.9074240

www.manaraa.com

IM-10T 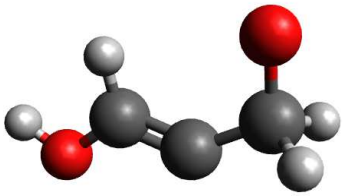 -266.9074240	TS-19T 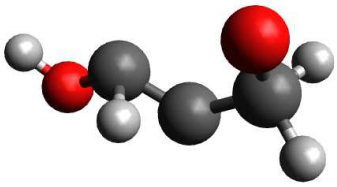 -266.8399542	IM-11T 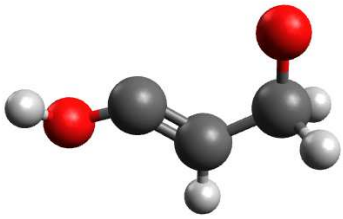 -266.9132697
IM-11T 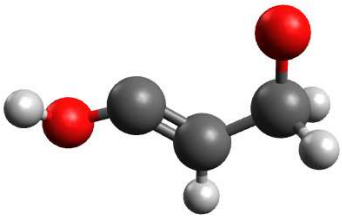 -266.9132697	TS-20T 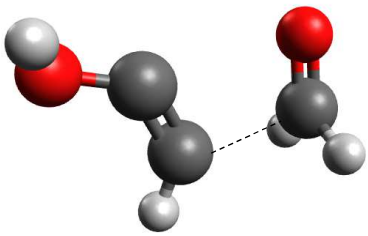 -266.8636594	CH_2O + CHCOH 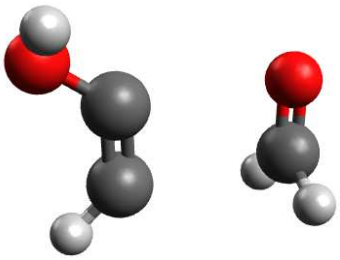 -266.8671552

www.manaraa.com

O(^{3}P) + 3-Butyn-1-ol Structures: Triplet Surface, M06-2x/cc-pVTZ

IM-0T 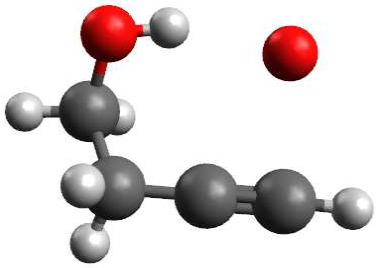 -305.6798844	TS-1T 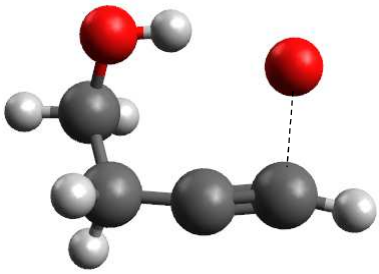 -305.6788671	IM-1T 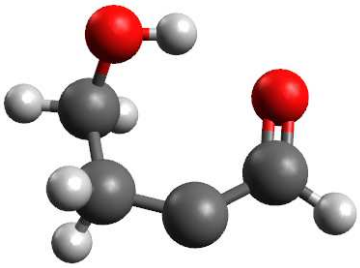 -305.7648724
TS-2T 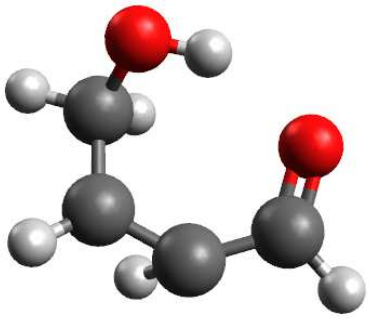 -305.6991794	IM-2T 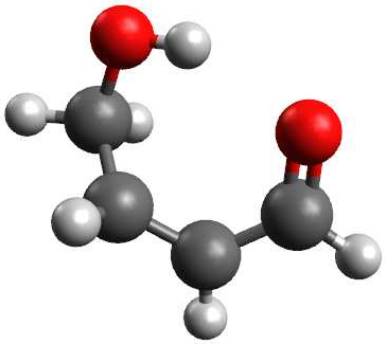 -305.7719352	TS-3T 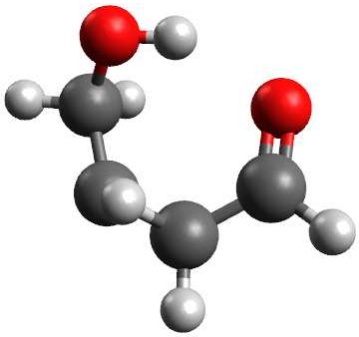 -305.7000171

www.manaraa.com

IM-3T 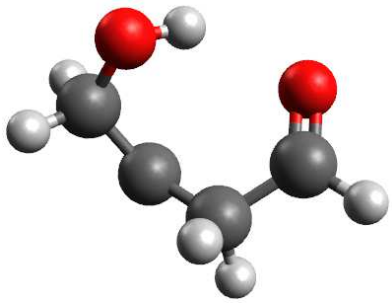 -305.7502373	TS-4T 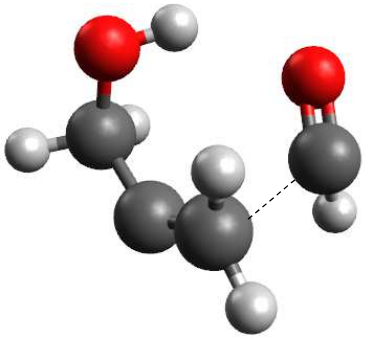 -305.7092163	$HCO + CH_2CCH_2OH$ 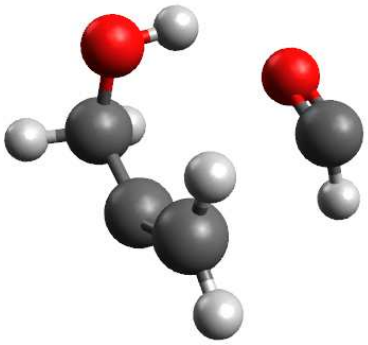 -305.72496
IM-2T 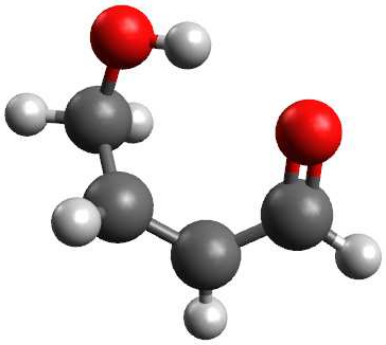 -305.7719352	TS-5T 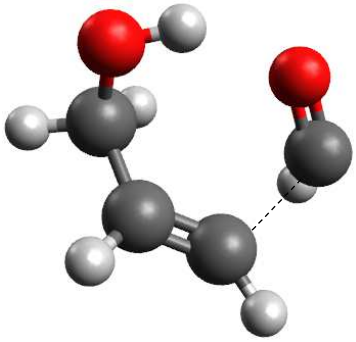 -305.707762	$HCO + CHCHCH_2OH$ 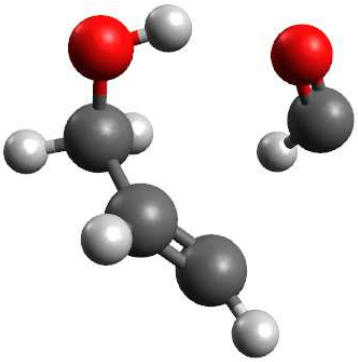 -305.7154736

www.manaraa.com

IM-1T 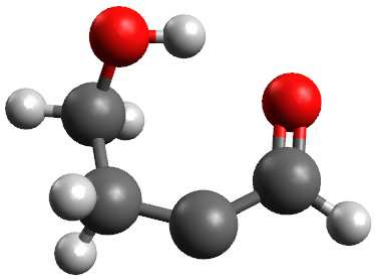 -305.7648724	TS-6T 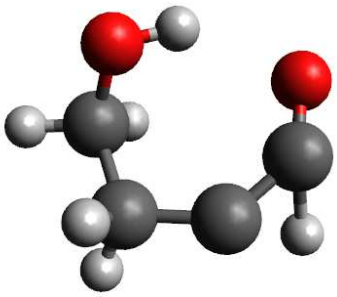 -305.6954378	IM-4T 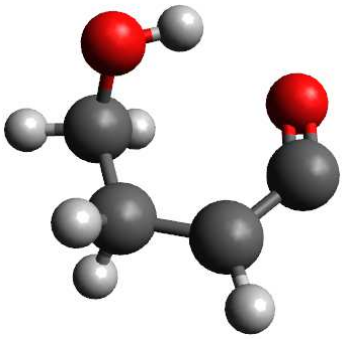 -305.7867939
TS-7T 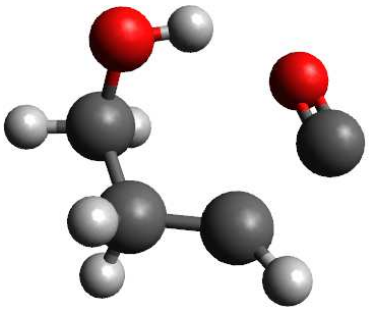 -305.7451153	$CO + CHCH_2CH_2OH$ 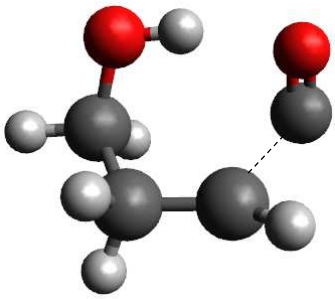 -305.7508826	TS-8T 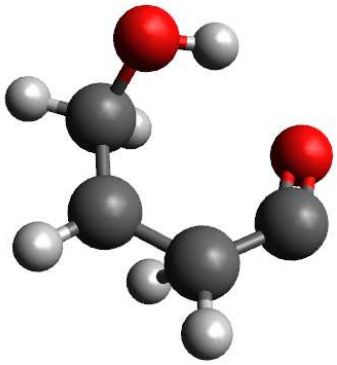 -305.725939

www.manaraa.com

IM-5T 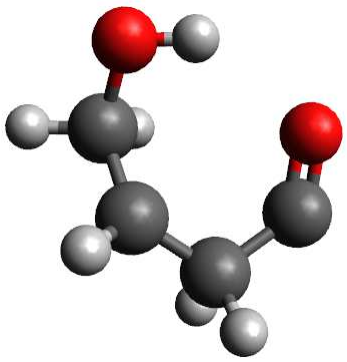 -305.7737809	TS-9T 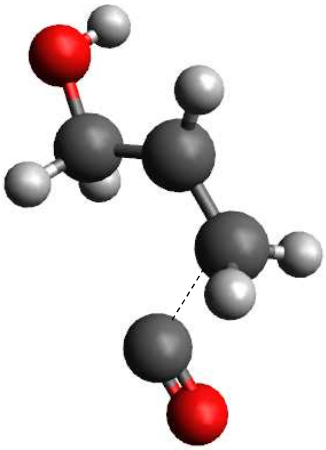 -305.751009	$CO + CH_2CHCH_2OH$ 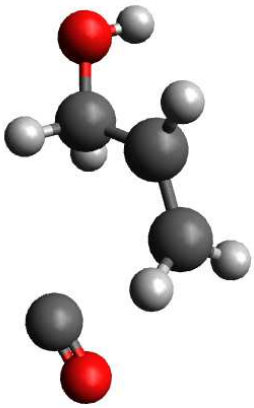 -305.7626263
IM-5T 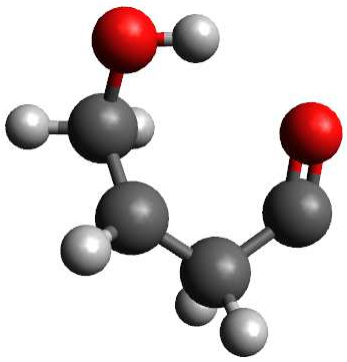 -305.7737809	TS-15T 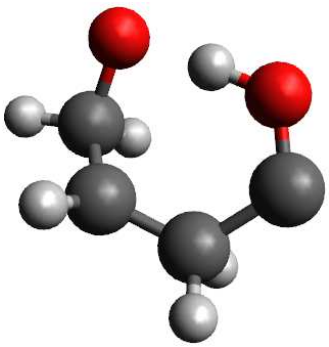 -305.6712636	IM-9T 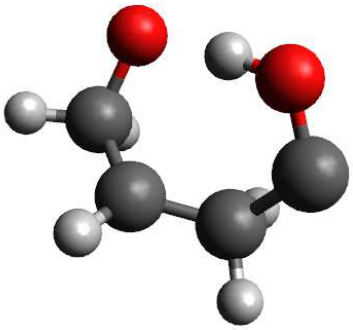 -305.6804459

www.manaraa.com

TS-18T 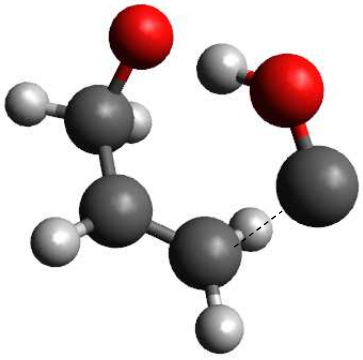 -305.7440635	HOC + CH_2CHCH_2O 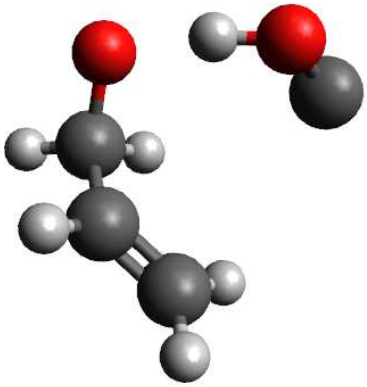 -305.7575225	TS-10T 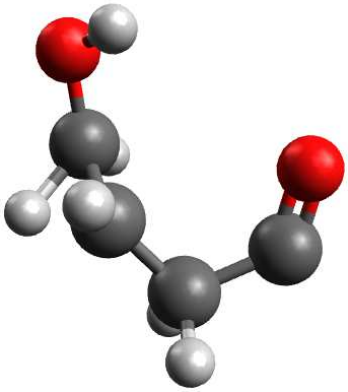 -305.7067748
IM-6T 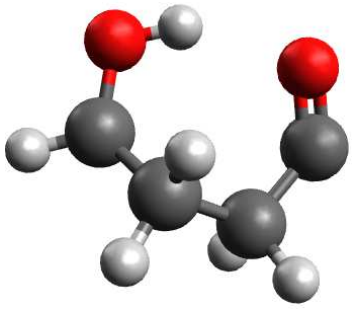 -305.783955	TS-11T 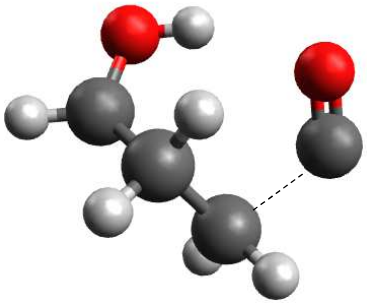 -305.7598468	CO + CH_2CH_2CHOH 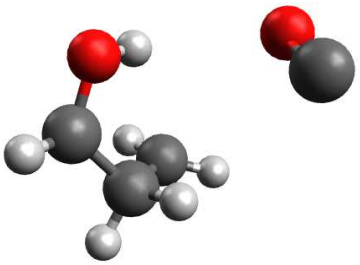 **MP2 Structure: -305.7722276

*TS-10T splits off from IM-5T
**M06-2x structure did not converge, and so MP2/6-311++G(d,p) was employed here.

www.manaraa.com

IM-2T 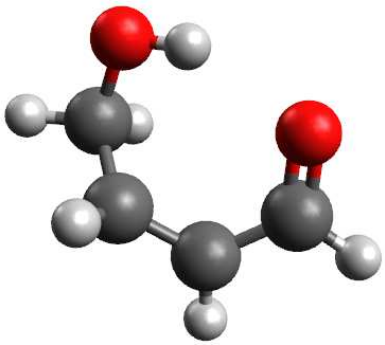 -305.7719352	TS-12T 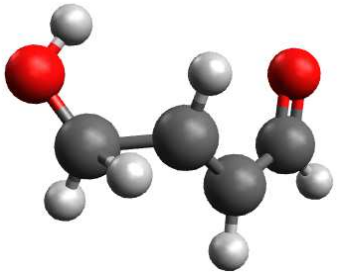 -305.7069876	IM-7T 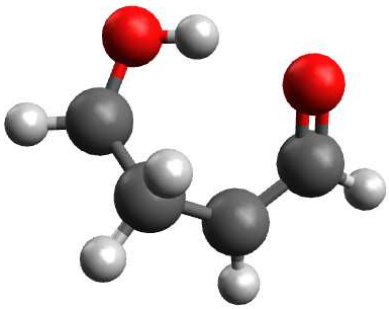 -305.7841507
TS-13T 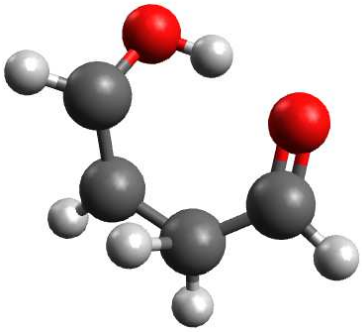 *MP2 Structure: -305.7161589	IM-8T 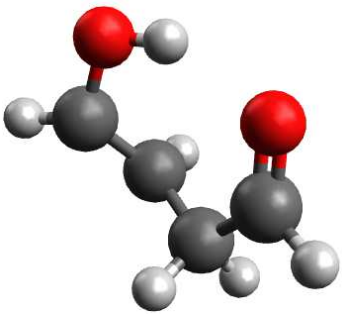 -305.7700823	TS-14T 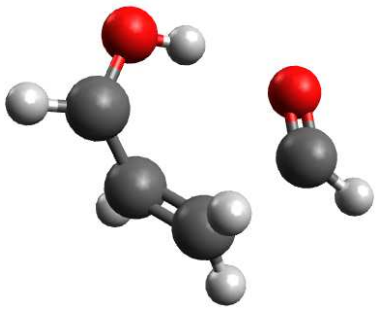 -305.727546

www.manaraa.com

HCO + $CH_2CHCHOH$ 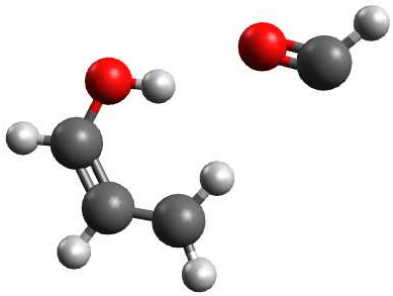 -305.7662484	TS-16T 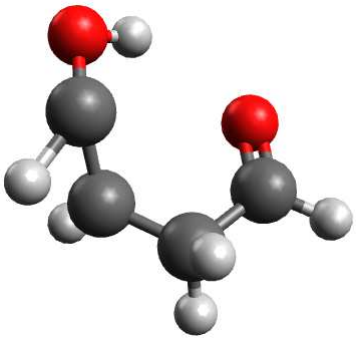 -305.6842905	IM-10T 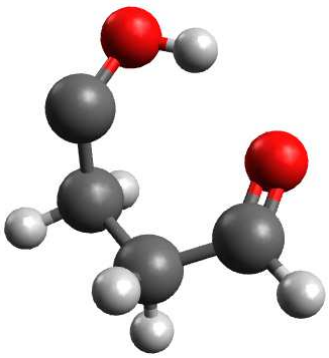 -305.7578898
IM-10T 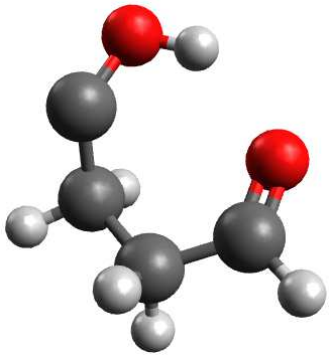 -305.7578898	TS-17T 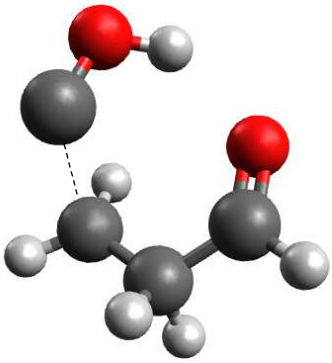 -305.6962129	HOC + CH_2CH_2CHO 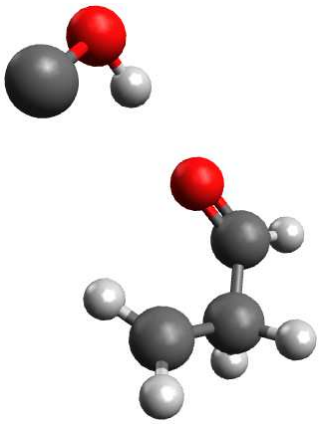 *B3LYP Structure: -305.7724339

*HOC + CH_2CH_2CHO structure did not converge with M06-2x and so B3LYP, another DFT method, was employed.

www.manaraa.com

Subsequent Dissociation Pathway Structures: Doublet Surface, M06-2x/cc-pVTZ

CH_2CCH_2OH 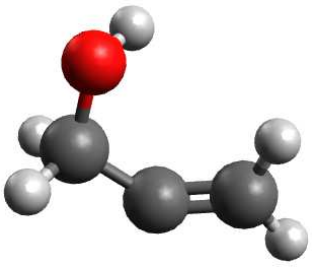 -192.0468151	TS-1D 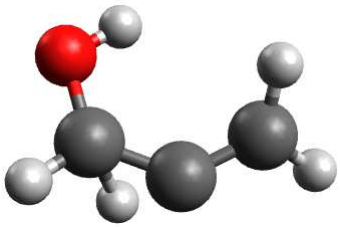 -191.9896934	IM-1D 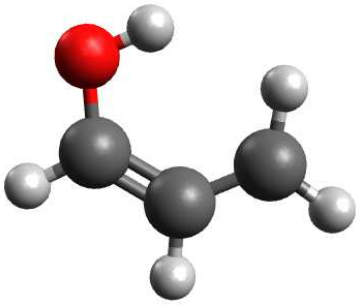 -192.0922389
IM-1D 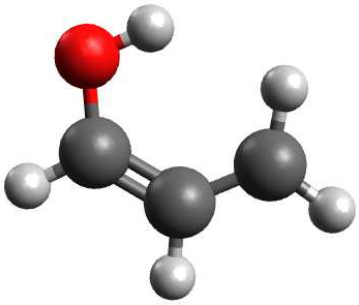 -192.0922389	TS-2D 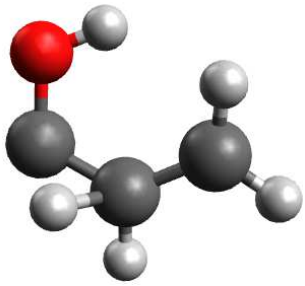 -191.9742786	IM-2D 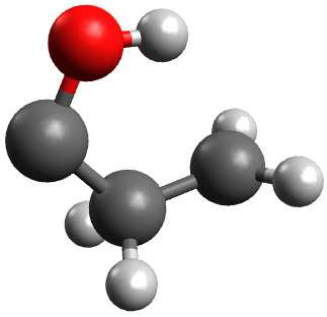 -192.0000518

www.manaraa.com

IM-2D 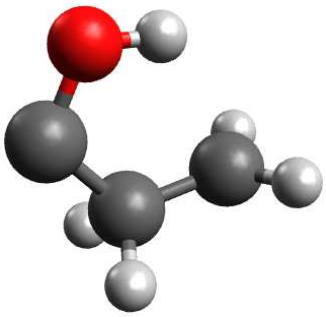 -192.0000518	TS-3D 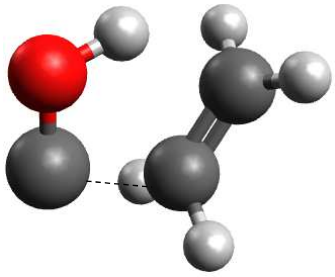 -191.9836849	HOC + C_2H_4 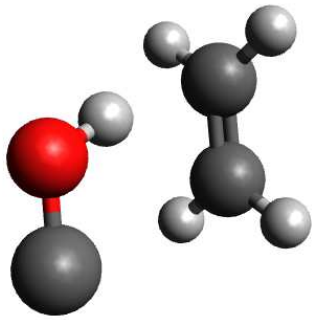 -191.9983663
$CHCHCH_2OH$ 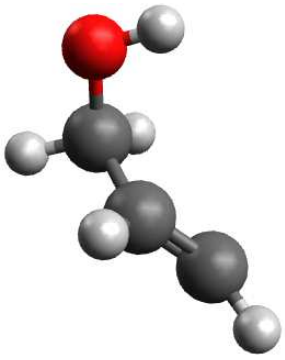 -192.0429802	TS-4D 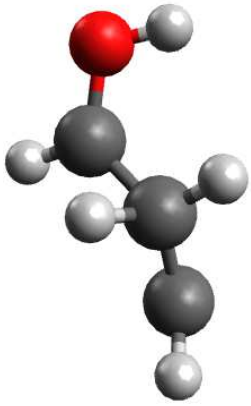 -191.930567	IM-3D 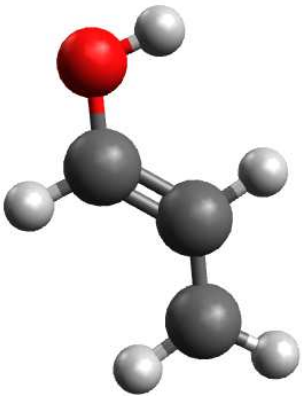 -192.090249

www.manaraa.com

IM-3D 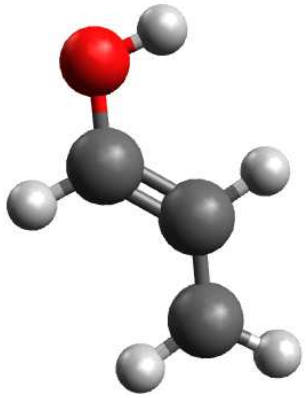 -192.090249	TS-5D 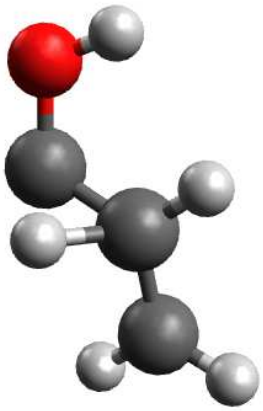 -191.9737315	IM-4D 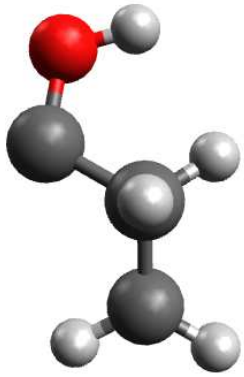 -191.9977047
IM-4D 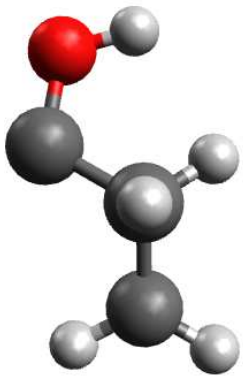 -191.9977047	TS-6D 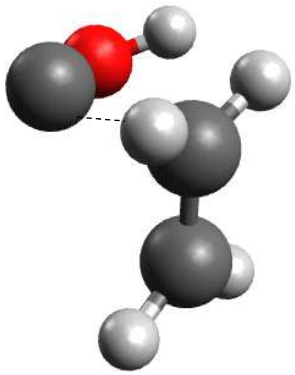 -191.9720546	$HOC + C_2H_4$ 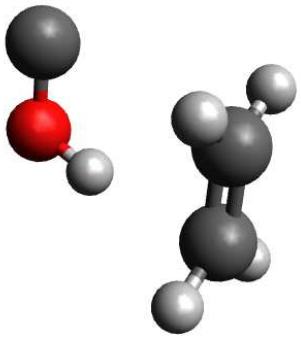 -191.9983624

www.manaraa.com

CH_2CH_2CHO	TS-7D	$HCO + C_2H_4$
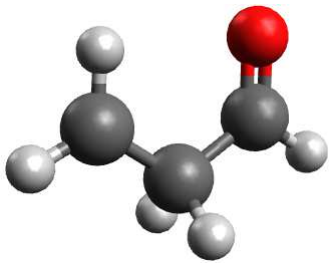	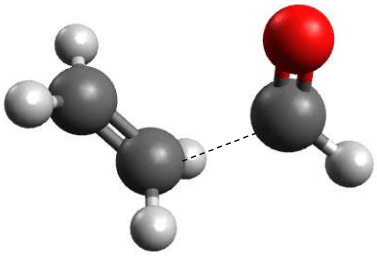	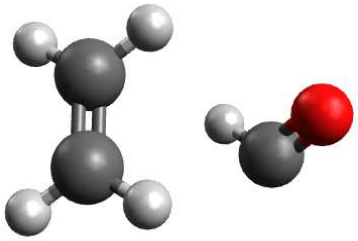
-192.0491309	-192.0416406	-192.0582518

www.manaraa.com

APPENDIX B: CARTESIAN COORDINATES FOR ALL OPTIMIZED STRUCTURES FOR $O(^3P)$ + PROPARGYL ALCOHOL AND $O(^3P)$ + 3-BUTYN-1-OL AT THE M06-2X/CC-PVTZ LEVEL

M06-2x/cc-pVTZ Cartesian Coordinates for the Triplet State Surface of $O(^3P)$ + Propargyl Alcohol

Propargyl Alcohol

C	-1.90771	-0.21543	-0.01289
H	-2.91716	-0.54622	-0.02884
C	-0.77209	0.16278	-0.00509
C	0.63088	0.58771	0.03511
H	0.83074	1.26248	-0.79642
H	0.80372	1.14552	0.96083
O	1.53624	-0.48759	-0.09609
H	1.28634	-1.17141	0.53037

TS-1T

C	-1.37318	-0.83850	-0.10782
H	-2.39712	-1.10119	-0.22956
C	-0.15916	-0.88809	-0.01687
C	1.25621	-0.54661	0.14066
H	1.55387	-0.78051	1.16815
H	1.86250	-1.16090	-0.52636
O	1.49504	0.80493	-0.17499
H	0.69439	1.30076	0.03771
O	-1.50215	1.11771	0.10677

IM-1T cis a

C	-1.50230	-0.50759	0.00069
H	-2.09972	-1.42861	0.00038
C	-0.09151	-0.62572	-0.02304
C	0.94898	0.41084	-0.03028
H	0.82693	1.01416	-0.94082
H	0.77015	1.08025	0.82260
O	2.21805	-0.20156	0.03132
H	2.88872	0.48435	0.02596
O	-2.03269	0.59964	0.01964

IM-1T cis b

C	-1.35867	0.39464	0.11736
H	-2.24812	0.98135	0.37854
C	-0.09764	1.03947	0.12634
C	1.23830	0.50370	-0.20319
H	1.38753	0.60180	-1.28879
H	2.01494	1.09949	0.27841
O	1.39754	-0.82716	0.22911
H	0.59989	-1.31104	-0.02020
O	-1.45331	-0.79765	-0.17799

www.manaraa.com

IM-1T trans a

C	-1.17744	-0.29718	0.00003
H	-0.81476	-1.33989	0.00014
C	-0.14860	0.67771	-0.00005
C	1.31792	0.62283	0.00003
H	1.69588	1.15435	-0.88304
H	1.69578	1.15418	0.88324
O	1.72129	-0.73555	-0.00008
H	2.68045	-0.77545	0.00030
O	-2.37237	-0.04112	-0.00001

IM-1T trans b

C	-1.36112	0.15316	0.27972
H	-1.29560	0.69664	1.24416
C	-0.12706	0.04897	-0.41795
C	1.23026	0.52469	-0.11421
H	1.60060	1.11193	-0.96302
H	1.17934	1.19622	0.75632
O	2.06158	-0.59021	0.14219
H	2.97017	-0.28735	0.20832
O	-2.42495	-0.29458	-0.10858

IM-1T trans c

C	1.37109	0.18442	0.25945
H	1.32239	0.84279	1.15032
C	0.12579	-0.00395	-0.39843
C	-1.22597	0.51179	-0.13930
H	-1.17237	1.23241	0.69107
H	-1.57535	1.05539	-1.02564
O	-2.08081	-0.57082	0.17002
H	-2.98404	-0.24791	0.20787
O	2.42880	-0.30872	-0.08927

TS-2T cis a

C	-1.50086	0.45887	-0.08185
H	-2.13547	1.35289	-0.12765
C	-0.09405	0.66371	0.08144
C	0.97694	-0.28473	0.23059
H	0.46543	0.57137	1.20632
H	0.72265	-1.31952	0.43752
O	2.19292	0.03341	-0.28601
H	2.87057	-0.50700	0.12900
O	-1.96984	-0.67401	-0.09228

www.manaraa.com

TS-2T cis b

C	1.44639	0.34150	0.02210
H	2.28909	1.02354	0.19367
C	0.15313	0.93052	-0.02650
C	-1.21630	0.51747	-0.11576
H	-0.63843	1.23883	0.91882
H	-1.91547	1.18330	-0.61052
O	-1.54411	-0.78887	0.05218
H	-2.47940	-0.86288	0.26388
O	1.59972	-0.87609	-0.05779

TS-2T trans a

C	1.39978	0.26451	-0.19958
H	1.36669	1.23903	-0.72922
C	0.10893	-0.19345	0.22695
C	-1.21105	0.38588	0.19925
H	-0.52822	-0.03257	1.31730
H	-1.29286	1.47199	0.17032
O	-2.23856	-0.37213	-0.27904
H	-3.07141	-0.04297	0.07045
O	2.45604	-0.30002	0.00547

TS-2T trans b

C	-1.21427	-0.32151	0.08366
H	-0.88004	-1.36463	0.24043
C	-0.13511	0.60597	0.03360
C	1.30019	0.56742	0.07879
H	0.51644	1.04507	-0.96015
H	1.83556	1.38791	0.54398
O	1.89916	-0.65514	-0.02712
H	2.80460	-0.55015	-0.33360
O	-2.39684	-0.04854	-0.05625

IM-2T cis a

C	-1.38868	0.25105	-0.17666
H	-2.22879	0.83983	-0.58102
C	-0.14188	0.95313	0.00379
C	1.04698	0.27071	0.50973
H	-0.10848	2.00602	-0.25506
H	1.03989	-0.13879	1.51256
O	1.76242	-0.39507	-0.44109
H	2.38539	-0.99138	-0.01805
O	-1.53574	-0.92556	0.10615

المنارة للاستشارات
www.manaraa.com

IM-2T cis b

C	1.38849	0.25087	-0.17671
H	2.22871	0.83919	-0.58151
C	0.14188	0.95339	0.00356
C	-1.04722	0.27144	0.50954
H	0.10877	2.00618	-0.25570
O	-1.76150	-0.39581	-0.44110
H	-1.04016	-0.13761	1.51259
O	1.53521	-0.92564	0.10662
H	-2.38594	-0.99034	-0.01781

IM-2T trans a

C	-1.18739	-0.27787	0.24099
H	-0.90893	-1.08482	0.94083
C	-0.12069	0.60156	-0.16561
C	1.24733	0.45386	0.31639
H	-0.38882	1.38589	-0.86664
H	1.51441	0.70165	1.33657
O	1.99650	-0.48419	-0.33245
H	2.85693	-0.55994	0.08863
O	-2.33514	-0.15432	-0.14880

IM-2T trans b

C	1.18737	-0.27786	0.24099
H	0.90892	-1.08478	0.94088
C	0.12068	0.60160	-0.16559
C	-1.24734	0.45387	0.31641
H	0.38881	1.38592	-0.86662
O	-1.99646	-0.48419	-0.33248
H	-1.51430	0.70139	1.33668
O	2.33511	-0.15434	-0.14882
H	-2.85691	-0.55993	0.08858

TS-3T isomer a

C	-1.46481	0.40483	-0.14617
H	-0.89401	1.41361	0.45880
C	-0.09693	0.48594	-0.28601
C	1.03740	-0.46583	-0.17330
H	0.74392	-1.24320	0.54506
H	1.16428	-0.94683	-1.15145
O	2.19462	0.22373	0.23001
H	2.92607	-0.39658	0.26550
O	-2.29390	-0.39581	0.20937

www.manaraa.com

TS-3T isomer b

C	-1.29795	0.44752	-0.03189
H	-1.09167	1.25182	0.97108
C	-0.04551	1.02172	-0.00059
C	1.33180	0.44062	-0.12819
H	2.02018	0.92880	0.55807
O	1.34051	-0.93189	0.17427
H	1.67210	0.64559	-1.15144
O	-1.73227	-0.68337	-0.06703
H	0.60335	-1.36333	-0.27161

IM-3T cis a

C	-1.52452	0.51327	0.00006
C	-0.10274	0.72741	-0.00019
H	0.29887	1.72927	-0.00003
C	0.82928	-0.42730	-0.00017
H	0.61461	-1.05035	0.87904
H	0.61503	-1.05013	-0.87963
O	2.15131	0.05731	0.00023
H	2.75955	-0.68448	-0.00017
O	-2.08883	-0.53538	0.00009

IM-3T cis b

C	1.33249	0.44898	-0.08385
C	0.05221	1.09686	-0.07674
H	0.02896	2.17449	-0.14756
C	-1.23266	0.36725	0.13215
O	-1.20682	-1.00115	-0.14736
H	-1.54708	0.56367	1.17202
H	-2.00041	0.81837	-0.50272
O	1.57739	-0.70736	0.08766
H	-0.35824	-1.36689	0.12641

IM-3T trans a

C	1.42026	0.33837	-0.00023
C	0.14010	-0.30871	0.00007
H	0.06912	-1.39177	0.00059
C	-1.10143	0.49544	0.00011
H	-1.09759	1.15413	0.88020
H	-1.09737	1.15464	-0.87960
O	-2.20542	-0.37743	-0.00027
H	-3.01512	0.13665	0.00081
O	2.50385	-0.14811	0.00006

www.manaraa.com

IM-3T trans b

C	1.11511	-0.33586	-0.00004
C	0.16609	0.74334	0.00002
H	0.54077	1.76266	0.00010
C	-1.29888	0.54177	-0.00002
O	-1.60678	-0.82757	0.00002
H	-1.71706	1.05408	0.87952
H	-1.71701	1.05401	-0.87964
O	2.30171	-0.25155	0.00001
H	-2.56007	-0.93324	0.00002

TS-4T

C	-1.35964	-0.33297	-0.39707
H	-0.79942	-1.29055	-0.50749
C	0.23315	1.07562	-0.14505
C	1.10764	0.27624	0.45788
H	0.16360	1.61636	-1.07072
H	1.10180	0.15099	1.53591
O	1.97408	-0.50963	-0.24449
H	2.41529	-1.11951	0.35216
O	-2.32010	-0.17419	0.26893

CHOHCH + HCO

C	-1.55016	0.12400	-0.09486
H	-2.57170	0.18181	-0.46395
C	-0.89817	1.21044	0.24511
C	1.81210	0.41311	-0.44726
H	2.01160	1.47163	-0.15017
O	1.82625	-0.49842	0.29170
H	-0.19613	-1.17684	0.24147
O	-1.11388	-1.15424	-0.05697
H	-1.12529	2.25930	0.27690

TS-5T out

C	-1.74903	0.31732	-0.33890
C	0.27315	1.22083	-0.08705
H	0.45164	2.10190	-0.68081
C	1.16658	0.21175	0.49239
H	2.09973	0.68965	0.81961
H	0.68800	-0.22550	1.37638
O	1.42988	-0.79189	-0.48174
H	1.82865	-1.54715	-0.04285
O	-1.83141	-0.64789	0.24788

www.manaraa.com

TS-5T in

C	-1.55846	-0.25750	0.48406
C	0.16930	0.96005	-0.22257
H	-0.03773	1.54574	-1.10495
C	1.40977	0.41020	0.33092
H	2.22717	1.13077	0.19446
H	1.27623	0.25175	1.40681
O	1.70692	-0.81768	-0.32517
H	2.46054	-1.22144	0.11237
O	-2.46316	-0.23024	-0.19522

$CH_2OHCH + CO$

C	1.31417	-0.22309	-0.14134
H	1.89369	-0.85557	0.51152
C	0.05692	0.50493	0.03198
H	0.06859	1.03441	0.99628
H	-0.03040	1.26404	-0.75444
O	-1.03832	-0.40400	-0.02096
H	-1.85186	0.09805	0.07046
C	0.00000	0.00000	-0.64106
O	0.00000	0.00000	0.48079

TS-6T cis a

C	-1.45907	0.43697	-0.10812
C	-0.04226	0.69502	-0.06557
H	-1.12651	1.04115	0.96230
C	0.88471	-0.33211	0.02664
H	0.28819	1.71773	-0.17539
H	0.57424	-1.36583	0.09027
O	2.19968	-0.04110	0.00565
H	2.71992	-0.84719	-0.04266
O	-2.04420	-0.62703	0.00032

TS-6T cis b

C	-1.25243	0.40756	-0.07351
C	0.01862	1.09151	-0.05043
H	-1.01627	0.99931	1.04390
C	1.21458	0.37944	-0.02498
H	0.01995	2.16732	-0.12186
O	1.26586	-0.94496	0.04226
H	2.17769	0.86361	-0.09716
O	-1.44345	-0.80518	-0.04016
H	0.35474	-1.30021	0.05192

www.manaraa.com

TS-6T trans a

C	-1.35561	0.34167	0.03375
C	-0.06015	-0.32139	-0.00241
H	-0.84314	0.23045	1.19030
C	1.11526	0.38894	-0.07207
H	-0.02917	-1.40899	-0.00881
H	1.12259	1.46943	-0.13676
O	2.29097	-0.26447	0.01909
H	3.02125	0.33686	-0.14473
O	-2.47454	-0.12091	-0.10104

TS-6T trans b

C	1.02289	-0.27406	0.04975
C	0.03627	0.79941	-0.01013
H	0.59178	0.07335	1.20523
C	-1.31106	0.50521	-0.04529
H	0.37420	1.82819	-0.07465
O	-1.77509	-0.74398	-0.01686
H	-2.07748	1.26379	-0.07386
O	2.23029	-0.25566	-0.10164
H	-1.01872	-1.35151	-0.07463

IM-4T cis a

C	1.52920	0.43374	-0.02488
C	0.06328	0.79953	0.03179
H	-0.13518	1.51510	-0.76998
H	-0.06963	1.36483	0.96487
C	-0.82780	-0.38620	-0.05412
H	-0.50558	-1.34156	0.33845
O	2.00428	-0.64038	-0.01391
O	-2.15433	-0.07693	-0.01601
H	-2.67732	-0.88232	-0.01077

IM-4T cis b

C	1.38181	0.22015	0.23544
C	0.11424	1.05006	0.14223
H	0.37077	1.92195	-0.46078
H	-0.09161	1.42369	1.15291
C	-1.04912	0.32117	-0.43850
O	-1.45332	-0.73609	0.31593
O	1.58699	-0.83951	-0.22307
H	-1.81098	0.86494	-0.98586
H	-2.21921	-1.15404	-0.08415

www.manaraa.com

IM-4T trans a

C	-1.38207	0.36983	0.04102
C	-0.09103	-0.42306	0.10863
H	-0.12785	-1.20589	-0.65559
H	-0.10378	-0.93305	1.08423
C	1.09230	0.45226	-0.05709
H	1.07482	1.46614	0.32368
O	-2.47117	-0.04399	-0.09256
O	2.27566	-0.22111	-0.05643
H	3.00564	0.39942	-0.11578

IM-4T trans b

C	1.14780	-0.10661	-0.39411
C	0.09711	0.81619	0.21101
H	0.35216	1.81700	-0.14239
H	0.22119	0.79529	1.30338
C	-1.27103	0.45829	-0.23013
O	-1.64720	-0.79585	0.14294
O	2.16790	-0.43583	0.08194
H	-2.04220	1.21210	-0.32182
H	-2.54005	-0.97813	-0.15877

TS-7T isomer a

C	1.67406	-0.53124	0.03320
C	-0.12130	0.63754	0.02219
H	0.11942	1.25364	-0.83837
H	0.02373	1.13183	0.98156
C	-1.16300	-0.37693	-0.10298
H	-0.97594	-1.40189	0.19220
O	2.63694	0.06870	-0.02194
O	-2.44295	0.09206	0.01537
H	-3.05782	-0.64590	0.00265

TS-7T isomer b

C	1.35066	-0.00792	-0.54352
C	-0.29761	1.20242	0.06575
H	-0.19858	1.98057	-0.68073
H	0.06978	1.47741	1.05356
C	-1.44168	0.29546	-0.03852
O	-1.15579	-1.04289	-0.00842
O	2.00996	-0.38713	0.30051
H	-2.39933	0.58843	0.38436
H	-1.97343	-1.54610	0.00381

www.manaraa.com

$CHOHCH_2 + CO$			
C	-1.27409	-0.13819	0.01359
H	-1.84664	-0.38202	-0.87158
H	-1.67795	-0.46029	0.96770
C	0.03246	0.48565	-0.08338
H	0.19311	1.50434	0.25545
O	1.10781	-0.36241	0.00676
H	1.91876	0.15250	0.01313
C	0.00000	0.00000	-0.64106
O	0.00000	0.00000	0.48079

HCO			
C	0.06197	0.58133	0.00000
H	-0.86759	1.20850	0.00000
O	0.06197	-0.58706	0.00000

M06-2x/cc-pVTZ Cartesian Coordinates for the Singlet State Surface of $O(^3P)$ + Propargyl Alcohol

IM-1S noncyclic			
C	-1.19396	0.46296	-0.18245
C	0.12305	1.06398	-0.13546
H	-1.63696	0.64287	-1.17150
H	-1.76583	1.13796	0.48051
O	-1.37879	-0.86023	0.24905
C	1.19081	0.27806	0.38247
H	1.68008	0.53217	1.33592
O	1.58880	-0.60768	-0.36157
H	-0.67682	-1.39966	-0.13215

IM-1S cyclic			
C	1.08189	-0.82586	-0.09224
C	0.15557	0.01112	0.65629
H	1.84757	-1.39050	0.42999
O	1.43761	0.60338	-0.24448
H	0.83240	-1.22662	-1.07102
C	-1.05549	0.42985	-0.01886
H	-1.06764	1.47849	-0.37484
O	-2.03603	-0.27842	-0.09101
H	2.08317	0.84822	0.42866

www.manaraa.com

TS-2S a

C	-1.41891	0.39289	0.05914
H	-1.77250	1.35184	0.48899
C	-0.09395	0.40122	-0.48699
C	0.96898	-0.00605	0.34569
H	0.86705	1.02629	0.83244
H	0.76213	-0.73327	1.14007
O	2.21232	-0.16673	-0.25211
H	2.85076	-0.43587	0.41264
O	-2.14284	-0.57544	-0.04555

TS-2S b

C	1.17245	0.29642	0.35685
H	1.59968	0.60139	1.32737
C	0.09330	1.04930	-0.20419
C	-1.20569	0.45382	-0.15662
H	-1.50063	1.13640	0.69246
H	-1.87600	0.75389	-0.96545
O	-1.38910	-0.88567	0.20176
H	-0.60935	-1.38292	-0.07160
O	1.64235	-0.60257	-0.32164

IM-2S cis a

C	-1.45221	0.40185	0.00004
H	-2.13461	1.27030	0.00021
C	-0.02432	0.73154	-0.00003
C	0.86761	-0.26011	0.00002
H	0.28949	1.76575	-0.00006
H	0.52788	-1.29098	0.00009
O	2.19112	-0.04387	-0.00003
H	2.66617	-0.87787	0.00024
O	-1.90305	-0.71948	-0.00004

IM-2S cis b

C	-1.23389	0.34362	-0.00001
H	-2.17781	0.90860	-0.00010
C	-0.00814	1.09757	0.00004
C	1.17400	0.43513	-0.00002
H	-0.02786	2.17478	0.00007
O	1.29068	-0.87331	0.00002
H	2.12726	0.95280	-0.00020
O	-1.27580	-0.88354	-0.00001
H	0.36755	-1.23928	-0.00001

www.manaraa.com

IM-2S trans a

C	-1.06865	-0.34383	0.00020
H	-0.64956	-1.36378	0.00048
C	-0.09325	0.74757	0.00031
C	1.22494	0.54464	-0.00011
H	-0.47146	1.75901	0.00014
H	1.92227	1.37559	-0.00054
O	1.77350	-0.68830	0.00003
H	2.73068	-0.63021	-0.00058
O	-2.26228	-0.16557	-0.00026

IM-2S trans b

C	1.08345	-0.37142	-0.00010
C	-0.03725	0.35423	0.00006
O	2.34199	0.08259	0.00005
H	-0.03238	1.43757	-0.00024
H	1.05357	-1.45505	-0.00037
C	-1.32586	-0.32819	0.00007
H	-1.26448	-1.43473	0.00029
O	-2.39515	0.22722	-0.00004
H	2.34646	1.04608	0.00006

TS-3S isomer a

C	1.35826	0.25595	0.19060
C	0.05078	0.47413	-0.22507
C	-1.02585	-0.40545	0.12053
O	-2.33367	0.05406	-0.00593
H	-0.74860	-1.12723	-0.70283
H	-0.94709	-0.98544	1.04158
H	1.28466	0.90508	1.13304
O	2.38811	-0.24888	-0.16869
H	-2.32363	0.81838	-0.59123

TS-3S isomer b

C	1.14386	0.17735	0.29495
C	0.05845	1.00825	0.00292
C	-1.25605	0.46864	-0.14352
H	-2.07979	1.10058	0.18042
H	-1.16589	0.68949	-1.25605
O	-1.58228	-0.86016	0.12545
H	1.12322	0.30105	1.42906
O	1.99376	-0.46299	-0.27049
H	-0.84695	-1.43143	-0.11922

www.manaraa.com

TS-3S isomer c

C	-1.18189	-0.34437	-0.06453
C	0.09482	-0.54934	-0.59599
C	1.25151	-0.54447	0.33103
H	2.10828	-1.14718	0.04068
O	1.41073	0.84428	0.00496
H	1.06631	-0.61142	1.40088
H	-1.43932	-1.45894	0.03448
O	-1.97960	0.52227	0.16521
H	1.82909	0.91422	-0.86037

IM-3S isomer a

C	-1.52452	0.51327	0.00006
C	-0.10274	0.72741	-0.00019
H	0.29887	1.72927	-0.00003
C	0.82928	-0.42730	-0.00017
H	0.61461	-1.05035	0.87904
H	0.61503	-1.05013	-0.87963
O	2.15131	0.05731	0.00023
H	2.75955	-0.68448	-0.00017
O	-2.08883	-0.53538	0.00009

IM-3S isomer b

C	1.33249	0.44898	-0.08385
C	0.05221	1.09686	-0.07674
H	0.02896	2.17449	-0.14756
C	-1.23266	0.36725	0.13215
O	-1.20682	-1.00115	-0.14736
H	-1.54708	0.56367	1.17202
H	-2.00041	0.81837	-0.50272
O	1.57739	-0.70736	0.08766
H	-0.35824	-1.36689	0.12641

TS-6S

C	-1.25239	0.26655	0.41130
H	-1.53557	1.41618	0.26135
O	-2.07118	-0.63763	-0.24181
H	-1.23436	0.14693	1.49389
C	-0.18554	0.92772	-0.21962
H	-0.34442	0.84989	-1.30371
C	1.63936	-0.31435	-0.27158
O	2.65503	-0.20651	0.20141
H	-2.76502	-0.93942	0.35111

www.manaraa.com

$CHOHCH_2 + CO$

C	-1.27409	-0.13819	0.01359
H	-1.84664	-0.38202	-0.87158
H	-1.67795	-0.46029	0.96770
C	0.03246	0.48565	-0.08338
H	0.19311	1.50434	0.25545
O	1.10781	-0.36241	0.00676
H	1.91876	0.15250	0.01313
C	0.00000	0.00000	-0.64106
O	0.00000	0.00000	0.48079

TS-8S

C	-1.25963	0.23199	0.07351
H	-0.39817	0.90091	1.13110
C	-0.03015	0.87821	-0.10289
C	0.91981	-0.11286	-0.49744
H	0.55192	-0.99673	-0.99844
O	2.06295	-0.24133	0.25978
O	-2.07534	-0.59651	0.07396
H	0.00206	1.96139	-0.20773
H	2.16315	-1.14693	0.56610

Cyclopropanone-2-ol

C	-0.76993	-0.02738	0.07589
C	0.63883	0.08619	0.48620
C	-0.11718	1.25337	-0.20239
H	0.86020	0.24834	1.53726
O	1.63106	-0.54331	-0.25996
H	0.13695	1.43826	-1.23957
H	-0.32202	2.13072	0.39614
O	-1.71842	-0.73115	-0.07274
H	1.51341	-1.49469	-0.19043

TS-10S

C	1.35826	0.25587	0.19055
H	1.28439	0.90514	1.13289
C	0.05076	0.47377	-0.22509
O	2.38830	-0.24868	-0.16858
C	-1.02598	-0.40560	0.12050
O	-2.33371	0.05416	-0.00610
H	-0.94741	-0.98580	1.04144
H	-0.74879	-1.12725	-0.70300
H	-2.32312	0.81982	-0.58966

المنارة للاستشارات
www.manaraa.com

TS-11S

C	1.47317	-0.36098	-0.00075
C	-0.11346	0.80854	-0.00048
C	-1.12791	0.10414	-0.00016
H	0.30995	-1.62579	-0.00109
H	0.39365	1.74670	-0.00072
H	-0.49371	-1.40207	-0.00062
O	-2.43353	-0.08592	0.00056
O	2.56385	-0.03959	0.00079
H	-2.64320	-1.02504	-0.00004

COHCH + H_2 + CO

C	-1.31737	0.01676	0.00016
C	-0.12357	-0.01245	-0.00037
H	-2.37721	0.04264	0.00015
O	1.18088	-0.10529	0.00013
H	1.57574	0.77384	0.00008
C	0.00000	0.00000	-0.64106
O	0.00000	0.00000	0.48079
H	0.00000	0.00000	0.36915
H	0.00000	0.00000	-0.36915

TS-12S isomer a

C	-0.99652	0.17775	-0.13235
H	-0.30643	2.05597	0.40395
C	0.00816	1.20171	-0.19143
C	0.91036	0.26787	0.51950
O	1.33482	-0.83928	-0.21978
H	0.71755	0.08028	1.56581
O	-1.63654	-0.77073	0.05039
H	0.26970	1.50568	-1.20380
H	2.20094	-0.64573	-0.58519

TS-12S isomer b

C	0.97792	0.26526	-0.06470
H	-0.27240	1.50277	-1.24131
C	-0.08078	1.25869	-0.19725
C	-0.88742	0.24059	0.45645
H	-0.89860	0.18326	1.53495
O	-1.31434	-0.83940	-0.27620
O	1.52732	-0.76404	0.05887
H	0.12767	2.14586	0.39209
H	-0.71885	-1.59163	-0.11412

www.manaraa.com

$CHOHCH_2 + CO$

C	-1.27409	-0.13819	0.01359
H	-1.84664	-0.38202	-0.87158
H	-1.67795	-0.46029	0.96770
C	0.03246	0.48565	-0.08338
H	0.19311	1.50434	0.25545
O	1.10781	-0.36241	0.00676
H	1.91876	0.15250	0.01313
C	0.00000	0.00000	-0.64106
O	0.00000	0.00000	0.48079

M06-2x/cc-pVTZ Cartesian Coordinates for the Novel HCO/HOC Pathways, Triplet Surface of $O(^3P)$ + Propargyl Alcohol

TS-HCO to HOC

C	0.06901	0.73038	0.00000
H	-0.96612	-0.09097	0.00000
O	0.06901	-0.53641	0.00000

HOC

C	0.05965	0.78801	0.00000
O	0.05965	-0.48065	0.00000
H	-0.83507	-0.88287	0.00000

TS-8T

C	-1.13825	-0.54938	-0.15550
H	-2.00300	-1.14778	-0.42111
C	0.12643	-1.08244	-0.10180
C	1.34543	-0.28287	0.25144
H	1.45057	-0.25457	1.34586
H	2.24017	-0.75620	-0.17203
O	1.00564	0.89532	-0.34180
H	-0.49277	1.12392	0.17416
O	-1.40522	0.67003	0.23033

www.manaraa.com

IM-5T

C	1.16525	0.52955	-0.21783
H	1.97913	1.10675	-0.63795
C	-0.06472	1.00091	-0.10495
C	-1.30567	0.32737	0.34905
H	-1.25660	0.12548	1.42701
H	-2.17049	0.96854	0.13877
O	-1.33793	-0.83100	-0.41041
H	0.79656	-1.24388	0.35631
O	1.57321	-0.68198	0.23019

TS-9T

C	1.22392	0.51043	0.03295
H	2.15044	1.06807	0.03690
C	-0.01830	1.09873	0.08255
C	-1.27072	0.37065	0.03172
H	-2.19914	0.90484	0.24544
H	-0.90370	0.95115	-1.08447
O	-1.20806	-0.90298	0.02058
H	0.37160	-1.14852	-0.01570
O	1.32948	-0.80382	-0.02877

IM-6T

C	-1.23352	0.47743	0.00013
H	-2.14296	1.05289	0.00013
C	0.09868	1.08083	-0.00003
C	1.28810	0.33497	-0.00003
H	2.24159	0.86678	-0.00014
O	1.26381	-0.93221	0.00007
H	-0.43698	-1.21736	-0.00007
O	-1.35600	-0.84564	-0.00010
H	0.15626	2.16116	-0.00014

TS-10T

C	1.38301	0.27265	0.05697
H	2.40057	0.55252	0.32396
C	0.47571	1.20902	-0.11767
C	-1.59898	0.42475	0.24481
H	-1.92398	1.24938	-0.43454
O	-1.58608	-0.72258	-0.07007
H	0.30107	-1.27226	-0.16521
O	1.23367	-1.05877	-0.01861
H	0.48318	2.28268	-0.11940

www.manaraa.com

$CH_2CH_2OH + HCO$

C	-1.55016	0.12400	-0.09486
H	-2.57170	0.18181	-0.46395
C	-0.89817	1.21044	0.24511
C	1.81210	0.41311	-0.44726
H	2.01160	1.47163	-0.15017
O	1.82625	-0.49842	0.29170
H	-0.19613	-1.17684	0.24147
O	-1.11388	-1.15424	-0.05697
H	-1.12529	2.25930	0.27690

TS-11T cis a

C	-0.93376	-0.34099	-0.09741
H	-0.27730	1.72535	0.14104
C	0.08221	0.71468	-0.01249
C	1.48323	0.37835	0.07398
O	1.90643	-0.76236	0.02126
H	2.16178	1.24320	0.15620
O	-2.25230	-0.17375	-0.00435
H	-0.36671	0.31165	-1.12708
H	-2.54093	-0.30363	0.91007

TS-11T cis b

C	1.48591	0.36947	-0.07284
H	2.17416	1.22593	-0.15988
C	0.09023	0.72238	0.03981
C	-0.93502	-0.31180	0.11854
H	-0.25596	1.74010	-0.10068
O	-2.21919	-0.15570	-0.20929
H	-0.37587	0.35554	1.16163
O	1.89539	-0.77741	-0.02493
H	-2.79861	-0.53701	0.45962

TS-11T trans a

C	-1.07122	-0.33852	0.13051
H	-0.61914	-1.28776	0.46927
C	-0.14480	0.76696	-0.02920
C	1.30351	0.57986	0.00923
H	-0.52770	1.72073	-0.36708
H	0.51921	0.85678	1.06432
O	1.94891	-0.57465	-0.18807
H	2.58768	-0.74595	0.51229
O	-2.25954	-0.24956	-0.10468

www.manaraa.com

TS-11T trans b

C	1.07122	-0.33852	0.13049
H	0.61913	-1.28778	0.46920
C	0.14480	0.76696	-0.02920
C	-1.30351	0.57987	0.00920
H	0.52770	1.72073	-0.36704
O	-1.94891	-0.57465	-0.18806
H	-0.51923	0.85677	1.06431
O	2.25954	-0.24955	-0.10466
H	-2.58766	-0.74595	0.51232

IM-7T cis a

C	-1.10670	0.50617	-0.32528
H	0.06667	1.06438	1.37521
C	0.10862	1.10634	0.28182
C	1.18163	0.17271	-0.24323
O	1.29337	-0.95959	0.15725
H	1.78519	0.53586	-1.09250
O	-1.58561	-0.67707	0.02835
H	0.25967	2.12621	-0.06112
H	-0.87491	-1.34450	0.01371

IM-7T cis b

C	1.48690	0.32301	0.01740
H	2.23260	1.13973	0.04264
C	0.05330	0.78299	0.00755
C	-0.90801	-0.33483	-0.09349
H	-0.06148	1.49707	-0.82129
O	-2.23761	-0.18832	-0.06504
H	-0.10306	1.37732	0.92104
O	1.83160	-0.82349	0.00507
H	-2.61308	-0.54667	0.74866

IM-7T trans a

C	-1.09608	-0.35385	0.18419
H	-0.70299	-1.33111	0.52079
C	-0.08814	0.78366	0.21297
C	1.16624	0.37723	-0.46831
H	-0.53346	1.65053	-0.27036
H	0.12063	1.03189	1.26305
O	2.02809	-0.52783	0.00680
H	2.80481	-0.11028	0.40164
O	-2.22572	-0.23257	-0.19283

www.manaraa.com

IM-7T trans b

C	1.09608	-0.35386	0.18419
H	0.70298	-1.33112	0.52078
C	0.08814	0.78366	0.21297
C	-1.16625	0.37725	-0.46830
H	0.53347	1.65053	-0.27036
O	-2.02809	-0.52784	0.00678
H	-0.12061	1.03190	1.26304
O	2.22572	-0.23258	-0.19283
H	-2.80473	-0.11031	0.40179

TS-12T

C	-1.31748	0.59673	-0.55715
H	0.42350	1.09533	1.36469
C	0.82306	1.14338	0.36266
C	1.19754	-0.07602	-0.30716
O	0.93930	-1.18896	0.12965
H	1.73053	0.03600	-1.26289
O	-1.71376	-0.31705	0.23020
H	1.06079	2.10221	-0.07066
H	-1.23788	-1.16994	0.10002

HOC + CH_2CHO

C	1.99787	0.86125	0.00066
H	-0.39298	1.52429	0.00018
C	-1.39709	1.11085	-0.00020
C	-1.56859	-0.29844	-0.00002
O	-0.62907	-1.09967	0.00040
H	-2.59155	-0.69368	-0.00024
O	1.89387	-0.39029	-0.00063
H	-2.26079	1.75871	-0.00060
H	0.93373	-0.71165	-0.00011

TS-13T

C	1.18810	0.50400	0.19411
C	-0.10858	1.17292	0.00744
H	-0.13720	1.69881	-0.95839
H	-0.30598	1.92118	0.77737
C	-1.21199	0.16630	-0.06804
O	-0.96589	-1.05307	0.13020
O	1.36229	-0.69853	-0.15595
H	-2.19733	0.46591	-0.42568
H	0.26408	-1.13242	0.01154

www.manaraa.com

IM-8T

C	-1.10461	0.50387	-0.37458
C	0.17077	1.11905	0.04889
H	0.11647	1.55831	1.05798
H	0.45871	1.93354	-0.61865
C	1.29695	0.10818	0.08596
O	1.14979	-1.06534	-0.12335
O	-1.64393	-0.56582	0.20473
H	2.29356	0.51161	0.34443
H	-1.09428	-1.34073	0.00361

TS-14T

C	-1.31766	0.59672	-0.55699
C	0.82305	1.14341	0.36267
H	0.42361	1.09523	1.36475
H	1.06018	2.10232	-0.07079
C	1.19765	-0.07591	-0.30722
O	0.93972	-1.18888	0.12968
O	-1.71394	-0.31722	0.23017
H	1.73032	0.03621	-1.26312
H	-1.23850	-1.17026	0.09950

HOC + CH_2CHO

C	1.99787	0.86125	0.00066
H	-0.39298	1.52429	0.00018
C	-1.39709	1.11085	-0.00020
C	-1.56859	-0.29844	-0.00002
O	-0.62907	-1.09967	0.00040
H	-2.59155	-0.69368	-0.00024
O	1.89387	-0.39029	-0.00063
H	-2.26079	1.75871	-0.00060
H	0.93373	-0.71165	-0.00011

TS-15T

C	-1.15762	0.12897	-0.35985
C	-0.69161	1.21457	0.27466
H	-0.51095	1.18009	1.34434
H	-0.75006	2.18362	-0.19790
C	1.32568	0.49921	-0.20175
O	1.52125	-0.60454	0.20902
O	-1.12376	-1.12820	-0.01031
H	1.42535	0.80288	-1.26436
H	-0.20286	-1.36114	0.24989

www.manaraa.com

HCO + CH_2COH

C	-1.11874	-0.09344	-0.37727
C	-1.97778	0.79887	0.06242
H	-2.39694	0.71403	1.06048
H	-2.28441	1.62063	-0.56573
C	1.95141	0.89060	0.09474
O	1.99257	-0.26977	-0.07112
O	-0.70599	-1.23765	0.13956
H	1.00840	1.46770	0.26493
H	0.25099	-1.31914	0.01353

TS-16T

C	1.54822	0.42070	-0.14920
C	0.16682	0.96036	0.05178
H	-0.15776	1.50738	-0.83981
H	0.20663	1.68793	0.87020
C	-0.79183	-0.20200	0.33317
H	0.55479	-1.14847	0.17253
O	1.56481	-0.83309	-0.01487
O	-1.99552	-0.26711	-0.23985
H	-2.69725	-0.31955	0.42037

IM-9T

C	1.47422	0.34223	-0.33737
C	0.15298	1.01868	0.02540
H	-0.17519	1.60120	-0.84148
H	0.44288	1.75184	0.78576
C	-0.95245	0.15485	0.52377
H	0.68295	-1.16194	0.52258
O	1.51751	-0.87955	0.07117
O	-1.80267	-0.49856	-0.27762
H	-2.71790	-0.26081	-0.08610

TS-17T-A

C	1.72148	0.29181	-0.36769
C	-0.19334	1.19964	0.02452
H	-0.32288	1.58489	-0.98217
H	0.22663	1.88447	0.74771
C	-1.03416	0.22864	0.46079
H	0.65968	-0.95649	0.55257
O	1.57818	-0.83481	0.15539
O	-1.69094	-0.68319	-0.27813
H	-2.62523	-0.68945	-0.04198

www.manaraa.com

TS-17T-B

C	1.32560	0.17222	-0.42349
C	0.65828	1.22847	0.11707
H	0.48389	2.11464	-0.47673
H	0.64013	1.34368	1.19586
C	-0.96050	-0.28179	0.46903
H	0.29384	-1.09300	0.36442
O	1.37552	-1.00994	0.03433
O	-1.98526	-0.17493	-0.29964
H	-2.68026	0.40019	0.06329

HOC + CH_2COH-A

C	-2.61937	0.22240	0.18607
C	0.55601	1.15845	0.04708
H	0.43361	1.32855	1.11284
H	0.00821	1.78478	-0.64086
C	1.38419	0.23751	-0.39573
H	-0.90627	-0.44782	-0.20821
O	-1.85293	-0.73110	-0.13064
O	2.05840	-0.70523	0.24422
H	2.89566	-0.88505	-0.19693

HOC + CH_2COH-B

C	1.53702	0.04161	-0.37897
C	1.28877	1.22553	0.14314
H	1.53541	2.12653	-0.39686
H	0.87940	1.31299	1.14652
C	-1.44880	-0.31256	0.49121
H	0.35095	-1.25604	0.27220
O	1.29342	-1.19184	0.01012
O	-2.30629	0.10614	-0.33309
H	-2.92471	0.77462	0.02966

TS-18T

C	-1.48059	0.46113	-0.03668
H	-2.07377	1.33847	-0.31375
C	-0.01211	0.63094	-0.10740
C	0.97533	-0.28759	-0.03895
H	-0.91512	0.82961	1.05696
H	0.73443	-1.34599	-0.04907
O	2.26929	0.07865	0.03215
H	2.83198	-0.69859	-0.01048
O	-1.95345	-0.69744	0.01965

www.manaraa.com

IM-10T

C	1.45659	-0.53216	0.00006
H	1.89732	-1.05010	-0.86734
C	-0.01806	-0.61392	-0.00026
C	-0.99053	0.26037	0.00004
H	1.89695	-1.05010	0.86763
H	-0.75709	1.32402	0.00034
O	-2.31181	-0.07872	0.00020
H	-2.84192	0.71997	-0.00122
O	1.95139	0.75003	-0.00000

TS-19T

C	1.43466	-0.49417	-0.07131
H	1.71064	-0.98793	-1.01307
C	-0.03841	-0.67602	0.12478
C	-0.98690	0.22757	-0.10797
H	1.99579	-1.03606	0.70799
H	-0.34858	0.36452	0.96079
O	-2.31216	0.02216	-0.01557
H	-2.75725	0.86113	-0.16302
O	1.93006	0.78460	-0.00514

IM-11T

C	1.44266	0.42963	0.00384
H	1.91647	0.90134	0.88268
C	-0.03006	0.72056	-0.03218
C	-0.93980	-0.22577	-0.01971
H	1.96273	0.90715	-0.84477
O	-2.26222	-0.15377	0.08949
H	-2.67646	-0.81695	-0.47228
O	1.80071	-0.88352	0.01014
H	-0.34742	1.76025	-0.07431

TS-20T

C	1.87478	0.29427	-0.06241
H	2.06035	0.95644	0.80028
C	-0.27895	0.95864	0.00777
C	-0.99261	-0.13917	-0.06247
H	2.00300	0.74893	-1.05688
O	-2.30110	-0.28816	0.09716
H	-2.65571	-0.85254	-0.60056
O	1.73590	-0.90445	0.07809
H	-0.50535	2.00564	0.15781

www.manaraa.com

H_2CO + CHCOH

C	-2.06671	0.29016	0.06903
H	-2.20446	0.97705	-0.78377
C	0.61089	1.17740	-0.01763
C	1.02186	-0.07240	0.04104
H	-2.14134	0.74051	1.07299
O	2.27268	-0.50651	-0.08215
H	2.47654	-1.12360	0.63123
O	-1.85589	-0.87874	-0.08768
H	1.13877	2.11706	-0.11646

M06-2x/cc-pVTZ Cartesian Coordinates for the Triplet State Surface of $O(^3P)$ + 3-Butyn-1-ol

IM-0T, $O(^3P)$ + 3-Butyn-1-ol

C	0.75511	-1.22806	-0.08594
C	-0.69126	-1.03761	-0.08280
C	-1.87993	-0.86172	-0.06164
H	-2.93534	-0.74154	-0.04664
C	1.50203	0.00924	0.42678
H	1.00111	-2.09112	0.53629
H	1.08832	-1.44097	-1.10277
H	2.56609	-0.22097	0.46707
H	1.16582	0.24002	1.44291
O	1.35475	1.10996	-0.43018
H	0.44752	1.42739	-0.35480
O	-1.53590	1.58205	0.16512

www.manaraa.com

TS-1T

C	0.78333	-1.20711	-0.12257
C	-0.65689	-1.01772	-0.08995
C	-1.82196	-0.67183	-0.02776
H	-2.88506	-0.67690	-0.00162
C	1.51331	0.03879	0.41458
H	1.04986	-2.08021	0.47704
H	1.10109	-1.38844	-1.15030
H	2.58394	-0.16263	0.40249
H	1.20862	0.20888	1.45238
O	1.29105	1.16316	-0.38566
H	0.36566	1.42484	-0.27575
O	-1.58241	1.31455	0.14191

IM-1T

C	-0.76932	1.20385	-0.12175
C	0.69220	1.16818	-0.14082
C	1.71673	0.20488	-0.00310
C	-1.42404	-0.07397	0.44081
H	-1.09415	2.07245	0.46046
H	-1.13566	1.35461	-1.14300
H	-2.49624	0.10673	0.51660
H	-1.03914	-0.26325	1.44796
O	-1.24530	-1.17623	-0.40049
H	-0.32278	-1.45297	-0.30952
O	1.50096	-1.00025	0.15166
H	2.74922	0.57661	-0.03265

TS-2T

C	-0.65704	1.19447	-0.15257
C	0.77006	1.11345	-0.19990
C	1.72461	0.07347	-0.01719
C	-1.45460	0.04788	0.43655
H	0.26650	1.82970	0.67406
H	-1.13608	1.97173	-0.73344
H	-2.49774	0.34766	0.51571
H	-1.08231	-0.17456	1.44172
O	-1.39909	-1.08432	-0.39052
H	-0.49097	-1.41976	-0.33318
O	1.38171	-1.10194	0.14375
H	2.78155	0.35981	0.00792

IM-2T

C	-0.43853	1.06926	-0.41825
C	0.94153	1.08852	0.03917
C	1.71626	-0.11554	0.13122
C	-1.49929	0.36162	0.37275
H	1.40615	2.01232	0.37058
H	-0.62852	1.20626	-1.47754
H	-2.46014	0.86101	0.24705
H	-1.24502	0.37506	1.43769
O	-1.67283	-0.96135	-0.09793
H	-0.79404	-1.36219	-0.15187
O	1.25282	-1.22663	-0.10595
H	2.76192	-0.01171	0.45580

www.manaraa.com

TS-3T

C	-0.47683	1.23615	0.09348
C	0.94423	1.09005	-0.14564
C	1.64965	-0.16425	0.00336
C	-1.54631	0.24823	0.38794
H	1.52422	1.99467	-0.27286
H	0.14046	1.03378	-1.10107
H	-2.51968	0.72850	0.28924
H	-1.43900	-0.07692	1.43189
O	-1.51460	-0.84878	-0.49267
H	-0.68774	-1.32083	-0.30071
O	1.11713	-1.24150	0.25072
H	2.73706	-0.09806	-0.14568

IM-3T

C	-0.50012	1.00891	0.49422
C	0.76261	1.12857	-0.24250
C	1.67931	-0.07501	-0.12595
C	-1.72941	0.25759	0.18271
H	1.33794	2.00271	0.07955
H	0.59211	1.27256	-1.32133
H	-2.36279	0.81262	-0.51891
H	-2.31613	0.11142	1.09649
O	-1.43585	-0.97577	-0.45256
H	-0.71176	-1.38952	0.03337
O	1.37285	-1.12414	0.36867
H	2.69032	0.06914	-0.54892

TS-4T

C	0.53849	1.09143	-0.41722
C	-0.33381	1.45046	0.52276
C	-1.75403	-0.04773	-0.18988
C	1.43586	-0.07683	-0.57103
H	-0.93268	2.34796	0.42746
H	-0.26844	1.00828	1.51434
H	2.46156	0.25345	-0.73815
H	1.13158	-0.64943	-1.45604
O	1.43796	-0.88419	0.58756
H	0.57495	-1.30954	0.65204
O	-1.46087	-1.18039	-0.00072
H	-2.10266	0.36193	-1.16215

$HCO + CH_2CCH_2OH$

C	-1.03145	0.78183	0.53723
C	-0.78771	1.68116	-0.37870
C	2.00687	0.50071	-0.05244
C	-1.15966	-0.69137	0.59048
H	-0.74102	2.73978	-0.15155
H	-0.64687	1.38622	-1.41750
H	-2.17159	-0.95600	0.89951
H	-0.47424	-1.09170	1.34452
O	-0.94219	-1.29177	-0.67183
H	0.00618	-1.30430	-0.83347
O	1.90483	-0.66173	0.07087
H	2.15801	1.22002	0.78681

www.manaraa.com

TS-5T

C	-0.71120	1.19499	-0.09728
C	0.55796	1.47653	-0.17605
C	1.95149	-0.14135	0.05755
C	-1.28230	-0.04160	0.56551
H	1.18196	2.25255	-0.58812
H	-1.42207	1.85697	-0.59287
H	-2.22261	0.21446	1.05127
H	-0.59013	-0.40387	1.32775
O	-1.57500	-1.04030	-0.38345
H	-0.73386	-1.39271	-0.69357
O	1.38787	-1.18237	-0.07281
H	2.18803	0.32260	1.04725

HCO + $CHCHCH_2OH$

C	-1.23616	0.83187	-0.24032
C	-0.43931	1.85007	-0.07634
C	2.15173	0.37956	0.24078
C	-1.18219	-0.44245	0.56615
H	-0.28853	2.82275	-0.51453
H	-1.99663	0.85512	-1.02277
H	-2.14145	-0.59394	1.06249
H	-0.41624	-0.35697	1.34324
O	-0.97874	-1.57203	-0.25121
H	-0.08072	-1.53028	-0.59441
O	1.90134	-0.62460	-0.30783
H	1.77835	0.66204	1.25667

TS-6T

C	-0.87926	1.16667	-0.07653
C	0.59291	1.18413	-0.24978
C	1.60407	0.25386	-0.13810
C	-1.36658	-0.18919	0.46711
H	-1.19741	1.98617	0.56847
H	-1.32684	1.32198	-1.06254
H	-2.44654	-0.13047	0.60288
H	-0.91112	-0.37552	1.44425
O	-1.11203	-1.23275	-0.43214
H	-0.19132	-1.50604	-0.33331
O	1.68394	-0.90923	0.21098
H	1.79122	1.34687	0.53331

IM-4T

C	-0.61730	1.21720	0.03431
C	0.84900	1.13607	-0.22153
C	1.68183	-0.02445	-0.07196
C	-1.31086	-0.06507	0.47608
H	-0.78186	2.00482	0.77995
H	-1.09788	1.57808	-0.88274
H	-2.34963	0.17036	0.70749
H	-0.84639	-0.45193	1.38693
O	-1.32900	-1.03831	-0.54168
H	-0.49597	-1.51770	-0.50245
O	1.40431	-1.13687	0.26132
H	1.35316	2.03525	-0.54771

www.manaraa.com

TS-7T

C	-1.19633	0.99177	0.13667
C	0.12315	1.47046	-0.30813
C	2.03923	0.37851	0.00450
C	-1.23446	-0.49047	0.51019
H	-1.53199	1.57588	1.00399
H	-1.92936	1.15627	-0.66219
H	-2.23307	-0.73751	0.86783
H	-0.53036	-0.68859	1.32397
O	-0.99006	-1.33052	-0.59454
H	-0.05315	-1.29998	-0.80223
O	1.92284	-0.72912	0.22299
H	0.42618	2.36941	-0.81833

$CO + CHCH_2CH_2OH$

C	-1.59808	0.71165	0.16263
C	-0.51646	1.51835	-0.41686
C	2.25927	0.43168	0.64410
C	-1.10705	-0.67938	0.56930
H	-2.02847	1.20393	1.04407
H	-2.40602	0.59196	-0.56852
H	-1.92426	-1.24337	1.01630
H	-0.31821	-0.57712	1.32388
O	-0.66178	-1.43064	-0.53591
H	0.03570	-0.93431	-0.97513
O	2.26984	-0.22328	-0.26865
H	-0.44926	2.29643	-1.15905

TS-8T

C	-0.51922	1.22029	0.03593
C	0.92553	1.07429	-0.25539
C	1.65111	-0.15945	-0.11837
C	-1.35980	0.05363	0.45822
H	0.56459	1.47475	0.84998
H	-0.96014	2.17290	-0.21878
H	-2.37219	0.40283	0.65250
H	-0.97391	-0.38332	1.38425
O	-1.44739	-0.92912	-0.55348
H	-0.63756	-1.45042	-0.51486
O	1.29360	-1.22619	0.28803
H	1.42381	1.89314	-0.75178

IM-5T

C	-0.28566	1.12960	-0.29580
C	1.18249	1.01130	-0.03015
C	1.67224	-0.40832	0.14521
C	-1.29689	0.35481	0.47784
H	1.48884	1.55320	0.87449
H	-0.62082	1.82875	-1.04841
H	-2.14462	0.98964	0.73743
H	-0.85835	-0.01236	1.41267
O	-1.84632	-0.71937	-0.27238
H	-1.11783	-1.30925	-0.49228
O	1.07523	-1.40660	-0.03168
H	1.78849	1.43349	-0.83400

www.manaraa.com

TS-9T

C	-0.74489	0.89627	0.00622
C	0.68442	1.18481	-0.00151
C	1.77621	-0.65716	0.06243
C	-1.30347	-0.48213	0.12374
H	1.14167	1.57401	0.90544
H	-1.44679	1.71028	0.16068
H	-1.10092	-0.89955	1.11706
H	-0.80538	-1.15121	-0.58837
O	-2.70661	-0.50929	-0.03065
H	-2.91892	-0.16930	-0.90334
O	2.89595	-0.52547	-0.08492
H	1.14207	1.56311	-0.91217

$CO + CH_2CHCH_2OH$

C	-1.10111	0.97440	0.05822
C	0.22877	1.54694	-0.02932
C	2.30989	-0.91488	0.14122
C	-1.31943	-0.49999	0.14596
H	0.81183	1.76536	0.85844
H	-1.95473	1.60021	0.30393
H	-1.07762	-0.86785	1.15035
H	-0.63540	-1.01623	-0.53955
O	-2.66443	-0.86806	-0.08299
H	-2.91975	-0.53547	-0.94712
O	3.21771	-0.31561	-0.13573
H	0.64063	1.88451	-0.97271

TS-10T

C	-0.29489	0.85866	-0.45936
C	1.10930	1.03997	0.03948
C	1.84126	-0.28499	0.19938
C	-1.31328	0.27594	0.43730
H	1.14576	1.53533	1.01361
H	-0.49279	0.77776	-1.51878
H	-1.30733	1.51933	0.06594
H	-1.07892	0.21612	1.49462
O	-2.21346	-0.63384	-0.04452
H	-1.75950	-1.18987	-0.69212
O	1.42838	-1.34745	-0.08551
H	1.71910	1.65424	-0.62384

IM-6T

C	-0.42527	1.09282	-0.44124
C	0.95566	1.08339	0.23186
C	1.65475	-0.25536	0.20467
C	-1.47343	0.29496	0.26404
H	0.88591	1.36524	1.28487
H	-0.31449	0.74624	-1.47610
H	-2.42024	0.74437	0.52301
O	-1.57480	-1.04237	0.06156
H	-0.71378	-1.40114	-0.19021
O	1.25037	-1.29183	-0.18353
H	1.64289	1.79274	-0.23322
H	-0.75515	2.13132	-0.48861

www.manaraa.com

TS-11T

C	0.72605	0.96845	0.50142
C	-0.44187	1.47471	-0.29745
C	-1.94777	-0.09189	-0.31974
C	1.58781	-0.02438	-0.19922
H	-0.31753	1.57161	-1.36820
H	0.36344	0.55783	1.45447
H	2.63238	0.16314	-0.39065
O	1.29091	-1.35060	-0.16182
H	0.38336	-1.48078	0.13084
O	-1.64770	-1.00034	0.30239
H	-1.09727	2.20274	0.16460
H	1.34457	1.83170	0.77429

$CO + CH_2CH_2CHOH$ (MP2, M06-2x DNC)

C	1.30012	0.60879	0.63128
C	1.07411	1.47257	-0.56964
C	-2.65220	0.13378	0.70770
C	1.51368	-0.83277	0.28026
H	1.72328	1.36858	-1.43169
H	0.45089	0.71987	1.32412
H	1.96594	-1.50782	0.99674
O	0.55265	-1.46149	-0.46658
H	0.15074	-0.79677	-1.03751
O	-2.34283	0.04066	-0.38539
H	0.42813	2.33967	-0.51783
H	2.18818	0.94880	1.18427

TS-12T

C	0.35402	0.35174	0.61075
C	-0.82467	0.92628	-0.00677
C	-1.98965	0.13242	-0.24995
C	1.65227	0.42286	-0.12856
H	-0.83308	1.96465	-0.31506
H	0.25673	-0.48831	1.28413
H	1.44182	1.04928	0.96222
H	1.74127	1.14507	-0.93040
O	2.45414	-0.67469	-0.24101
H	1.94416	-1.46347	-0.02341
O	-2.06034	-1.05796	0.03627
H	-2.85313	0.65416	-0.69235

IM-7T

C	0.55712	1.09120	0.42144
C	-0.78821	1.09588	-0.22176
C	-1.63941	-0.04688	-0.19339
C	1.56806	0.20052	-0.25398
H	-1.14301	1.98031	-0.73401
H	0.42853	0.75159	1.46137
H	2.59423	0.53234	-0.31917
O	1.43880	-1.13881	-0.14729
H	0.52040	-1.35709	0.09032
O	-1.30110	-1.12567	0.29405
H	-2.64002	0.06043	-0.63441
H	0.95296	2.10387	0.44787

www.manaraa.com

TS-13T (MP2, M06-2x DNC)

C	0.54019	1.22430	-0.14087
C	-0.92412	1.07440	-0.08722
C	-1.61548	-0.19977	0.06094
C	1.48849	0.19612	0.36223
H	-1.51710	1.90572	-0.45933
H	-0.30346	1.53641	0.87073
H	2.44668	0.53837	0.73394
O	1.54332	-1.00513	-0.25472
H	0.60740	-1.30058	-0.31883
O	-1.08809	-1.30318	0.06713
H	-2.71373	-0.10364	0.14605
H	0.90392	2.11994	-0.64228

IM-8T

C	-0.41477	1.08426	0.41268
C	0.96724	1.07933	-0.14370
C	1.62110	-0.28512	-0.14180
C	-1.50774	0.41478	-0.28742
H	1.63945	1.75980	0.38666
H	-2.39955	0.95445	-0.57647
O	-1.75353	-0.90114	-0.03548
H	-0.91567	-1.31177	0.22727
O	1.07591	-1.30767	0.17949
H	2.67442	-0.30379	-0.47426
H	-0.54383	1.41302	1.44059
H	0.97116	1.39929	-1.19433

TS-14T

C	-0.75389	1.00332	0.42660
C	0.28341	1.52091	-0.27320
C	1.89373	-0.02132	-0.08428
C	-1.69673	0.04295	-0.16362
H	0.92937	2.27316	0.16433
H	-2.76135	0.23089	-0.15591
O	-1.40681	-1.28816	-0.08292
H	-0.45079	-1.40182	0.00681
O	1.59802	-1.13953	0.12536
H	2.91501	0.39996	0.07174
H	-0.82369	1.21742	1.49292
H	0.30261	1.42682	-1.35232

$HCO + CH_2CHCHOH$

C	-1.91527	0.64711	0.00024
C	-0.87828	1.54967	-0.00021
C	2.95848	0.45927	-0.00036
C	-1.80158	-0.73037	0.00014
H	-1.07077	2.61080	-0.00007
H	-2.66451	-1.37844	0.00044
O	-0.64643	-1.41508	-0.00036
H	0.11358	-0.82014	-0.00043
O	2.16496	-0.40135	0.00036
H	4.06402	0.29586	0.00121
H	-2.93067	1.02276	0.00073
H	0.15990	1.24652	-0.00078

www.manaraa.com

TS-16T

C	-0.27637	1.11431	0.35497
C	1.14174	0.98449	-0.12529
C	1.59494	-0.45837	-0.10561
C	-1.32763	0.42794	-0.34298
H	1.84648	1.57825	0.46174
H	-1.32901	1.72094	-0.22959
O	-2.05619	-0.65895	-0.04633
H	-1.41623	-1.34251	0.21792
O	0.88674	-1.38968	0.17120
H	2.65172	-0.63213	-0.38150
H	-0.44869	1.33003	1.40685
H	1.25534	1.32430	-1.16087

IM-10T

C	-0.33156	1.21778	0.34012
C	1.09492	0.95280	-0.15229
C	1.51500	-0.48516	-0.10024
C	-1.36970	0.45613	-0.40318
H	1.83390	1.53145	0.41178
O	-1.91379	-0.69763	-0.02644
H	-1.20810	-1.36416	0.03777
O	0.79910	-1.40827	0.19391
H	2.57154	-0.67908	-0.36027
H	-0.41051	0.95226	1.39979
H	1.20595	1.26931	-1.19508
H	-0.52726	2.28817	0.25976

TS-17T

C	0.40134	1.40906	0.56199
C	1.37559	0.65168	-0.25622
C	1.19043	-0.83903	-0.26110
C	-1.51467	0.56518	-0.72195
H	2.41511	0.81455	0.07421
O	-2.04847	-0.24465	0.09924
H	-1.44588	-1.00296	0.29839
O	0.39003	-1.45297	0.40151
H	1.89000	-1.38924	-0.91456
H	0.04362	0.98866	1.48957
H	1.35759	0.97829	-1.29996
H	0.29093	2.47034	0.41007

HOC + CH_2CH_2CHO (B3LYP, M06-2x DNC)

C	1.48909	1.46703	0.15130
C	2.17522	0.18675	-0.13464
C	1.31454	-1.05039	-0.07329
C	-2.75720	1.17312	-0.14261
H	3.01307	-0.00697	0.56178
O	-2.82354	-0.43858	-0.01011
H	-1.87225	-0.64229	0.05276
O	0.13732	-1.07217	0.18540
H	1.85487	-1.99983	-0.26295
H	0.60992	1.48945	0.77620
H	2.66255	0.18799	-1.11877
H	1.89166	2.39859	-0.21599

www.manaraa.com

TS-15T

C	-0.42791	1.12118	-0.38344
C	0.95995	1.10354	0.11766
C	1.76579	-0.22200	0.08657
C	-1.48248	0.32710	0.29980
H	1.01315	1.33828	1.19135
H	-0.61857	1.41360	-1.40768
H	-2.49995	0.71256	0.15724
H	-1.33270	0.29738	1.39386
O	-1.48011	-1.00411	-0.12061
H	0.08415	-1.22075	-0.21064
O	1.08846	-1.29076	-0.06365
H	1.59503	1.83889	-0.37357

IM-9T

C	-0.50027	1.03344	-0.42858
C	0.77752	1.09703	0.31207
C	1.86211	0.00726	0.04951
C	-1.64750	0.21728	0.03804
H	0.62444	0.99756	1.39711
H	-0.56909	1.50015	-1.40085
H	-2.55760	0.36164	-0.55482
H	-1.93812	0.49048	1.07734
O	-1.38380	-1.13532	0.16427
O	1.36294	-1.15307	-0.20492
H	1.27914	2.04997	0.15560
H	0.37697	-1.22268	-0.17536

TS-18T

C	-0.74693	1.00816	-0.43973
C	0.30717	1.46560	0.29479
C	2.00631	0.11605	0.05846
C	-1.62623	-0.07316	0.07193
H	0.33613	1.28743	1.36582
H	-0.87751	1.31423	-1.46900
H	-2.59224	-0.16343	-0.43791
H	-1.89175	0.08778	1.13926
O	-1.04398	-1.33763	0.12591
O	1.54023	-1.01290	-0.16991
H	0.89468	2.30636	-0.04354
H	0.51875	-1.12813	-0.11538

HOC + CH_2CHCH_2O

C	-1.44086	0.25228	-0.40006
C	-1.36891	1.49662	0.04226
C	1.91526	0.80639	0.64049
C	-1.00955	-0.93782	0.40665
H	-0.97214	1.72134	1.02519
H	-1.82367	0.03908	-1.39213
H	-1.82210	-1.65180	0.58589
H	-0.65414	-0.60544	1.40042
O	0.08587	-1.59940	-0.10629
O	2.04389	0.21765	-0.46707
H	-1.69032	2.33133	-0.56561
H	1.34870	-0.48531	-0.60281

www.manaraa.com

M06-2x/cc-pVTZ Cartesian Coordinates for the Subsequent HCO/HOC Pathways of $O(^3P)$ + 3-Butyn-1-ol

CH_2CCH_2OH

C	-0.72566	-0.59238	0.05232
C	-1.65532	0.31943	-0.02420
C	0.74930	-0.63717	-0.01248
H	-2.70684	0.08164	0.08242
H	-1.39995	1.36022	-0.21881
H	1.06301	-1.15702	-0.91811
H	1.13900	-1.20597	0.83805
O	1.32729	0.65621	-0.07488
H	1.07659	1.13219	0.72165

TS-1D

C	-0.69533	-0.60211	-0.06706
C	-1.63571	0.36001	-0.01350
C	0.69995	-0.55885	-0.08713
H	-2.58501	0.21732	0.48202
H	-1.51710	1.27298	-0.59394
H	1.28526	-1.39642	-0.44471
H	0.07720	-1.12934	0.91155
O	1.45767	0.56752	0.04988
H	0.86484	1.30094	0.25215

IM-1D

C	-0.68283	0.61043	-0.00004
C	-1.50649	-0.48977	0.00003
C	0.69860	0.59319	0.00004
H	-2.57891	-0.37868	-0.00011
H	-1.13353	-1.50607	0.00032
H	1.29466	1.49207	0.00013
O	1.45161	-0.52336	0.00002
H	0.88123	-1.29876	-0.00051
H	-1.13199	1.59518	-0.00016

TS-2D

C	0.61760	0.62605	0.05520
C	1.45563	-0.53755	-0.00096
C	-0.81598	0.68445	0.05820
H	2.52340	-0.45102	0.12070
H	1.07712	-1.50494	-0.29903
H	-0.01065	1.01779	-0.99410
O	-1.42445	-0.50348	0.00313
H	-0.83073	-1.24736	0.20030
H	1.09301	1.57568	0.27240

www.manaraa.com

IM-2D

C	-0.61840	0.71216	0.00018
C	-1.39377	-0.55312	0.00010
C	0.91531	0.66652	0.00015
H	-1.71423	-1.01563	-0.92173
H	-1.70733	-1.01987	0.92219
H	-0.85388	1.33557	0.86829
O	1.37879	-0.54432	-0.00036
H	0.68055	-1.23473	-0.00086
H	-0.85418	1.33591	-0.86754

TS-3D

C	-0.89853	0.70976	-0.00001
C	-1.36140	-0.58818	0.00001
C	1.10414	0.68774	0.00001
H	-1.58415	-1.10729	-0.92249
H	-1.58414	-1.10727	0.92253
H	-0.95412	1.29963	0.90773
O	1.42641	-0.51700	-0.00001
H	0.60002	-1.10460	-0.00002
H	-0.95412	1.29960	-0.90777

HOC + C_2H_4

C	-1.30421	0.74140	-0.00001
C	-1.61833	-0.54945	0.00001
C	1.81980	0.63455	-0.00001
H	-1.77504	-1.09354	-0.92315
H	-1.77503	-1.09352	0.92318
H	-1.16541	1.29402	0.91983
O	1.49858	-0.58105	0.00000
H	0.50867	-0.71148	0.00001
H	-1.16542	1.29400	-0.91986

$CHCHCH_2OH$

C	-0.73793	-0.09856	0.38745
C	-1.82902	-0.04261	-0.32460
C	0.55552	0.57139	0.00535
H	-2.83473	-0.42488	-0.26417
H	-0.71125	-0.67745	1.31234
H	0.84315	1.28669	0.77638
H	0.42403	1.11666	-0.93300
O	1.61981	-0.35776	-0.07163
H	1.38895	-1.02025	-0.72775

www.manaraa.com

TS-4D

C	-0.67643	-0.29889	0.15927
C	-1.96523	0.06506	-0.32299
C	0.54889	0.46369	0.03584
H	-2.86291	0.10923	0.28026
H	-0.48067	-1.37272	0.28124
H	-0.43338	0.15005	1.22856
H	0.54646	1.54232	0.03133
O	1.76414	-0.09876	-0.08680
H	1.67403	-1.01795	-0.35971

IM-3D

C	-0.58334	-0.38293	0.00003
C	-1.87904	0.08229	0.00001
C	0.53677	0.41764	0.00003
H	-2.71600	-0.59698	-0.00020
H	-0.42043	-1.45834	0.00007
H	-2.08990	1.14245	-0.00004
H	0.48400	1.49674	0.00007
O	1.81058	-0.03596	-0.00005
H	1.81125	-0.99825	0.00009

TS-5D

C	0.51303	0.34278	0.06902
C	1.87079	-0.07211	-0.09219
C	-0.58040	-0.56803	-0.02369
H	2.67170	0.64814	-0.08240
H	0.31746	1.42361	0.10399
H	2.09703	-1.12381	-0.17534
H	0.09929	-0.32421	1.10467
O	-1.78430	0.02189	-0.06017
H	-1.73157	0.98534	-0.18834

IM-4D

C	0.50727	0.42108	0.21583
C	1.80307	-0.17407	-0.19402
C	-0.62025	-0.57180	0.21439
H	2.63033	0.45506	-0.47987
H	0.27809	1.34064	-0.35219
H	1.95584	-1.23531	-0.08030
H	0.54256	0.72742	1.27915
O	-1.73639	-0.03120	-0.16895
H	-1.65634	0.91054	-0.43241

المنارة للاستشارات
www.manaraa.com

TS-6D

C	0.94457	0.63805	-0.27519
C	1.41216	-0.59282	0.06814
C	-0.82757	0.35960	0.66787
H	1.19666	-1.46666	-0.53077
H	0.55649	0.82027	-1.27347
H	1.94068	-0.74993	0.99681
H	1.26388	1.51797	0.26348
O	-1.58516	-0.30460	-0.14143
H	-1.45143	-0.11380	-1.08951

HOC + C_2H_4

C	1.30400	0.74143	0.00010
C	1.61790	-0.54946	0.00009
C	-1.81961	0.63449	-0.00001
H	1.77557	-1.09331	-0.92304
H	1.16637	1.29432	-0.91976
H	1.77342	-1.09382	0.92329
H	1.16413	1.29378	0.91993
O	-1.49814	-0.58104	-0.00012
H	-0.50812	-0.71135	-0.00049

CH_2CH_2CHO

C	-1.44196	-0.56656	0.00008
C	-0.63131	0.67044	-0.00008
C	0.85685	0.43461	0.00006
H	-0.84957	1.31412	0.86427
O	1.37422	-0.64638	0.00001
H	1.47431	1.35265	0.00019
H	-0.95233	-1.52668	-0.00053
H	-0.84934	1.31375	-0.86480
H	-2.51830	-0.51371	0.00042

TS-7D

C	-1.64189	-0.56047	0.00591
C	-1.07034	0.66273	-0.00716
C	1.15107	0.43312	-0.00001
H	-0.98619	1.24149	0.90486
O	1.66901	-0.61534	-0.00373
H	1.68887	1.41417	0.03935
H	-1.84356	-1.07728	0.93341
H	-0.99199	1.22512	-0.92959
H	-1.85222	-1.09308	-0.91063

www.manaraa.com

$HCO + C_2H_4$

C	1.52671	-0.67841	-0.02275
C	1.59895	0.62931	0.16563
C	-1.49401	0.33878	-0.53962
H	2.32959	1.23774	-0.35136
O	-1.87329	-0.18003	0.43757
H	-1.06000	-0.19976	-1.41899
H	2.19816	-1.19226	-0.69861
H	0.93267	1.14006	0.84953
H	0.79599	-1.28363	0.49931

www.manaraa.com